

## Chapter 1: Selection on a Single Trait

© Stevan J. Arnold 2016

*Overview.*- Phenotypic selection can be measured by its effects on trait distributions within a generation. Our fundamental approach contrasts trait distribution before and after selection. This contrast is less intuitive than the comparison of traits in survivors and nonsurvivors, but it has an important statistical advantage. The difference in trait means before and after selection is equivalent to the covariance between a trait and fitness. Such selection differentials have been measured in a wide variety of natural populations and show that trait means are usually shifted by less than a half a phenotypic standard deviation (mean about 0.6) and that the modal value is close to zero. A similar perspective on trait variances shows that they usually contract by 0-50 percent within a generation or expand by 0-25 percent as a consequence of selection, with a mode close to zero.

In this chapter we will focus on simple descriptive characterizations of selection. Our account goes only a little way beyond older treatments of selection on quantitative traits in which correlations with other traits are ignored and no attempt is made to relate selection coefficients to equations for evolutionary change (Cook 1971, Endler 1986). In later chapters we will correct for the effects of selection on correlated characters, deduce modes of selection and fitness functions from changes in trait distributions, and use our measures of selection to model evolution.

### 1.0 Traits and trait distributions.

Many important traits show continuous distributions within populations, rather than discrete polymorphisms. Such traits are represented by multiple values rather than a few, so that the resulting distribution is continuous, and it is often unimodal (Wright 1968). Although normal distributions are not universal, many traits approach such a distribution, or can be transformed so that they approach normality more or less closely (Wright 1968). In the following sections of this chapter, and in most of the chapters that follow we will assume normality of trait distributions. This assumption is less restrictive than it may appear. In many theoretical situations that follow the crucial assumptions are actually unimodality and symmetry rather than normality *per se*.

A few examples will illustrate the kinds of traits that are continuously distributed. The examples that follow were chosen because not only because their



statistical distributions are well known, but because they are the subjects of research from diverse points of view. Because this extensive backlog of information, we will use them as examples throughout this book.

**Figure 1.0.** Radiograph of a natricine snake showing vertebrae in the body and tail. The distinction between the two kinds of vertebrae is not arbitrary. Ribs are attached to body vertebrae, but not to tail vertebrae. These two vertebral numbers can be assessed, without recourse to radiography, by counting ventral and subcaudal scales. The electronic object is a radiotransmitter used to study thermoregulation in free-ranging females during pregnancy.

Vertebral numbers in snakes (Fig. 1.0) have been important characters in systematics since the time of Linnaeus because they often differentiate even closely related species, as well as higher taxa. Vertebral counts also serve as markers for the occupancy of different adaptive zones; as few as 100 in fossorial species, as many as 300 in arboreal species (Marx & Rabb 1972). In most snakes the vertebrae show a 1:1 correspondence with external scales, so counts can be made using those scales (ventral and subcaudal) without recourse to radiography (Alexander & Gans 1966, Voris 1975). Furthermore, the transition from body vertebrae (with ribs) to tail vertebrae (with ribs) is marked by the anal scale, so counts on both body regions can be made in any specimen without a broken tail. In most snakes, both counts are sexually-dimorphic, typically with more vertebrae in males. Counts from females in a single population of the garter snake *Thamnophis elegans* are shown in Fig. 1.1. Distributions of body and tail vertebrae are generally unimodal and closely approximate normal or lognormal distributions (Kerfoot & Kluge 1971), as in these examples.

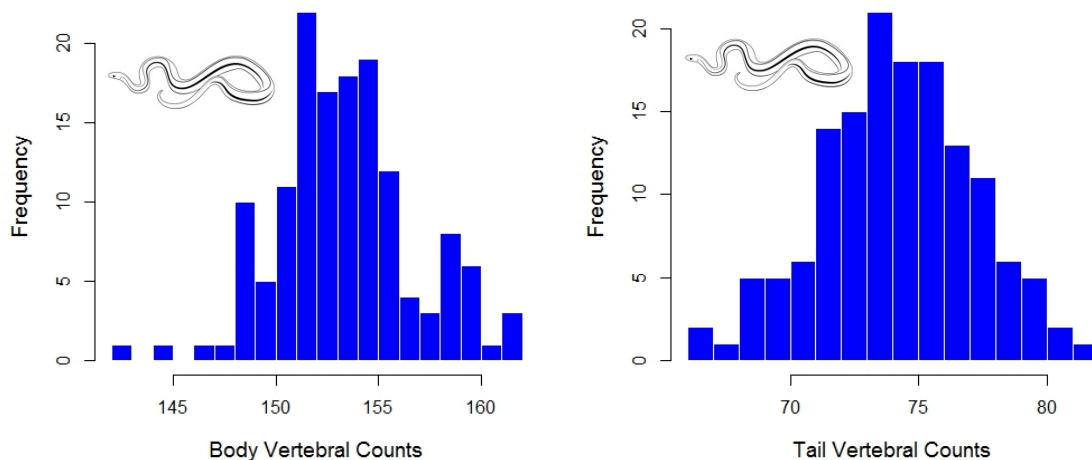


**Figure 1.1** Distributions of body and tail vertebral numbers in 143 newborn garter snakes, *Thamnophis radix* (data from Arnold & Bennett 1984).

Counts of bristles on the thorax and abdomen of *Drosophila melanogaster* have been used in studies of inheritance and responses to deliberate selection since the 1940s (Mather 1941, 1942). Usually two kinds of counts are made: abdominal bristles (on the sternites located on the ventral surface of the abdomen) and sternopleural bristles (on the sternopleuron located laterally on the thorax, Fig. 1.2). The bristles are actually the moving parts of a mechanoreception system. When the bristles are moved they activate an electrical signal that is sent to the brain, keeping the fly aware of changes in its environment. Because the larger bristles (macrochaetae) on the sternopleuron are fewer in number and almost completely invariant, they are sometimes ignored and so that the count is based only on the smaller, more numerous bristles (microchatae) (Clayton et al. 1957b). Distributions of abdominal and sternopleural bristle numbers closely approach normal distributions (Fig. 1.3).

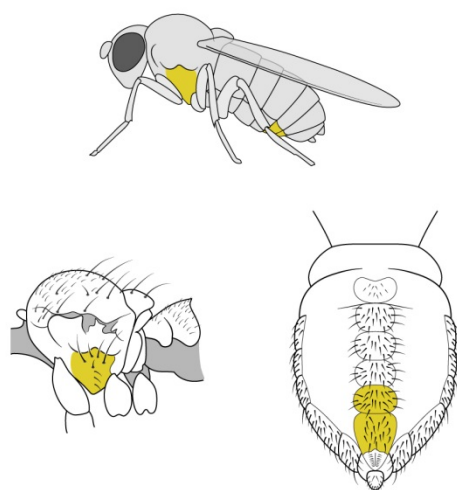


**Figure 1.2.** *Drosophila*, showing sites of important bristle counts. (Left). The sternopleuron (colored) on the thorax, showing eight sternopleural bristles (after Wheeler 1981). (Right). Abdominal tergites, showing abdominal bristles on the 4<sup>th</sup> and 5<sup>th</sup> tergites (colored).

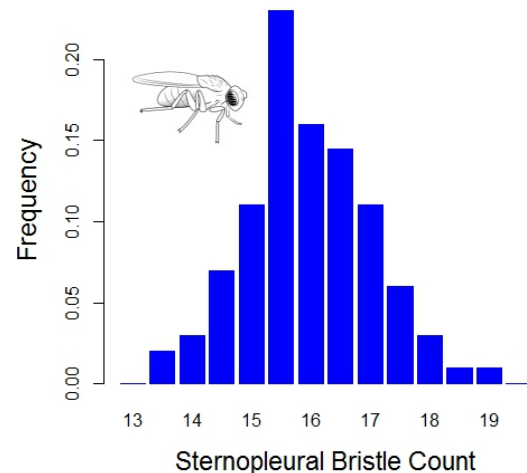
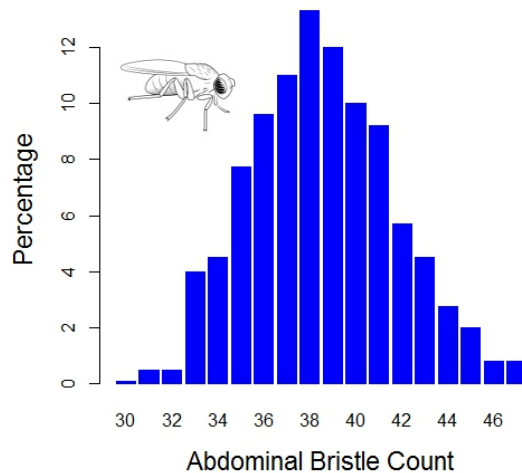


**Figure 1.3.** Histograms illustrating variation in *Drosophila melanogaster* bristle counts. (Left). Abdominal bristle number (Falconer & Mackay 1989). (Right). Sternopleuroal bristle number (i.e., sum of right and left sides). This histogram shows just the contributions to total variation from chromosome 2 (Mackay & Lyman 2005).

The dimensions of bird bills often reflect differences in food habits among species and so capture an essential feature of adaptive radiations (Schluter 2000). Diversification of bills is a pivotal feature of the adaptive radiation of the ground finches of the Galapagos, and for this reason many aspects of bills have been intensively studied (Lack 1947, Bowman 1961, Abbott et al. 1977, Grant 1986). The measurements are made on individuals that have reached adult size so that there are no ontogenetic complications. Distributions of bill depth, for example, often approximate a normal distribution (Fig. 1.4).

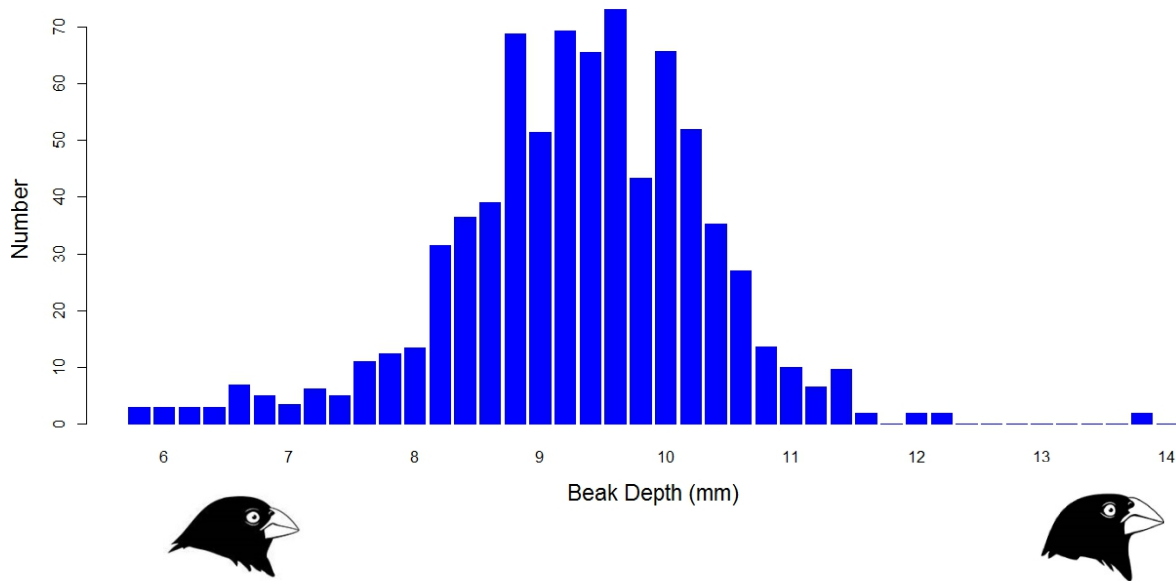


**Figure 1.4.** The distribution of beak depth of the Medium Ground Finch (*Geospiza fortis*) on Daphne Major, Galapagos Islands, in 1976 before a drought (n=751, from Grant 1986).

In this and the chapters that follow, we will assume that the trait does not change during ontogeny, as a result of age, growth or experience. Some traits are naturally of this kind. Vertebral numbers in snakes and other vertebrates, for example, are determined relatively early in development and do not change during the postnatal ontogeny. Likewise, bristle numbers do not change once the fly ecloses from its pupal stage. In other cases ontogeny-invariance can be achieved by defining age-specific traits (e.g., size at age three years), as in the beak dimensions of *Geospiza*. A general solution to the issue of traits that vary with age, size, experience, environment, etc. can be achieved by treating them as function-valued or infinite dimensional attributes (Kirkpatrick 1989, Gomulkiewicz & Kirkpatrick 1992, Kingsolver et al. 2001). In this approach, the phenotypic size of an individual is represented as a continuous function of age. The resulting theory closely follows the more simple theory for point-valued traits that is sketched here and in later chapters. In general, the main expressions remain the same except those involving traits values are transformed to continuous functions. In any case, the general point in trying to achieve size- and age-independence is that we want to define a phenotype that enables us to separate the effects of ontogeny from the effects of selection.

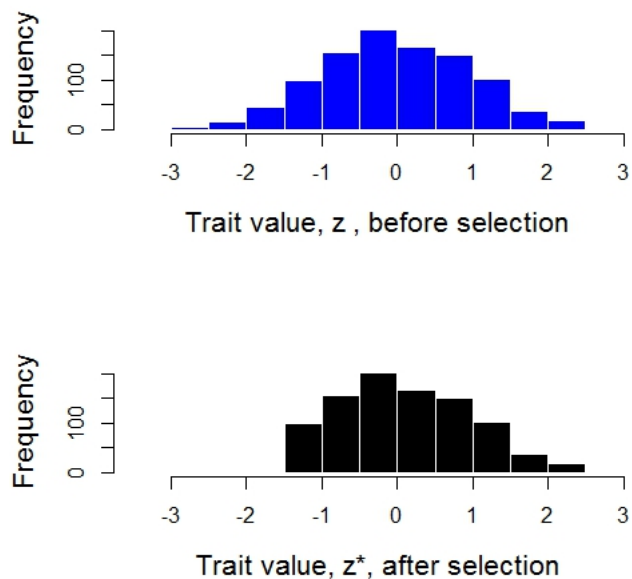
The choice of scale for a particular trait can be based on practical concerns. Homogeneity of variance among populations or higher taxa is often desirable for then the evolution of the trait mean can be divorced from concerns about the evolution of trait variance. The logarithmic scale is often useful in attaining this kind of invariance and has useful properties in its own right (Wright 1969). On the other hand, transforming a trait with the sole goal of making its distribution approach normality is seldom useful. Most statistical tests assume that the distribution of errors is normal (not the trait distribution itself) and, in any case, are robust to even appreciable departures from normality.

### 1.1 Selection changes the trait distribution.

We are concerned here not with the agents of selection but with the statistical effects of those agents on a particular trait,  $z$ . Those statistical effects are evolutionarily important even though they fail to capture the personality of selection. Imagine the statistical distribution of the trait in a population before selection has acted (Fig. 1.5). We will call the continuous version of that distribution  $p(z)$ , a distribution function that might take any of a variety of forms. Later we will assume that the function is a normal

distribution, but for the moment we will not make any assumptions about its form. Now imagine that as a consequence of selection some phenotypes increase in frequency, while others decrease (Fig. 1.5).

**Figure 1.5.** A single hypothetical trait in a sample of 1000 individuals is subjected to truncation selection. (above) The histogram of trait values for these individuals before selection is shown in blue (mean = -0.02, variance = 0.96). (below) Only individuals with trait values greater than -1.5 (n=921) survived selection. The trait distribution after selection is shown in black. Selection has shifted the trait mean and contracted its variance (mean = 0.11, variance = 0.75).  $s = \bar{z}^* - \bar{z} = 0.13$ ;  $(P^* - P)/P = -0.22$ ;  $(P^* - P + s^2)/P = -0.21$ .



We ascribe those changes in frequency to differences in fitness as a function of phenotype. The essence of selection is that all individuals with a particular phenotype,  $z$ , have an expected absolute fitness, which we will call  $W(z)$ . To determine average absolute fitness in the population we need to weight each value of fitness by its frequency, in other words,

$$\bar{W} = \int p(z)W(z)dz. \quad (1.00)$$

The differences in fitness are crucial in determining how the frequency of individuals with phenotype  $z$  will be changed from  $p(z)$  before selection to  $p^*(z) = w(z)p(z)$  after selection, where  $w(z) = W(z)/\bar{W}$  is relative fitness of an individual with phenotype  $z$  (Fig. 1.5). Note that because mean relative fitness is

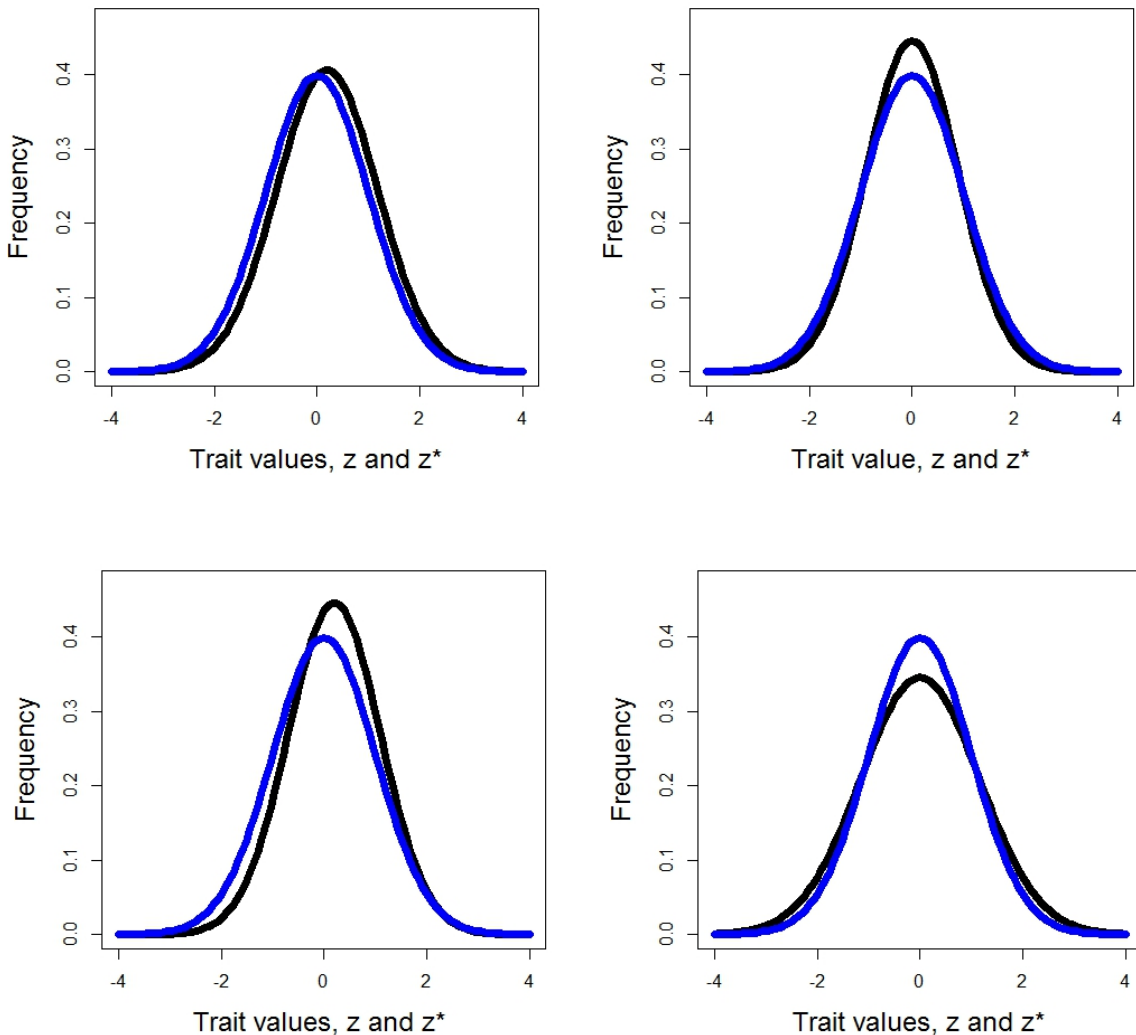


**Figure 1.6** Hypothetical examples of selection acting on normally-distributed trait distributions. Trait distributions are shown in blue before selection and in black after selection. (upper left) An upward shift in mean with little change in variance;  $\bar{z} = 0.00$ ,  $P = 1.00$ ,  $\bar{z}^* = 0.02$ ,  $P^* = 0.96$  (upper right) a contraction in variance with no shift in mean;  $\bar{z} = 0.00$ ,  $P = 1.00$ ,  $\bar{z}^* = 0.00$ ,  $P^* = 0.80$ . (lower left) An upward shift in mean with a contraction in variance;  $\bar{z} = 0.00$ ,  $P = 1.00$ ,  $\bar{z}^* = 0.20$ ,  $P^* = 0.80$ . (lower right) An expansion of variance with no shift in mean;  $\bar{z} = 0.00$ ,  $P = 1.00$ ,  $\bar{z}^* = 0.00$ ,  $P^* = 1.33$ .

$$w = \int p(z)w(z)dz = \int p(z)\frac{W(z)}{\bar{W}}dz = \int p(z)^*dz, \quad (1.01)$$

it equals 1. We will need the crucial function,  $p(z)^*$ , the frequency distribution after selection, to calculate various coefficients that can be used to characterize selection (Lande 1976).

To simplify particular theoretical results it will sometimes be useful to assume that the trait distribution before selection is normal. Under this assumption we have the following expression for  $p(z)$ ,

$$p(z) = \frac{1}{\sqrt{2\pi P}} \exp\left\{-\frac{(z - \bar{z})^2}{2P}\right\}. \quad (1.02)$$

The  $1/\sqrt{2\pi P}$  term is a normalization factor which insures that the trait probabilities sum to one.

### 1.2 Shift in the trait mean, the linear selection differential.

A fundamental question is to ask what does selection do to the mean of our trait distribution. The mean before selection is, using the standard definition of the mean,

$$\bar{z} = \int p(z)zdz. \quad (1.03)$$

Using that same, familiar definition, the mean after selection must be

$$\bar{z}^* = \int p(z)^*zdz. \quad (1.04)$$

A natural way to express the effect of selection on the mean is to take the difference between the mean after selection and mean before selection. The difference is taken in this order so that it will be positive, when the mean is shifted upwards. This difference is called the *directional selection differential*,

$$s = \bar{z}^* - \bar{z}. \quad (1.05)$$

It is useful to measure the shift in mean given by  $s$  in units of within-population phenotypic standard deviation. If we let the variance in the population for trait  $z$  be  $P$  before selection, then the trait standard deviation is  $P^{1/2}$ , and our *standardized directional selection differential* is  $s/P^{1/2}$ . A standardized selection differential of 2 means that the mean has been shifted upward by two phenotypic standard deviations (Lande & Arnold 1983).

### 1.3 The directional selection differential as a covariance.

The directional selection differential is an especially powerful descriptor of selection because it is a covariance as well as a shift in mean. Recall that the covariance between two variables, call them  $x$  and  $y$ , is defined as

$$\text{Cov}(x, y) = \int p(x, y)(x - \bar{x})(y - \bar{y})dxy , \quad (1.06)$$

where  $p(x,y)$  is the frequency of observations with values  $x$  and  $y$ . With a little rearrangement we can express this same equation as

$$\text{Cov}(x, y) = \int p(x, y)xydxy - \bar{xy} . \quad (1.07)$$

Substituting  $w(z)$  for  $x$  and  $z$  for  $y$  into these two expressions, and remembering that the mean of  $w(z)$  is 1, we obtain

$$\text{Cov}(w, z) = \int p(z)[w(z)-1][z - \bar{z}]dz = \int p(z)* zdz - \bar{z} = \bar{z}^* - \bar{z} = s . \quad (1.08)$$

In other words, the directional selection differential,  $s$ , is the covariance between relative fitness and trait values (Robertson 1962). This second definition of the directional selection differential will be of special importance in later sections. An example, showing the equivalence of  $\text{Cov}(x,z)$  and the directional

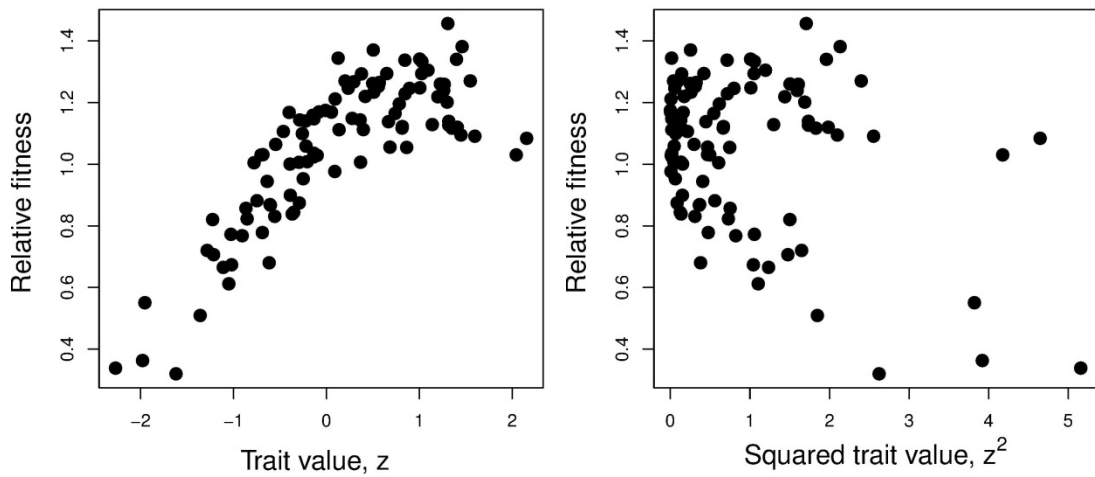


**Figure 1.7.** Scatterplots plots showing the equivalence between covariance and selection differentials. The sample of 100 individuals in these plots were drawn from the trait and fitness distributions,  $p(z)$  and  $w(z)$ , used in Fig. 1.1c. (a) Relative fitness as a function of trait value,  $z$  ( $\bar{z} = -0.13$ ,  $P = 0.98$ ,  $w = 0.97$ ,  $\text{cov}(z,w)=0.21$ ,  $r(z,w)=0.81$ ). (b) Relative fitness as a function of squared trait values,  $z^2$  (mean  $z^2 = 0.99$ ,  $\text{var}(z^2)= 0.98$ ,  $\text{cov}(z^2,w)=-0.17$ ,  $r(z^2,w)=-0.46$ ). \*pull in correct values from program file\*

selection differential is provided in Fig. 1.7a, which shows relative fitness as a function of trait values. This sample was drawn from the trait and fitness distributions,  $p(z)$  and

$w(z)$ , used in Fig. 1.5c. As expected the covariance in Fig. 1.7a (0.21) is very close to the shift in mean in Fig. 1.1c (0.20)

#### 1.4 Change in the trait variance, the nonlinear selection differential.

We can expect that selection might change the variance of a trait, just as it might shift the trait mean. Applying the same logic as before, the variance before selection is, using the standard expression for variance,

$$P = \int p(z)(z - \bar{z})^2 dz \quad (1.09)$$

and after selection it is

$$P^* = \int p^*(z)(z - \bar{z})^2 dz. \quad (1.10)$$

By analogy with our treatment of the mean, we might measure the absolute effect of selection on the variance as  $P^*-P$  and its proportional effect as  $(P^*-P)/P$ . For example, when this proportional measure is -0.5, the trait variance has been reduced by 50%.

A slightly more complicated measure of effects on variance will prove useful because it leads to a equivalence with a covariance. The essential point behind this more complicated measure is that the same mode of selection that shifts the trait mean will also contract its variance. This effect of directional selection on variance is especially easy to characterize if the trait is normally distributed before selection. In that case, directional selection that shifts the mean by an amount  $s$  will contract the trait's variance by an amount  $s^2$ . Consequently, we can define a *nonlinear selection differential* so that it measures effects on variance from sources other than directional selection (e.g., from stabilizing and disruptive selection), viz.

$$C = P^* - P + s^2. \quad (1.11)$$

This same selection differential, not  $P^*-P$ , is equivalent to the covariance between relative fitness and squared deviations from the trait mean,

$$C = Cov[w, \tilde{z}^2], \quad (1.12)$$

where  $\tilde{z} = z - \bar{z}$  (Lande & Arnold 1983). An example, showing the equivalence of  $Cov(x,z)$  and the nonlinear selection differential is provided in Fig. 1.7b, which shows relative fitness as a function of squared trait values. As expected the covariance in Fig. 1.7b (-0.17) is very close to the corrected change in variance,  $C = P^* - P + s^2$ , observed in the parent distributions shown in Fig. 1.6c (-0.16), within the bounds of sampling error. As before, it is useful to standardize using the variance before selection to obtain a proportional measure of effects on variance, a *standardized nonlinear selection differential*,  $C/P$ . In the next section we will show that  $s$  and  $C$  reflect selection acting on correlated traits, as well as selection acting directly on the trait in question.

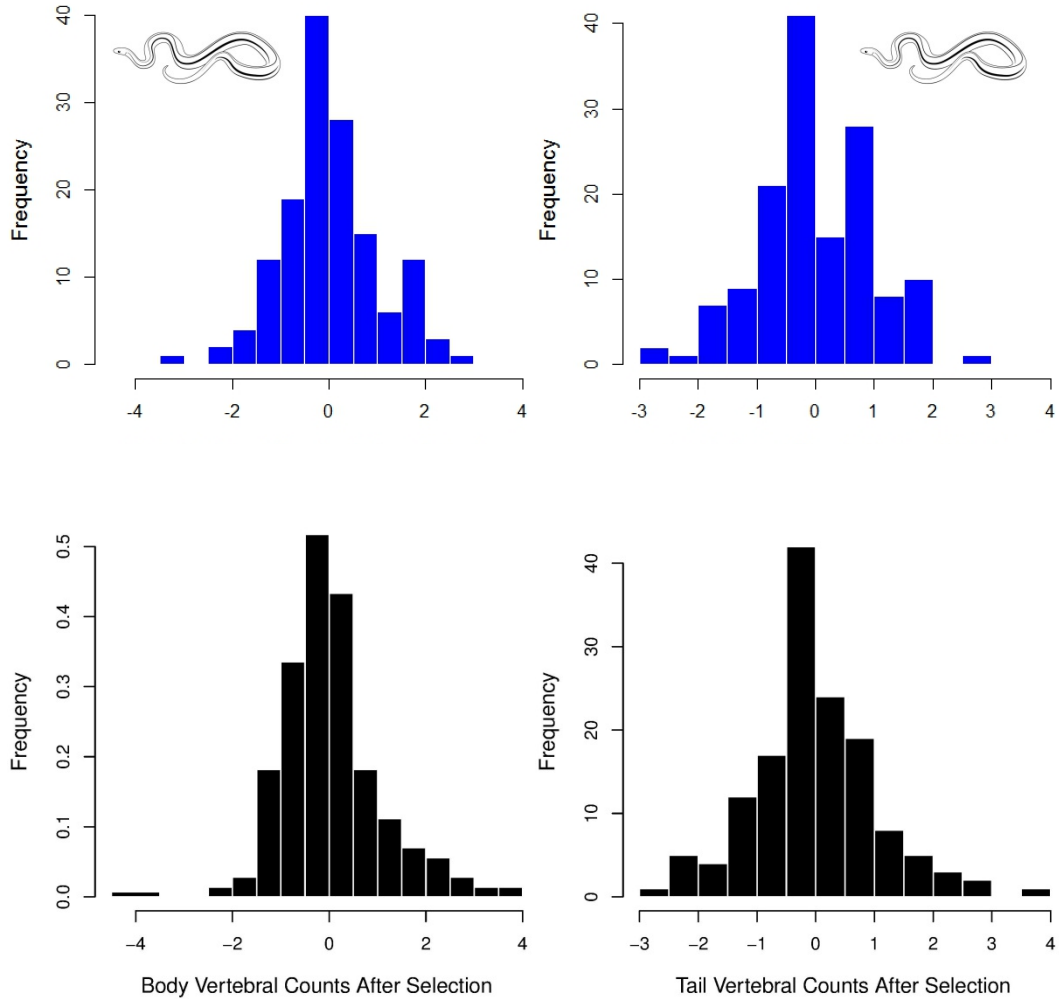


**Figure 1.75.** Samples of body and tail vertebral counts in the garter snake *T. radix* ( $n=143$ ) before and after selection. The samples before selection are standardized to zero means. In the samples after selection, the vertebral count of each individual is weighted by relative crawling speed.

### 1.5 Estimates of univariate selection differentials

Statistics associated with traits distributions before and after selection allow us to visualize the impact of selection. The following example illustrates how various

univariate statistics contribute to our visualization of selection. In this example, crawling speed of newborn garter snakes (*Thamnophis radix*) was measured in the laboratory and related to counts of body and tail vertebrae (Arnold & Bennett 1988). Crawling speed is plausibly related to vertebral counts because larger vertebral counts promote the flexibility needed for snake locomotion (Fig. zz.x)

**Figure zz.x** Diagram of a crawling snake showing how the body pushes against points in the environment. Contractions of musculature in particular segments of the body (black) produce the pressure that moves the snake forward (from Jayne 1985 = PhD dissertation).

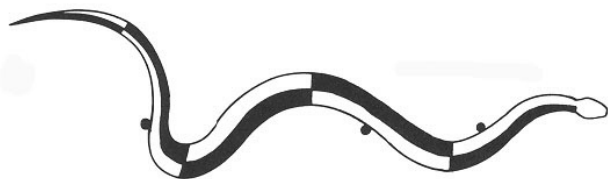


**Table 1.1** Selection differentials describing effects of numbers of body and tail vertebrate on crawling speed in newborn garter snakes (*Thamnophis radix*) (n=143). Standardized measures are denoted with a '. Bootstrap estimates of 95% confidence limits are shown in parentheses.

	BODY		TAIL	
	mean	variance	mean	variance
Before selection	153.414	11.437	74.257	9.094
Before selection'	0.000	1.000	0.000	1.000
After selection'	0.031	1.122	0.004	1.142
		$P_1^* - P_1$		$P_2^* - P_2$
Change in variance		0.122 (-0.062, 0.342)		0.142 (-0.015, 0.327)
	$s_1$	$C_1$	$s_2$	$C_2$
Selection	0.031	0.123	0.004	0.142

As is typical in snakes, males had several more tail vertebrae than females and a few more body vertebrae, so the sex

differential	(-0.032, 0.096)	(-0.062, 0.328)	(-0.058, 0.063)	(-0.015, 0.327)
Correction term, $s^2$		0.077		0.001

difference in means was added to the counts of females, and the combined sample of 143 neonates was analyzed. The trait sample before selection was standardized by subtracting the trait mean from each observation and dividing by the trait standard deviation, so that the means of each trait were zero and variances were equal to one. This standardization simplifies the interpretation of selection statistics. The sample after selection,  $p(z)^*$ , in this example is not a sample of survivors, but is instead the trait distribution weighted by relative crawling speed (Fig. 1.75). Because of the trait standardization, we can immediately see the changes in trait means and variances before we calculate the selection differentials (Table 1.1). We see that the body mean has been shifted upward by slight amount (3.1% of standard deviation in the body vertebral count before selection). The tail mean has also been shifted upward but to a smaller degree (0.4% of standard deviation in the body vertebral count before selection). The 95% confidence intervals for these and other statistics were estimated by bootstrapping over the sample of 143 individuals and are reported in Table 1.1. We see that the confidence intervals for  $s_1$  and  $s_2$  do not overlap zero, so those estimates are not significant at the 0.05 level. Turning to the trait variance, we crawling performance has caused the body variance to expand by 12.2% ( $P_1^*-P_1$ ). The effect of directional selection on the trait variance will be to decrease the variance by 7.7% ( $s_2=0.077$ ), so when we add that amount to  $P_1^*-P_1$ , we obtain a selection differential of 12.3%, which represents the effect of disruptive selection, after correcting for directional selection. The effect on tail variance is similar, except the expansion is slightly larger and the effect of directional selection is smaller. Bootstrapped confidence intervals indicate that neither the uncorrected changes in variance nor the nonlinear selection differentials are different from zero. One could easily conclude the slight changes in means and variances - and from our analysis - that the trait distributions have not been changed by selection. See shall see in the next chapter that this conclusion is premature, because we have not considered effects on trait covariance!

Ground finches (*Geospiza fortis*) present an especially well understood example of selection. Intensive mark-recapture studies on Dapne Major, a small island in the Galapagos, provided measurements of beak depth on 751 adult birds in 1976. Shortly after this field work, a severe drought markedly changed the availability of seed types on the island. When a sample was taken after the drought in 1978, only 90 birds survived. An inspection of the beak depth distribution before and after selection (Fig. 1.8) reveals that the average beak depth was shifted upwards and variance contracted.

Indeed, the mean beak depth distribution shifted upward by 60% of a phenotypic standard deviation ( $s = 0.60$ ). Both tails of the distribution were trimmed by the drought condition, but especially the lower tail. Observation studies showed that birds with deep beaks were better able to open larger seeds that increased in frequency during the drought (Grant 1986).

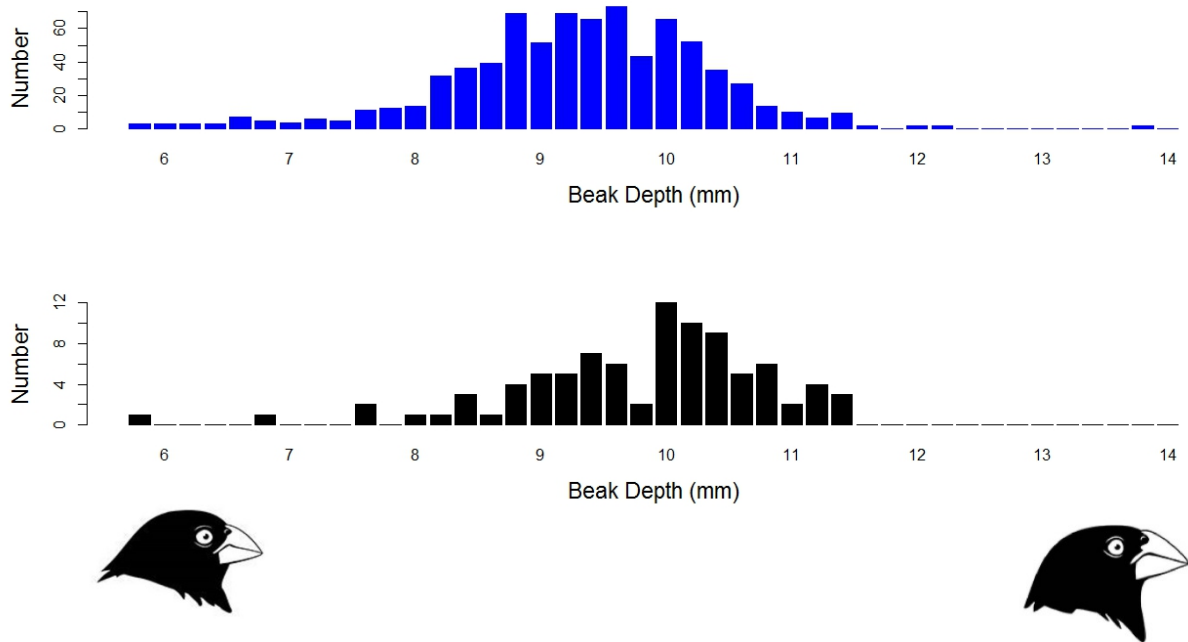


**Figure 1.8** Distributions of beak depth measurements before and after selection on the Daphne Major population of *Geospiza fortis*. (above) The distribution in 1976, before selection ( $n=751$ ). (below) The distribution in 1978, after a drought killed many birds ( $n=90$ ). (From Boag & Grant 1984, Grant 1986).

### 1.6 Technical issues in estimating and interpreting selection differentials

Different kinds of data are used to infer selection and measure its impact. It is useful to recognize two broad categories of samples. In *longitudinal samples*, a set of individuals is followed through time. Phenotypes are measured before selection, as well as after selection, and a particular value for fitness can be assigned to each individual. Because fitness values are attached to individuals, the covariance forms for selection differentials (1.07, 1.11) can be used. The significance of fitness assignments is apparent when we consider the contrasting case of *cross-sectional samples*. In a cross-sectional study, one sample is taken before selection and another is taken after selection, but individuals are

not tracked through time. As a consequence, more assumptions must be made to interpret selection differentials. In particular, one must assume that the sample before selection is representative of the statistical population that gave rise to the sample after selection. Although this assumption is straight-forward in some cases, it can be tortuous if the study begins with a sample of survivors and the probable population before selection must be reconstructed (Blanckenhorn et al. (1999)). The difference in samples also affects the estimation of standard errors. In the case of longitudinal data, estimation is straight-forward. The two key selection differentials are covariances which can be converted to correlations with well-characterized sampling properties, assuming a normal distribution of errors or by using nonparametric correlations. In the case of cross-sectional data, however, one must use the difference formulas (1.04, 1.10) to estimate selection differentials, and standard errors must be estimated by a re-sampling procedure (e.g., boot-strapping or jack-knifing).

Studies of selection are nearly always based on particular periods or episodes rather than lifetimes of exposure. Because this restriction is universally recognized by investigators, it may not always be acknowledged in print. For example, studies of sexual selection often use mating success as a fitness currency. The selection that is measured is distinct but it is usually not summed up over a lifetime of episodes. Instead, a snapshot of selection is taken at a particular place and time (e.g., one mating season), ignoring differences in age and the possibility of age-specific differences in selection. A similar restricted focus is often taken in studies of viability selection. Such restrictions are so common that they become a common denominator in comparisons across studies of a particular kind. The restriction to selection snapshots will make a difference when we consider responses to selection across generations (Chapters 9-10), for then the focus will necessarily be on lifetime measures of fitness and selection.

The use of standing, natural variation to assess fitness differences is powerful when it succeeds, but the approach can fail if variation is limited. Measuring selection on floral morphology has been challenging for precisely this reason (Fenster et al. 2004). Despite abundant evidence that pollinators shape the morphologies of the flowers they visit, selection on specific floral traits has often proved difficult to detect.

Throughout this chapter we have been concerned with viewing selection from the standpoint of a single trait. The univariate measures of selection that we have considered ( $s$ ,  $P^*-P$ , and  $C$ ) are all useful, but they share a common ambiguity. Each of these indices reflects the effects of selection on correlated traits as well as on the trait in question. In the next chapter we will consider techniques for separating these two kinds of effects.

### 1.6 Surveys of selection differentials

Endler (1986) surveyed about 30 studies of about 24 species published between 1904 and 1985 that measured selection in natural or experimental populations exposed to selection in nature. Those studies encompassed a wide range of organisms (plants, invertebrates, vertebrates) and traits (mostly linear measurements but some counts). Endler's survey indicates that selection typically changes trait means and variances by rather small amounts. The modal values for standardized change in mean,  $(\bar{z}^* - \bar{z})/\sqrt{P}$ , and standardized change in variance,  $(P^* - P)/P$ , are very close to zero (Figs. 1.9a, b). Note that in Fig. 1.9a, the positive and negative changes in the mean are grouped together, so that  $|(\bar{z}^* - \bar{z})/\sqrt{P}|$  is shown, since we are interested in the overall picture of how strong selection might be. In general, selection shifts the trait mean by less than half a phenotypic standard deviation (Fig. 1.9a). Likewise, selection generally causes a less than 50% change in trait variance (Fig. 1.9b). Contraction of variance is more common than expansion of variance; 68% of the values in Fig. 1.9b are negative. The distribution of changes in trait mean and variance are portrayed in Figs. 1.9 c-d, where for purposes of illustration the traits are assumed to be normally distributed before and after selection. Notice that the trait mean can be shifted by more than a standard deviation and the variance can change by more than 100%, but instances of such dramatic changes are relatively rare.

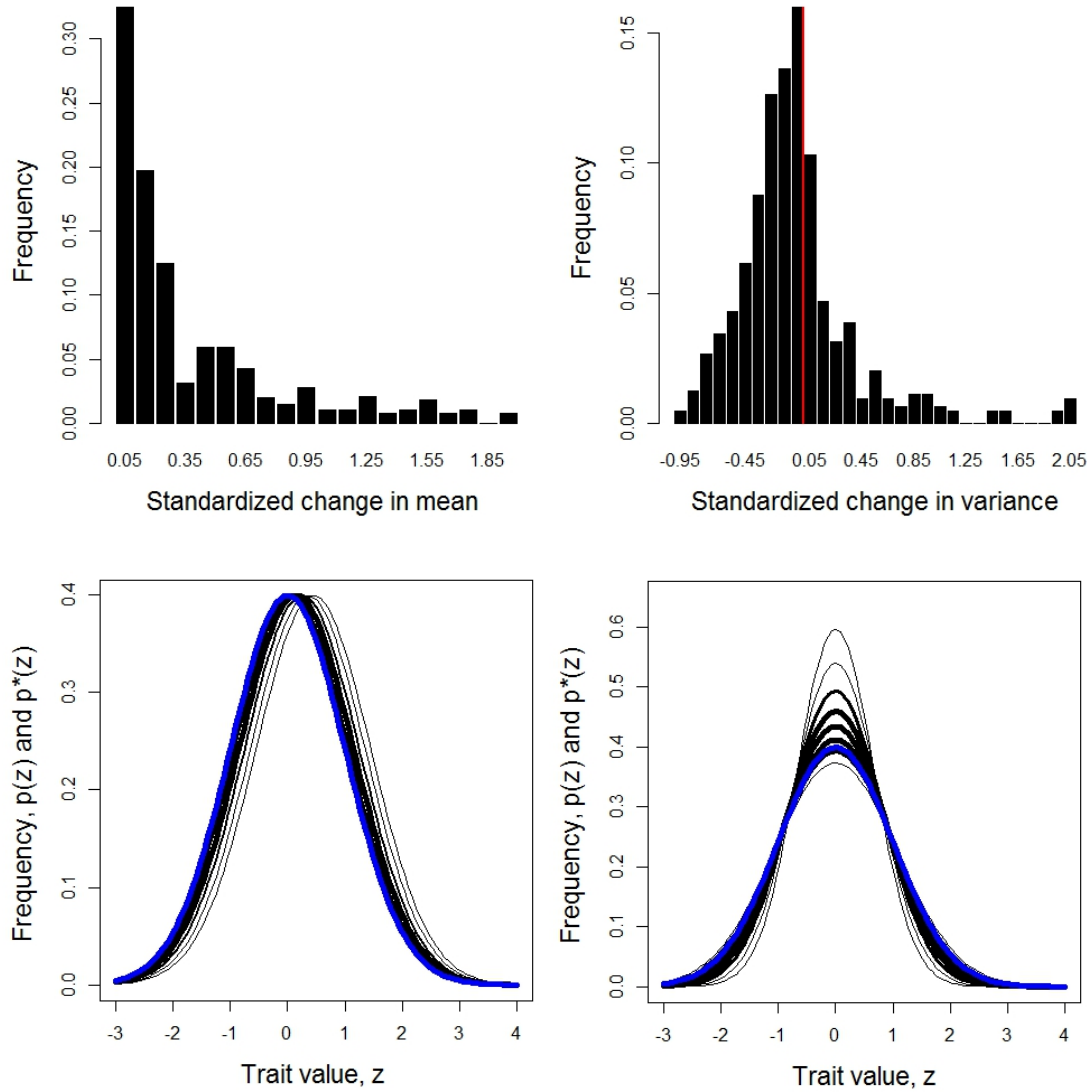
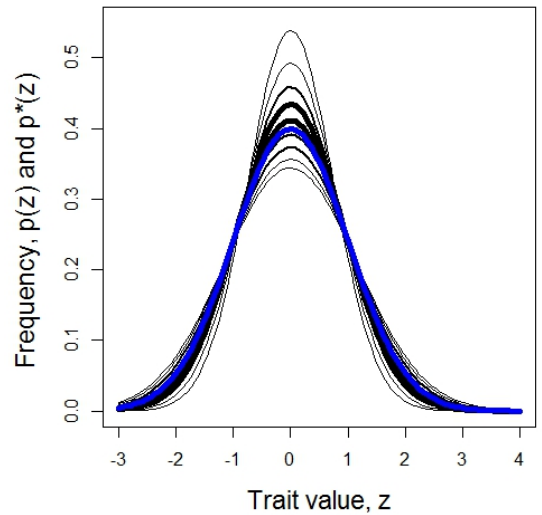
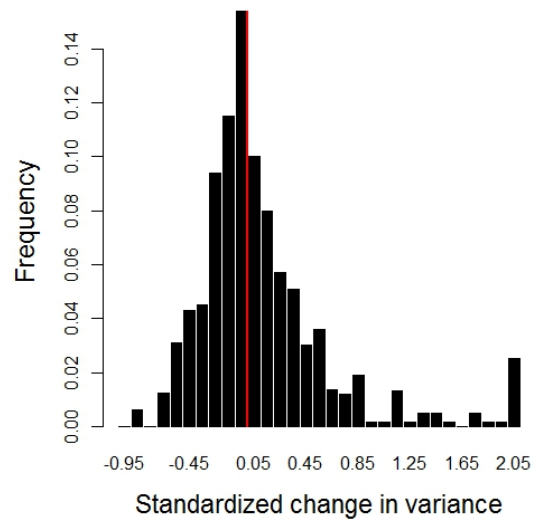


**Figure 1.9.** Distributions of standardized changes in means and variances. (Upper left) Distribution of estimates of the standardized change in mean,  $(\bar{z}^* - \bar{z}) / \sqrt{P}$ . From Endler (1986),  $n=262$ . (Upper right) Distribution of estimates of the standardized change in variance,  $(P^* - P)/P$ . From Endler (1986),  $n=330$ . The red vertical line shows the transition from negative to positive change in variance. (Lower left) Selection differential,  $s$ , illustrated as normal distributions after selection with mean shifted towards higher values. Line widths represent frequency in Endler's histogram; before selection (blue, with unit standard deviation and zero mean) and after selection (black). (Lower right) Standardized change in variance,  $(P^* - P)/P$  illustrated as normal distributions after selection with variance contracted or expanded. Line widths represent bin frequencies in Endler's histogram.

The consequences of correcting the change in variance for the effect of directional selection is shown in Fig. 1.10. The overall effect is, as Endler (1986) noted, extremely slight. Since the modal value of directional selection is close to zero, it is not surprising that correcting for this generally weak selection usually makes a small contribution to change in trait variance. The correction does however have the effect of making corrected expansions of variance nearly as common as contractions; only 52% of the values are negative in Fig. 1.10.

**Figure 1.10.** Distribution of estimates of the standardized change in variance, corrected for the effects of directional selection, showing that the predominant effect of selection is to contract variance. The red vertical line shows the transition from negative to positive change in variance. (Above) Distribution of estimates of the standardized change in variance,  $(P^*-P+s^2)/P$ . From Endler (1986),  $n=330$ . (Below) Standardized change in variance,  $(P^*-P+s^2)/P$ , illustrated as normal distributions after selection with variance contracted or expanded. Line widths represent bin frequencies in Endler's histogram, before (blue, with unit standard deviation and zero mean) and after selection (black).



## Chapter 2: Selection on Multiple Traits

© Stevan J. Arnold 2016

**Overview.**- The phenotypic effect of selection on multiple traits can be assessed by its effects on multivariate trait distributions. As in the case of a single trait, the fundamental approach is to compare the first and second moments of traits distributions before and after selection. Such a multivariate comparison of moments represents a major statistical improvement over trait-by-trait comparisons. By taking a multivariate approach we may be able to identify which traits are the actual targets of selection. Analysis of selection in natural systems reveals that the effects of selection on actual targets are often obscured by correlations between traits. In addition to identifying targets of selection, multivariate analysis also gives us a way to quantify functional interactions between traits. Measuring the strength of trait interactions is especially important because most traits belong to one or more functional complexes.

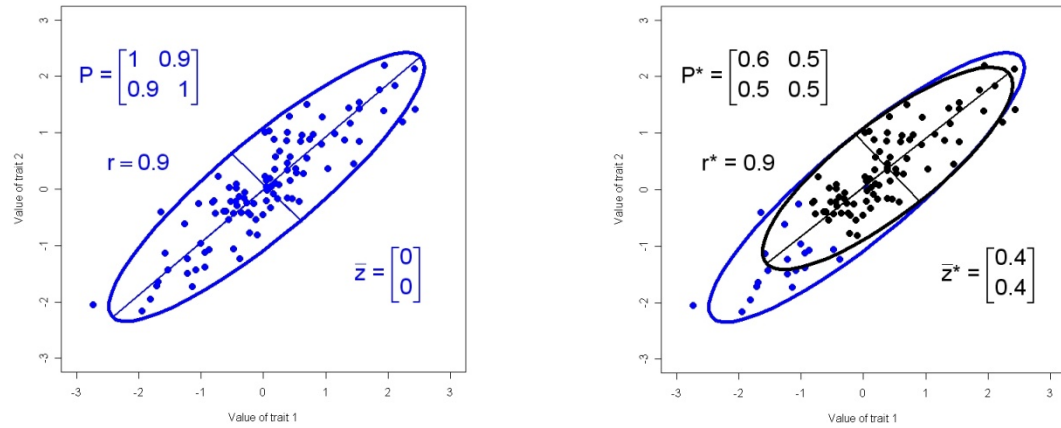
Animal and plant breeders may select on a single trait with the goal of improving their stocks. In the natural world, however, selection inevitably acts simultaneously on many traits. In this section we will introduce matrix algebra tools that will enable us to deal with this multivariate aspect of selection. In particular, we will move beyond the ambiguity of selection differentials.  $s$  and  $C$  are ambiguous because the shifts that they quantify could represent effects of selection acting on correlated traits as well as on the trait in question. Matrix algebra will help us to disentangle those direct and indirect effects and it will help us measure how strongly traits interact in functional complexes. The theoretical results that follow are from Lande & Arnold (1983), unless noted otherwise.

### 2.1 Selection changes the multivariate trait distribution.

Before we consider selection, we need to imagine the distribution of multiple traits before selection has happened. To visualize this distribution, picture a cloud of trait values in three-dimensional space. If more than three traits are involved, so that the cloud hangs in  $n$ -dimensional space, a standard convention is to depict those dimension two or three at a time. Some examples of actual two-dimensional trait distributions are shown in Fig. 2.0 {= examples of bivariate trait distributions, as in Fig. 1.0 drawing from show-cased examples, such as g-snake vertebral numbers ...}.

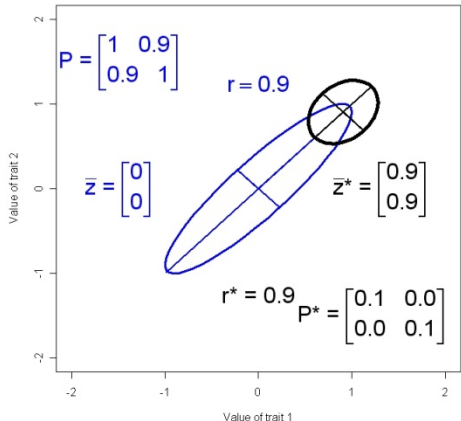
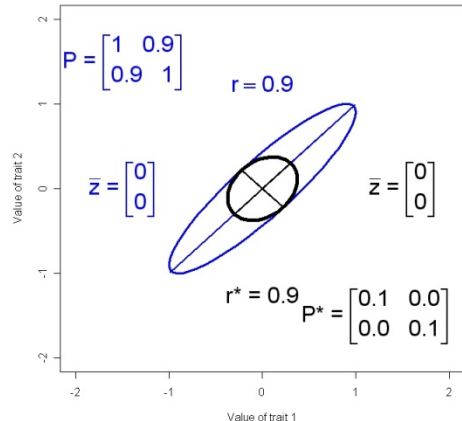
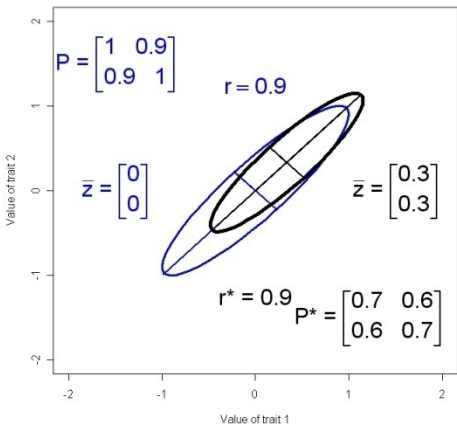
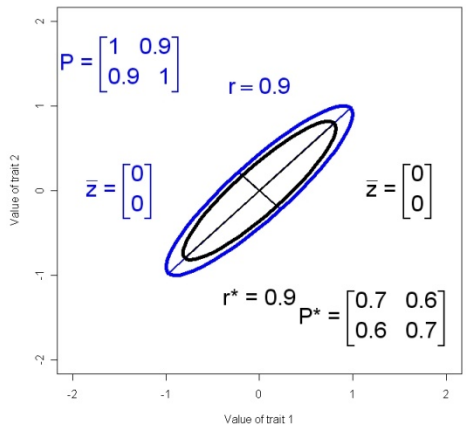
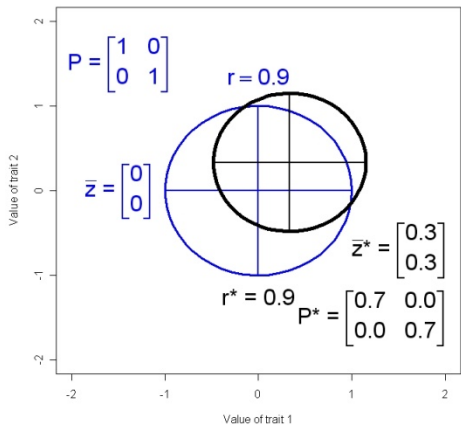
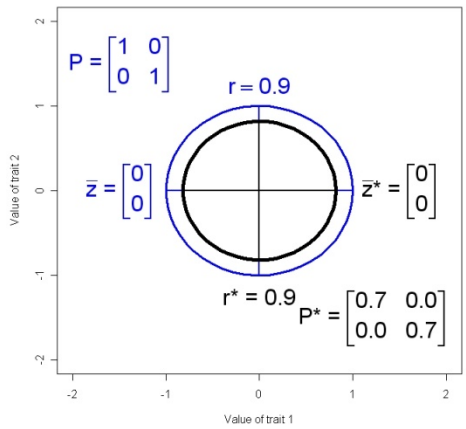
To consider how selection might affect such a bivariate distribution, it will be useful to consider the case of a hypothetical trait distribution that is subjected to truncation section. We will assume that the trait distribution is multivariate normal before selection, even though some of the results that follow do not depend on this

assumption. An example is provided in Fig. 2.1a, which shows a sample from normal distribution of just two hypothetical traits,  $z_1$  and  $z_2$ . We impose truncation selection, so that only individuals with  $z_1 > -1$  and  $z_2 > -1$  survive. The sample after selection is shown in Figure 2.1b. Calculation of selection measures (discussed below) confirm the impression that selection has shifted the bivariate mean and reduced dispersion in the sample.



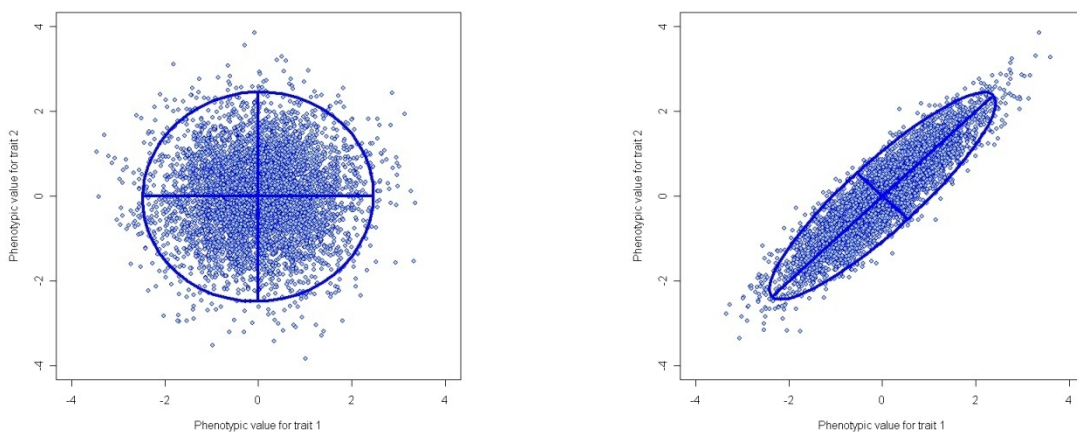
**Figure 2.1.** A two traits in a sample of 100 individuals are subjected to truncation selection. (a) A scatter plot trait values for these individuals before selection is shown in blue, along with the sample's 95% confidence ellipse. (b) Only individuals with trait values greater than -1.0 for both traits survived selection ( $n=81$ ). The scatter plot of the sample after selection is shown in black along with its confidence ellipse. Selection has shifted the trait means upwards and contracted both variances, the covariance, and the correlation.

Multivariate selection can change the trait distribution in a variety of ways that we might not have expected from a simple univariate view (Fig. 1.1). In particular, bivariate selection can change trait covariances and correlations, as well as means and variances. Only contractions of variance and covariance are shown in Fig. 1.1, but expansions can occur as well. As we shall see in later section, the hypothetical selection regimes used to produce Fig. 2.2 were, for the purposes of illustration, stronger than we would expect in nature.



**Figure 2.2.** Changes in hypothetical bivariate trait distributions induced by selection. All of the distributions are normal before and after selection; 95% confidence ellipses are shown before selection (blue) and after selection (black). The position of bivariate means is shown with crosses. (a) Contractions in both variances with no shift in mean. (b) Contraction in both variances with an increase in bivariate mean:  $\bar{z} = (0, 0)$ . (c) Contractions in both variances and covariance with no shift in mean. (d) Contractions in both variances and covariance with an upward shift in mean. (e) Substantial contractions in both variances and covariance with no shift in mean. (f) Substantial contractions in both variances and covariance with an upward shift in mean.

To get a better feel for the bivariate normal distribution consider the views in Fig. 2.3, which show large samples from distributions with no correlation (Fig. 2.3 a and c) and a strong positive distribution (Fig. 2.3b and d). With no correlation and equal variances for the two traits, the distribution is a symmetrical hill. Positive correlation converts the distribution into a symmetric, ridge-shaped hill.



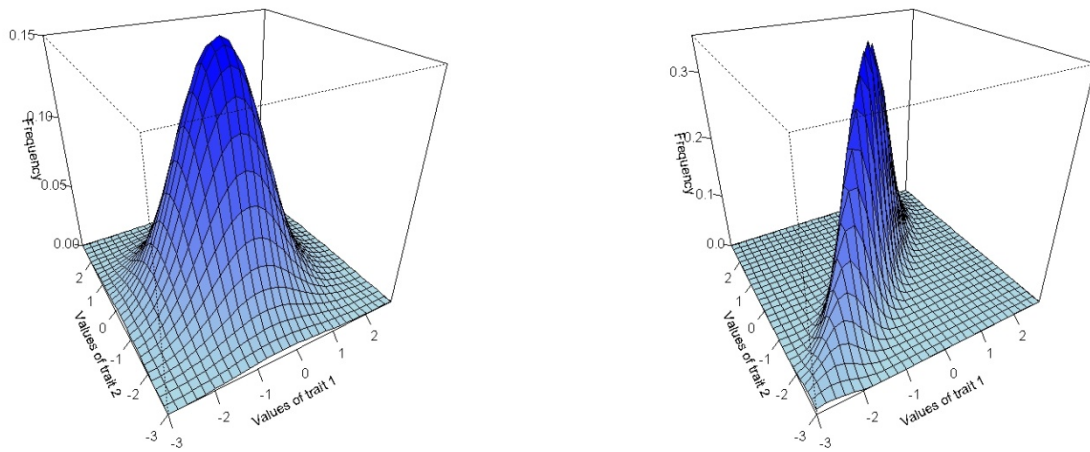


**Figure 2.3.** Large samples from two bivariate normal distributions of two traits, one with no trait correlation and the other with a strong positive correlation. (a) A bivariate scatter plot of the individuals sampled from a distribution with no correlation ( $\bar{z}_1 = 0.0$ ,  $\bar{z}_2 = 0.0$ ,  $P_{11} = 1.0$ ,  $P_{22} = 1.0$ ,  $P_{12} = 0.0$ ,  $r=0.0$ ). (b) A bivariate scatter plot of the individuals sampled from a distribution with a strong positive correlation ( $\bar{z}_1 = 0.0$ ,  $\bar{z}_2 = 0.0$ ,  $P_{11} = 1.0$ ,  $P_{22} = 1.0$ ,  $P_{12} = 0.9$ ,  $r=0.9$ ) (c) A 3-dimensional view of the probability distribution with no

correlation . (d) A 3-dimensional view of the probability distribution with a strong positive correlation

The points on the 3-dimensional surfaces shown in Fig. 2.3 are  $p(z)$ , the probabilities of observing a particular phenotypes as a function of particular traits values  $z_1$  and  $z_2$ . We now want to consider the formula for those probabilities for the case of a bivariate normal distribution. For convenience we can represent those two values as a column vector (Appendix 1 = basic conventions and rules of matrix algebra, see Arnold 1994), which we will call  $z$ . In the present case, the phenotype is represented by just two values, but in general it might be represented by  $n$  values, so that  $z$  might be a very tall vector. We can write an expression for a normal probability distribution in this general,  $n$ -trait case,

$$p(z) = \sqrt{(2\pi)^{-n} |P^{-1}|} \exp\left\{-\frac{1}{2}(z - \bar{z})^T P^{-1}(z - \bar{z})\right\}, \quad (2.0)$$

where  $P^{-1}$  is the inverse of the  $n \times n$  variance-covariance matrix  $P$ ,  $| \cdot |$  denotes determinate,  $\bar{z}$  is the column vector of means with  $n$  elements and  $T$  denotes transpose, the conversion of column vector into a row vector (Appendix 1). As in the univariate case (1.02), the square root term is a normalization factor that insures that the probabilities sum to one.

## 2.2 The directional selection differential, $s$ , a vector.

We need to consider the effects of selection on the multivariate distribution,  $p(z)$ . We recall from 1.1 that relative fitness is the variable that translated the distribution before selection,  $p(z)$ , into the distribution after selection,  $p(z)^*$ . In our multivariate world, absolute fitness,  $W(z)$ , and relative fitness,  $w(z)$ , are functions of a multi-trait phenotype,  $z$ . Indeed, we can substitute  $z$  for  $z$ , and a vector of trait means for  $\bar{z}$  in eq. (1.0-1.7) and those same expressions apply, without an assumptions about the multivariate distribution of  $z$ . We will pause to consider the selection differential, which is now an  $n$ -element column vector. In the 2-trait case it is

$$s = Cov(w, z) = \begin{bmatrix} Cov(w, z_1) \\ Cov(w, z_2) \end{bmatrix} = \bar{z} - \bar{z}^* = \begin{bmatrix} \bar{z}_1 - \bar{z}_1^* \\ \bar{z}_2 - \bar{z}_2^* \end{bmatrix} = \begin{bmatrix} s_1 \\ s_2 \end{bmatrix} \quad (2.01)$$

## 2.3 The directional selection gradient, $\beta$ , a vector.

We can now consider a new measure of selection, one that will account for correlations among the traits. That new measure is the *directional selection gradient*, an  $n$ -element column vector. In general and in the 2-trait case it is

$$\beta \equiv P^{-1}s = \begin{bmatrix} \beta_1 \\ \beta_2 \end{bmatrix}, \quad (2.02)$$

where  $\beta_1$  and  $\beta_2$  are the selection gradients for traits 1 and 2, respectively. We can rearrange this last expression in a way that disentangles the direct and indirect effects of directional selection,

$$s = P\beta = \begin{bmatrix} P_{11} & P_{12} \\ P_{12} & P_{22} \end{bmatrix} \begin{bmatrix} \beta_1 \\ \beta_2 \end{bmatrix} = \begin{bmatrix} P_{11}\beta_1 + P_{12}\beta_2 \\ P_{12}\beta_1 + P_{22}\beta_2 \end{bmatrix} = \begin{bmatrix} s_1 \\ s_2 \end{bmatrix}. \quad (2.03)$$

This portrayal of  $s$  tells us that the selection differential for a trait is composed of one term that represents the direct effect of selection on that trait on its mean, e.g.,  $P_{11}\beta_1$ , and another term that represents the indirect effect of selection on another trait, acting through the covariance between the two traits, e.g.,  $P_{12}\beta_2$  (Fig 2.z = path diagram). Of course, in the general case, with  $n$  traits, the indirect effects can be very numerous; the selection differential for trait 1 is

$$s_1 = P_{11}\beta_1 + P_{12}\beta_2 + P_{13}\beta_3 + \dots + P_{1n}\beta_n = P_{11}\beta_1 + \sum_{i=2}^n P_{1i}\beta_i. \quad (2.04)$$

Indeed, we see that it would be possible for the sum of indirect terms in (2.04) to overwhelm the direct effect, so that the selection differential,  $s_1$ , could have opposite sign to the selection gradient,  $\beta_1$ ! In other words, when we consider the actual value for a particular selection differential, e.g.,  $s_1$ , that value may reflect selection on other traits rather than selection on the trait in question.

## 2.4 The nonlinear selection differential, $C$ , a matrix.

In general, selection can change the variances and covariances of the traits, as well as shift their means (Fig. 2.ww = series of panels showing changes in 95% confidence ellipses of various bivariate Gaussian distributions; this same set of panels could correspond, in a coming chapter, to a set of panels showing the corresponding ISS and AL surfaces!). Change in second moments (variance and covariance) is considerably more complicated than in the univariate case, so we will need to consider it in detail. Focusing on the 2-trait case for concreteness, the phenotypic variance-covariance matrix before selection is

$$P = \int p(z)(z - \bar{z})^T(z - \bar{z})dz = \begin{bmatrix} P_{11} & P_{12} \\ P_{12} & P_{22} \end{bmatrix}, \quad (2.05)$$

where  $P_{11}$  and  $P_{22}$  are the variances of  $z_1$  and  $z_2$ , and  $P_{12}$  is their covariance before selection. Selection may change any or all of the elements in  $P$ , so that after selection the matrix becomes

$$P^* = \int p(z)^*(z - \bar{z})^T(z - \bar{z})dz = \begin{bmatrix} P_{11}^* & P_{12}^* \\ P_{12}^* & P_{22}^* \end{bmatrix}. \quad (2.06)$$

Following the argument in 1.4, we will want to employ a correction factor for effects of directional selection on variances and covariances. Here and hence forth we assume multivariate normality of the trait distribution before selection. In the 2-trait case, that correction factor is

$$ss^T = \begin{bmatrix} s_1^2 & s_1 s_2 \\ s_1 s_2 & s_2^2 \end{bmatrix}, \quad (2.07)$$

where the diagonal terms are effects on the trait variance (which will always be positive) and the off-diagonal term is the effect on the trait covariance (which may be positive or negative). In other words, we want to correct for the fact that directional selection on trait  $i$  will reduce its variance by an amount  $s_i^2$ , regardless of the sign of  $s_i$ , while directional selection on traits  $i$  and  $j$  will change their covariance by an amount  $s_i s_j$ . In the 2-trait case, the stabilizing selection differential is

$$C = P^* - P + ss^T = \begin{bmatrix} P_{11}^* - P_{11} + s_1^2 & P_{12}^* - P_{12} + s_1 s_2 \\ P_{12}^* - P_{12} + s_1 s_2 & P_{22}^* - P_{22} + s_2^2 \end{bmatrix} = \begin{bmatrix} Cov(w, \tilde{z}_1^2) & Cov(w, \tilde{z}_1 \tilde{z}_2) \\ Cov(w, \tilde{z}_1 \tilde{z}_2) & Cov(w, \tilde{z}_2^2) \end{bmatrix}. \quad (2.08)$$

Directional selection shifts the expected value of  $z$ , the mean (1.7); nonlinear selection shifts the expected values of the quadratic variables  $\tilde{z}_1^2$ ,  $\tilde{z}_2^2$ , and  $\tilde{z}_1 \tilde{z}_2$ . Notice that by the nature of  $ss^T$  (2.07), the nonlinear selection differential for a particular trait will be  $C_{ii} = P_{ii}^* - P_{ii} + s_i^2$ , regardless of how many traits are under selection. In other words, the diagonal elements in  $C$  correct for the effects of directional selection on the trait in question and not for effects exerted through correlations with other traits.

## 2.5 The nonlinear selection gradient, $\gamma$ , a matrix.

Just as we can solve for a vector,  $\beta$ , that corrects for trait correlations in measuring directional selection, we can by similar operations obtain a set of selection coefficients that correct for trait correlations in measuring nonlinear selection. Those coefficients constitute the *nonlinear selection gradient*, an  $n \times n$  symmetric matrix, defined here in the general case and illustrated in the 2-trait case,

$$\gamma \equiv P^{-1}CP^{-1} = \begin{bmatrix} \gamma_{11} & \gamma_{12} \\ \gamma_{12} & \gamma_{22} \end{bmatrix}, \quad (2.09)$$

where  $\gamma_{11}$  and  $\gamma_{22}$  represent, respectively, the direct effects of stabilizing/disruptive selection on the variances of traits 1 and 2, and  $\gamma_{12}$  represents the direct effect of correlational selection on the covariance of traits 1 and 2, i.e.,  $P_{12}$ . To see what constitutes direct and indirect effects, we can rearrange the  $2 \times 2$  version of (2.09) to obtain

$$C = P\gamma P = \begin{bmatrix} P_{11} & P_{12} \\ P_{12} & P_{22} \end{bmatrix} \begin{bmatrix} \gamma_{11} & \gamma_{12} \\ \gamma_{12} & \gamma_{22} \end{bmatrix} \begin{bmatrix} P_{11} & P_{12} \\ P_{12} & P_{22} \end{bmatrix} = \begin{bmatrix} P_{11}^2\gamma_{11} + 2P_{11}P_{12}\gamma_{12} + P_{12}^2\gamma_{22} & P_{11}P_{12}\gamma_{11} + P_{12}^2\gamma_{12} + P_{11}P_{12}\gamma_{12} + P_{12}P_{22}\gamma_{22} \\ P_{11}P_{12}\gamma_{11} + P_{12}^2\gamma_{12} + P_{11}P_{12}\gamma_{12} + P_{12}P_{22}\gamma_{22} & P_{12}^2\gamma_{11} + 2P_{12}P_{22}\gamma_{12} + P_{22}^2\gamma_{22} \end{bmatrix} = \begin{bmatrix} C_{11} & C_{12} \\ C_{12} & C_{22} \end{bmatrix}. \quad (2.10)$$

The  $P_{11}^2\gamma_{11}$ ,  $P_{22}^2\gamma_{22}$ , and  $P_{12}^2\gamma_{12}$  terms represent, respectively, direct effects on  $\tilde{z}_1^2$ ,  $\tilde{z}_2^2$ , and  $\tilde{z}_1\tilde{z}_2$ . All of the other terms represent indirect effects mediated through covariances between the quadratic variables  $\tilde{z}_1^2$ ,  $\tilde{z}_2^2$ , and  $\tilde{z}_1\tilde{z}_2$ .

## 2.55 The canonical form of the gamma-matrix

The picture of multivariate nonlinear selection presented by  $\gamma$  may be easier to visualize if we use a different coordinate system. A natural alternative to the original trait axes is one in which the  $\gamma$ -matrix takes a diagonal form in which all the off-diagonal terms, which describe correlational selection, are zero. This diagonal form of the  $\gamma$ -matrix is known as its canonical form (Phillips & Arnold 1989)

$$\Lambda = \mathbf{M}^T \gamma \mathbf{M}, \quad (2.11)$$

where  $\Lambda$  is matrix with the eigenvalues of  $\gamma$ ,  $\lambda_i$ , on its diagonal and zeros as its off-diagonal elements, and  $\mathbf{M}$  is a matrix whose columns are the eigenvectors of  $\gamma$  (normalized to unit length). The new axes, the eigenvectors, are a rotation of the original axes, and like those axes, they are orthogonal to one another.

## 2.6 Estimates of multivariate selection gradients

Selection on beak dimensions (mm) in a Galapagos finch, illustrates a surprising case in which a selection gradient is strikingly different from the corresponding selection gradient.

Table 2.2 Directional selection on body size and beak dimension in a Galapagos finch (*Geospiza fortis*) arising from drought conditions on Daphne Major (Price et al. 1984). The sample size before selection is 640; after selection the sample is 96. An asterisk indicates significance at the 0.05 level. The test statistic for the selection differential is a T-test comparing the means of samples before and after selection.

trait	Selection differential, $s$	Selection gradient, $\beta \pm \text{s.e.}$
Weight (g)	0.62*	0.51±0.14*
Beak length	0.49*	0.17±0.18
Beak depth	0.60*	0.79±0.23*
Beak width	0.49*	-0.47±0.21*

The focus is on directional selection associated with a change in environmental conditions and, indeed, this form of selection is dramatically stronger than in the preceding example. For example, selection associated with drought conditions shifted average body weight by 62% of the standard deviation in this trait before selection. Although this and the other selection differentials suggest that heavier birds with larger beak dimensions were favored by selection, the directional selection gradients tell a different story. They suggest that while selection favored heavier birds, it also favored birds with deep, narrow beaks. The picture of selection revealed by the selection gradients is consistent with ecological observations during the drought. Hard seeds became disproportionately common during the drought, and only large birds could crack these seeds. Birds with narrow beaks are apparently favored by selection because birds with this morphology could twist and open the woody seed pods of *Tribulus cistoides* (Price et al. 1984). But how can the selection gradient for beak width have a different sign than its selection differential? We see from expression 2.04 that a shift in the mean,  $s_i$ , is composed of contributions from correlated traits. If those contributions ( $\beta_j P_{ij}$ ) have positive signs, they can overwhelm the direct effect of selection on beak width ( $\beta_i P_{ii}$ ), which has a negative sign. Calculating  $\beta$  can help untangle the direct and indirect effects and reveal the actual targets of selection. Finally, this example illustrates the value of standardized selection coefficients. In the case of weight,  $\beta=0.51$  means that if direct selection increased body weight by a before-selection standard deviation, relative fitness would be increased by 51%. Decreasing beak width by a standard deviation would increase relative fitness by 47%.

## 2.7 Functional complexes

Correlation among traits is a fact of life that motivates the calculation of the selection gradients that we introduced in the preceding sections. Those calculations enable us to account for trait correlations in assessing the effects of selection. But, trait correlations also have a deeper meaning. We can view trait correlations as the product of selection that occurs when traits work together to perform a common function (Olson & Miller 1958). Functional interactions of this kind can help to build trait correlations (covariances) (cite Lande, Cheverud, Wagner). Consequently, it follows that we can detect functional interactions by assessing the effects of selection on trait covariances. The tools for that assessment are the off-diagonal elements of the C-matrix and especially of the  $\gamma$ -matrix. But, before turning to the assessment value of those two matrices, let's focus on the biology of functional interaction and the grouping of traits into functional complexes. As we shall see in the chapters ahead, these functional interactions have diverse and important effects on evolutionary processes and patterns.

Functional interaction between characters is a ubiquitous feature of life, especially in metazoans. The organization of interacting characters into functional complexes is particularly obvious if we focus on complexes that are dedicated to well-defined ecological or social functions. Spider web ... venom delivery in *Conus* snails ...

pheromone delivery in

plethodontid salamanders ...

pollinator attraction and

attachment of pollinia in orchids

... In all of these instances a

particular measure of whole

organism performance

summarizes the interactions of

characters in the complex ... prey

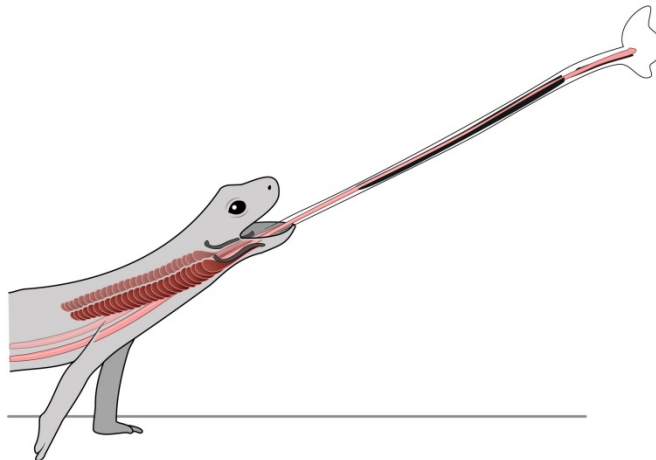
capture in spiders and *Conus* ...

tongue projection in chameleons

and bolitoglossine salamanders

... mating success in male

salamanders ... pollen export in orchids ...



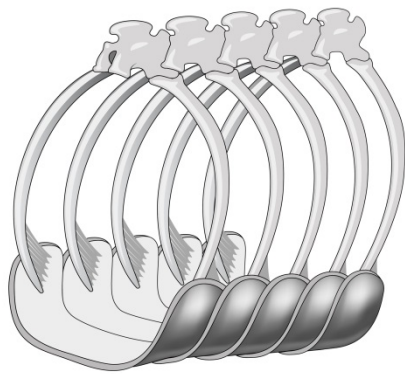
{In the next few paragraphs, portray traits showcased in multiple chapters as parts of functional complexes: snake vertebrae in locomotion ...}

**Fig x.yy** The tongue projection mechanism of a plethodontid salamander. The tongue skeleton (black) is normally folded inside the body cavity but is projected forward during prey capture by contracted protractor muscles (dark red). Retractor muscles (light red), attached to the tongue skeleton, run the full length of the body and attach to the pelvis. The contraction of these muscles pulls the tongue and attached prey back into the body (after Deban et al. 1997)

Functional complexes are equally recognizable when sets of characters participate in well understood physiological functions ... in vertebrates for example ... cardio-vascular system ... heart, vessels, lungs ... delivery of oxygen to peripheral tissues

during exercise ... water transport system in plants ... phloem, xylem, root system ... water delivery to

**Figure 4.qq.** A five-vertebrae segment of the vertebral column of a natricine snake (*Natrix natrix*), showing functional connection between three elements. Ribs articulate with the vertebral column, but muscles also connect the tips of the ribs of the ventral scales on the snake's ventral surface. Furthermore, a complicated system of muscles (not shown) connects between the ribs. (after a 19<sup>th</sup> century instructional poster).



peripheral tissues ... {one or two additional examples} ... As in the case of functional complexes directed at mates and prey, the performance of physiological character complexes can often be summarized by one or a few metrics that capture the salient features of operation in the entire complex.

The unifying feature in all of these examples is interaction and coordination between the elements in the complex that can be summarized and expressed in measures of performance. The ease with which such functional complexes can be listed suggests that trait organization of this kind is so common as to be virtually ubiquitous. In any case, the ease of inventory suggests that functional complexes are extremely common, so that they subsume many if not all traits in organisms. The significance of this ubiquity is that the mode of selection required to account for functional complexes is likewise ubiquitous and important. In the chapters that follow we will identify multivariate stabilizing selection, and especially correlational selection, as the mode of selection chiefly responsible for the assembly and maintenance of functional complexes. To see this connection more clearly we must first tackle the problem of how the performance of functional complexes is related to lifetime fitness.

## 2.8 Morphology, performance, and fitness

\*Introduce performance here, at the start of this paragraph\* Important measures of performance have been called ‘surrogates for fitness’. This characterization is unfortunate because it suggests that we are pretending that performance is fitness. Instead of that pretense, we wish to understand how performance is related to fitness, for with that understanding we will also be able characterize selection on functional complexes.

The solution to our problem lies in recognizing that selection on a trait in a functional complex can be subdivided into two parts: the relationship between the trait and performance, and the relationship between performance and fitness. Consider the example of the traits that come into play when a snake swallows a large prey item. Snakes ingest their prey whole

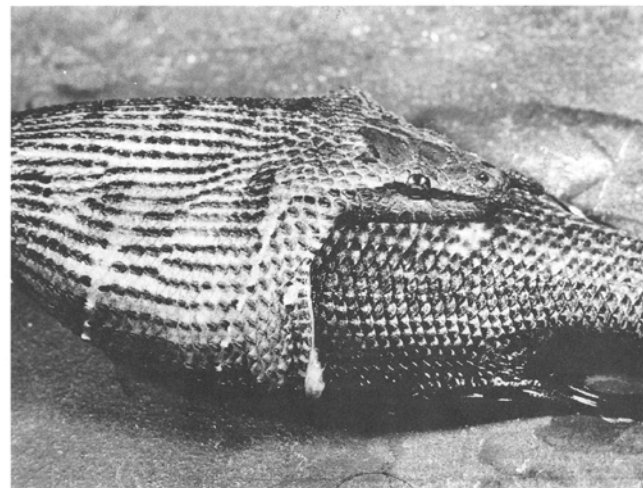


**Figure 4.xx** A tentacled snake (*Erpeton tentaculum*) in the process of swallowing a large fish (from Arnold 1983)

(Fig. 4.xx) and consequently the maximum size that can be ingested is a function of the sizes of a series of five structural elements (Fig. 4.xy). In an experimental study of swallowing performance our model of performance,  $f$ , might be

$$f = \beta_{fz1}z_1 + 2\beta_{fz2}z_2 + 2\beta_{fz3}z_3 + 2\beta_{fz4}z_4 + \beta_{fz5}z_5 + \varepsilon_f, \quad (zz)$$

where the subscripted  $\beta$ s represent directional coefficients describing the effect of each of the 5 traits on performance, and the factors of 2 account for traits that participate twice in effects on performance. These  $\beta$  coefficients are not directional selection gradients, which would represent effects of traits on fitness, so we will call them *directional performance gradients*.

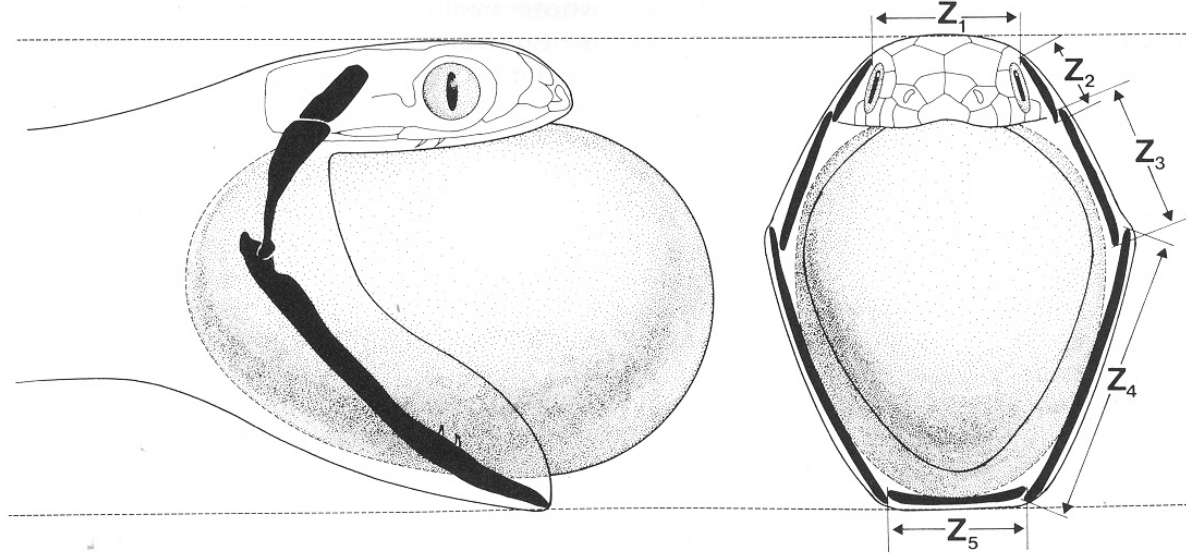


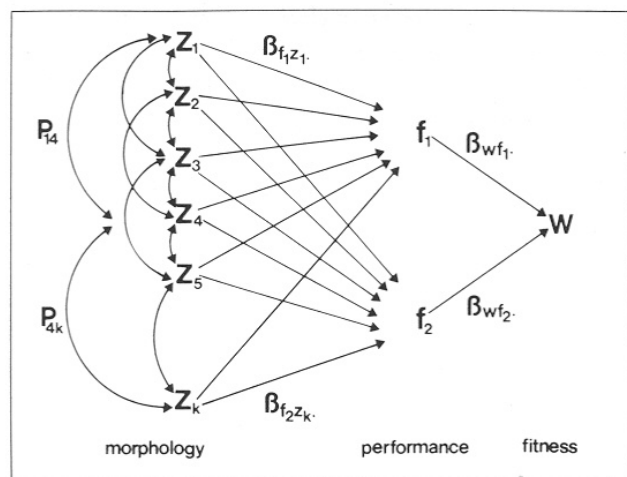
**Figure 4.xy** An African egg-eating snake (*Dasypeltis* sp.) in the process of swallowing its prey. The lengths of 5 structural elements determine the maximal cross-sectional area of prey than can be ingested: width of the brain case ( $z_1$ ), and the lengths of the supratemporal ( $z_2$ ), quadrate ( $z_3$ ), mandible ( $z_4$ ), and mandibular symphysis ( $z_5$ ) (from Arnold 1983).

The relationship between a performance gradient and an ordinary selection gradient becomes clear if we construct a path diagram. In Fig. 4.yy, we have made our example slightly more general by including two performance measure,  $f_1$  and  $f_2$ , and by increasing the number of traits from 5 to  $k$ . Figure 4.yy is a diagram that portrays a nested regression model. We have taken our regular expression for multivariate directional selection,

$$w = \beta_1 z_1 + \beta_2 z_2 + \dots + \beta_k z_k + \varepsilon_w$$

and converted it into a model in which all of the  $k$  traits exert their effects on  $w$  via two performance measures. In other words,

$$w = \beta_{wf_1} f_1 + \beta_{wf_2} f_2 + \varepsilon_w,$$



where the two subscripted  $\beta$ s represent directional effects of performance on fitness, which we shall call *fitness gradients*. By substituting two expressions like (zz) into this last expression, we see that each directional selection gradient is the product of a performance gradient and a fitness gradient (Fig. 4.yz).

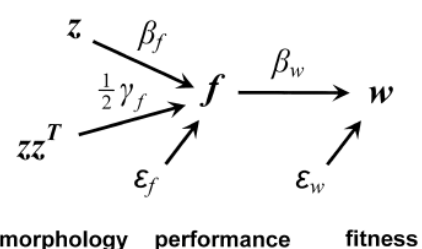
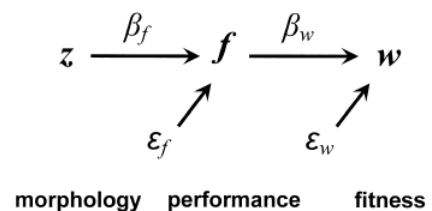
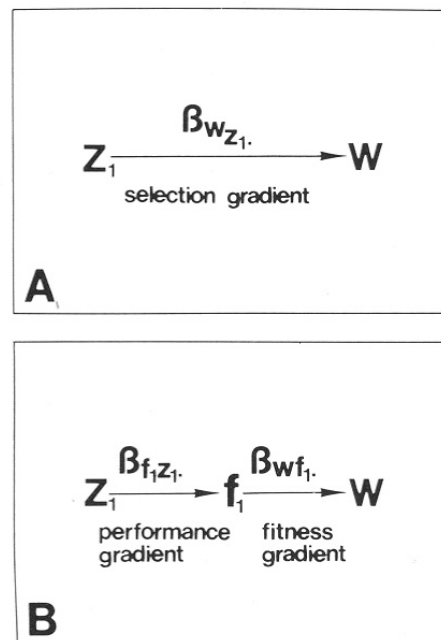
**Figure 4.yy.** Path diagram showing causal relationships (paths with single arrowhead) between  $k$  morphological traits ( $z_1, z_2, \dots, z_k$ ), two measures of performance ( $f_1$  and  $f_2$ ), and relative fitness ( $w$ ). Double-headed arrows represent phenotypic covariances between traits, before selection. Two of these covariances are labeled,  $P_{14}$  and  $P_{4k}$ . (from Arnold 1983)

**Figure 4.yz.** Total directional selection gradient on a trait (A) can sometimes be partitioned into two parts (B): a performance gradient and a fitness gradient.

The significance of this product rule (Fig. yz) is that even when it is not feasible to estimate selection gradients or fitness gradients, it may often be possible to estimate performance gradients. Performance gradients are more routinely tractable because they can be estimated in the laboratory via performance testing, whereas the other two kinds of gradients require assessment of fitness or its components under field conditions. Under ideal circumstances, all three kinds of gradients can be estimated in a combined laboratory and field study (e.g., Tsuji et al's *Sceloporus* study).

Clearly morphological and other kinds of traits can have curvilinear as well as directional effects on performance, so we need to consider a more general model that includes those effects.

The algebra of such a model is detailed by Arnold (2003). Without recounting those details here, we can note that in general the linear model that we have just considered can be represented by a multivariate path diagram in which all of the elements, except fitness, are vectors (Fig. 4.wz). If we add curvilinear



effects of traits on performance, that extended model can be represented by the path diagram shown in Fig. 4.wz. Although this model is tractable and estimable, it is obviously a considerable simplification. We have assumed that fitness is a planar rather than a curvilinear function of performance. Although that assumption is justified and appropriate if our goal is to estimate directional fitness gradients, we need empirical inquiries to establish whether the surface relating performance to fitness can indeed be approximated by a plane.

**Figure 4.wz.** A path diagram showing multivariate directional performance and fitness gradients in which all of the elements, except fitness, are vectors. (from Arnold 2003).

**Figure 4.zw.** A path diagram showing multivariate directional ( $\beta_f$ , a vector) and curvilinear ( $\gamma_f$ , a matrix) performance gradients. Other conventions as in Fig. 4.wz. (from Arnold 2003)

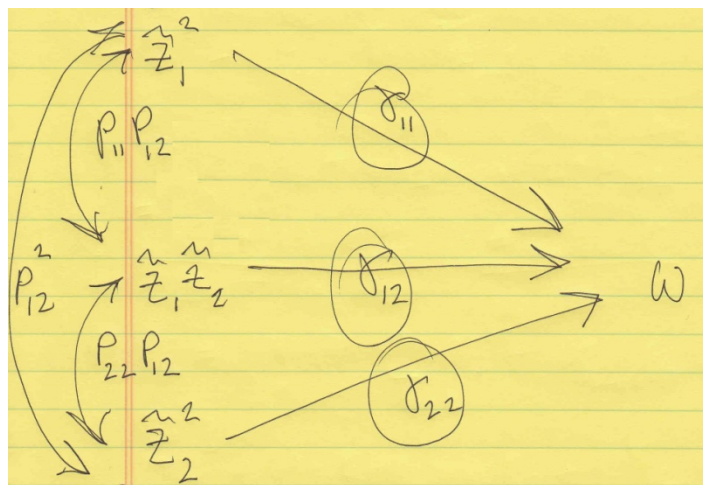


**Figure 4.zz** Path diagram view of (2.10) showing the effects of the quadratic variables  $\tilde{z}_1^2$ ,  $\tilde{z}_2^2$ , and  $\tilde{z}_1\tilde{z}_2$  on relative fitness,  $w$ . Coefficients are shown on each path. Double-headed arrows denote covariances between quadratic variables **##Include something like this figure? At a minimum it needs some work, e.g. coefficients of 1/2 on gamma11 and 22##**

{need a concluding paragraph here for this section, relating the above results to the issue of the mode of selection acting on functional complexes}

## 2.9 Morphology and performance in garter snakes

Returning to the example of crawling speed in newborn garter snakes introduced in Chapter 1, we now consider how accounting for trait covariance affects our concept of selection. This example is also an exercise in identifying the most important trait dimension for functional integration. In the first place, we have a new nonlinear selection differential to consider,  $C_{12}$ , which describes the total effect of nonlinear selection on the trait covariance,  $P_{12}$ . In the sample after selection, trait covariance has increased by 19.2%. Bootstrapping reveals that in only 1 boot sample out of 1000 did  $C_{12}$  take a value less than zero, so the change in covariance is highly significant ( $P=0.001$ ). Virtually all of the 19.2% expansion is due to nonlinear selection; directional selection contributes only a 0.8% decrease in covariance. The selection gradients, which account for trait covariance, give much the same picture of selection as the selection differentials. Although most gradients are nonsignificant, the nonlinear selection gradient describing the effect of the trait product,  $z_1z_2$ , on crawling speed is positive and

highly significant ( $P < 0.001$ ). The positive value for this coefficient,  $\gamma_{12}$ , indicates that selection directly increases trait covariance. In other words, comparing samples before and after selection we see a change in trait covariance (from 0.073 to 0.265), but that change largely reflects direct effects on covariance rather than indirect effect via trait means or variances. The direct effect of selection is to increase the integration of the two traits.

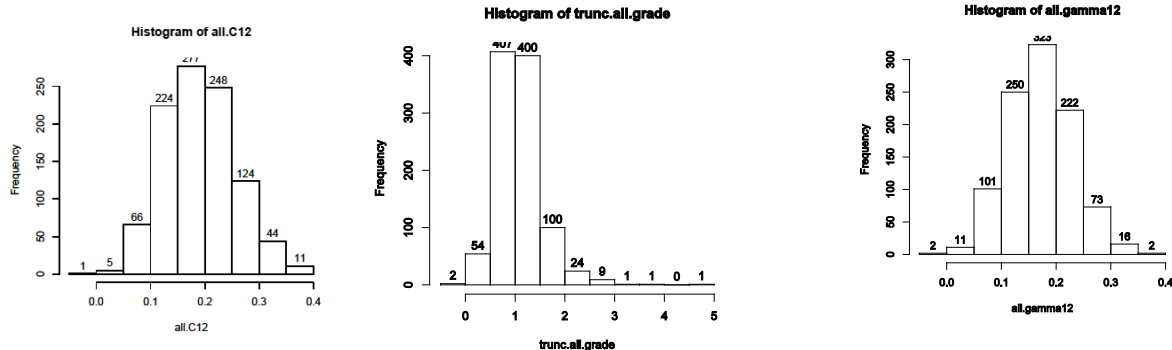
A useful way to visualize the picture presented by the  $\gamma$ -matrix is to rotate trait axes so that  $\gamma$  takes a so-called canonical form (Phillips & Arnold 1989). In this canonical form, the off-diagonal elements are zero, so no direct effects act on trait covariance. The  $\gamma$  coefficients (eigenvalues) corresponding to the new major and minor axes are, respectively 0.253 (0.95 CI = 0.136, 0.489) and -0.617 (0.95 CI = -0.221, 0.088). In other words, selection on the major axis is disruptive and highly significant, while selection on the minor axis might be either stabilizing (as it is in the point estimate) or disruptive, but non-significant. The major axis (leading eigenvector) is inclined at about a 45 degree angle in trait space with a slope of 1.055 (0.95 CI = 0.380, 2.156); the minor axis is perpendicular to the major axis. The leading eigenvector of  $\gamma$  is important to us because we have shown that it is the trait dimension of greatest functional integration (see next section), i.e., the trait direction in which trait covariance is most affected by selection exerted through crawling speed. We will return to the issue of visualization in Chapter 4 when we consider the topic of multivariate selection surfaces.

Using this example to illustrate (2.11), taking the values for  $M$  and  $\gamma$  from Table 2.1, we find that the canonical form of the the  $\gamma$ -matrix is

$$\Lambda = M^T \gamma M = \begin{bmatrix} 0.688 & -0.726 \\ 0.726 & 0.688 \end{bmatrix}^T \begin{bmatrix} 0.097 & 0.176 \\ 0.176 & 0.116 \end{bmatrix} \begin{bmatrix} 0.688 & -0.726 \\ 0.726 & 0.688 \end{bmatrix} = \begin{bmatrix} 0.282 & 0 \\ 0 & -0.069 \end{bmatrix}.$$

Table 2.1 Selection differentials and gradients describing effects of numbers of body and tail vertebrae on crawling speed in newborn garter snakes (*Thamnophis radix*) (n=143). Selection gradients were estimated using expressions 2.02 and 2.09. The standard errors of  $\beta$  and  $\gamma$  were estimated from the standard deviations of corresponding bootstrap distributions (n=1000 samples with replacement). Bootstrap estimates of 95% confidence limits are shown in parentheses. Significance levels: \*, P<0.05; \*\*, P<0.01; \*\*\*, P≤0.001. Eigenvalues of the  $\gamma$ -matrix corresponding to the leading and minor eigenvector are denoted  $\lambda_1$  and  $\lambda_2$ , respectively. 'Eigenvector' is the slope of the leading eigenvector.

	Body vertebrae		Tail vertebrae			
	mean	variance	mean	variance	covariance	correlation
Before selection	153.414	11.437	74.257	9.094	0.743	0.073
Before selection'	0.000	1.000	0.000	1.000	0.073	0.073
After selection'	0.031	1.122	0.004	1.142	0.265	0.234**
	s <sub>1</sub>	C <sub>11</sub>	s <sub>2</sub>	C <sub>22</sub>	C <sub>12</sub>	
selection differential	0.031 (-0.032, 0.096)	0.123 (-0.062, 0.348)	0.004 (-0.058, 0.063)	0.142 (-0.015, 0.327)	0.192*** (0.074, 0.328)	
correction term, $ss^T$		0.077		0.001	0.008	
	$\beta_1$	$\gamma_{11}$	$\beta_2$	$\gamma_{22}$	$\gamma_{12}$	eigenvector
selection gradient+	0.031 (-0.033, 0.095)	0.097 (-0.087, 0.301)	0.002 (-0.065, 0.059)	0.116 (-0.028, 0.292)	0.176** (0.066, 0.288)	1.055** (0.380, 2.156)
standard error++	0.033	0.098	0.031	0.082	0.059	$\lambda_1=0.282$ (0.136, 0.489) $\lambda_2=-0.069$ (0.136, 0.489)



\*Use these histograms; probably not\*\*

## 2.10 Technical issues in estimating and interpreting selection gradients

Several cautions, common to all multivariate statistical analyses, should be kept in mind in estimating  $\beta$  and  $\gamma$  and interpreting those estimates. As we will see in Chapter 4, the key formulas for  $\beta$  and  $\gamma$  (2.2 and 2.9) are equivalent to formulas for sets of multiple regression coefficients. Consequently, the issues we need to consider are usually discussed in the context of estimation by multiple regression (Lande & Arnold 1983, Mitchell-Olds & Shaw 1987); we will view them in that light in Chapter 4.

Not including correlated traits in the study can lead to biased estimates of  $\beta$  and  $\gamma$ . In particular, we need to consider the possibility that traits under directional and/or stabilizing selection are correlated with the measured traits but are not included in the study. This circumstance can cause us to over- or under-estimate our selection gradients, depending on the sign and magnitude of selection on the unmeasured trait and the pattern of correlation with the measured traits. In other words, what we interpret as direct effects of selection on our traits can be affected by traits that are excluded from the analysis for one reason or another. In practice, most investigators live with this limitation on interpretation because traits are included in the analysis precisely because they are likely to be under selection. In other words, prior information is brought to bear in choosing traits that partially mitigate the problem of influence from unmeasured traits. Nevertheless, the possibility of this kind of complication can never be completely eliminated and should be borne in mind in interpreting results.

Unmeasured environmental variables can produce an illusion of selection. This problem is related to the one just discussed, but here we are concerned with environmental effects that produce correlations between fitness and traits. Mitchell-Olds & Shaw (1987) discuss and tell a hypothetical example in which growing

conditions vary spatially and cause some plants to be both large and fecund and others to be small and barren. If we fail to include growing conditions in our analysis (e.g., as covariates), we might erroneously conclude that plant size is under strong selection. As in the case of correlated, unmeasured traits, biased estimates have lead us to a false conclusion. One antidote is the realization that correlational studies may not reveal causal relationships. In multivariate statistical analysis, we attempt to correct for correlations, but we may not succeed. For this reason, it is always wise to do a companion experimental study that manipulates traits of interest and gets us closer to an inference of causality.

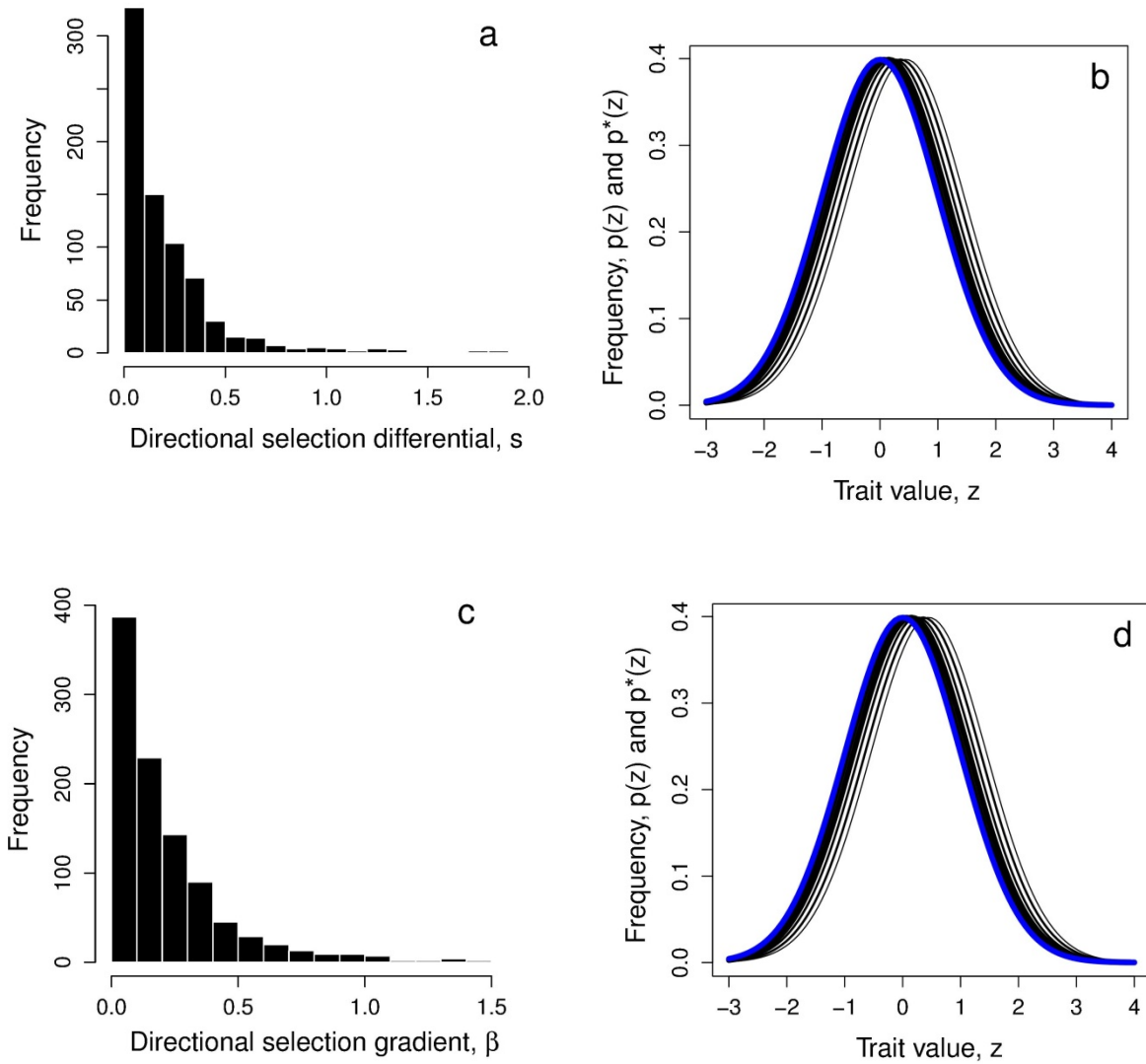
It is possible to make a strong inference of causality within the framework of correlational study. The argument is vividly portrayed in court cases that challenged the claim of tobacco companies that the link between smoking and lung cancer was not causal. Attorneys for cancer victims argued that three conditions help make a strong case for causality: plausibility, strength of correlation, and prevalence of correlation across replicate studies. All of these conditions can be considered in deciding whether a particular selection gradient represents a causal effect of phenotype on fitness.

The expressions presented in this chapter for estimating  $\beta$  and  $\gamma$  are useful when a population is sampled before and after selection (i.e., for the case of cross-sectional data). Those estimations require making assumptions about the two samples since they may no individual in common (Lande & Arnold 1983). A key assumption then is that the sample before selection closely resembles the actual set of individuals after selection before those individuals were exposed to selection. Alternatively, individuals may be followed through time so that their individual fitness values are assessed, bypassing these assumptions. In the case of such longitudinal data, a multiple regression approach can be used to estimate selection coefficients. That regression approach is described in Chapter 4. The notorious factor of 1/2 problem surrounding the estimates of  $\gamma$  in the literature before 2009 will also be discussed in Chapter 4 (Stinchcombe et al. 2009).

## 2.9 Surveys of selection gradients

The point of the surveys in this section is that the  $\beta$  and  $\gamma$  estimates correct for the effects of selection on multiple traits, unlike the surveys in Chapter 1 which showed shifts in mean and variance that reflect both direct and indirect effects. The advantage is that comparisons between  $s$  and *beta* and between  $C$  and *gamma* allow us to see how much the aggregated indirect effects contribute to the overall distribution of selection coefficients.

The surveys summarized here were compiled by Hoekstra et al. (2001), Kingsolver et al. (2001), and Stinchcombe (2009). Kingsolver et al. (2001) and Hoekstra et al. (2001) updated Endler's (1986) survey, using similar criteria and obtaining a sample about an order of magnitude larger. This more recent survey of 62 studies (63 species) focused on selection acting on natural populations in natural circumstances. Like Endler's sample, the survey included a wide range of organisms (plants, invertebrates, vertebrates) and an even wider range of traits (most were morphological measurements and counts, but some behavior and life history traits were included). The sample consists of studies published between 1984 and 1997 and so slightly overlaps with Endler's sample. Stinchcombe (2008) uncovered errors in the estimation of  $\gamma$  that



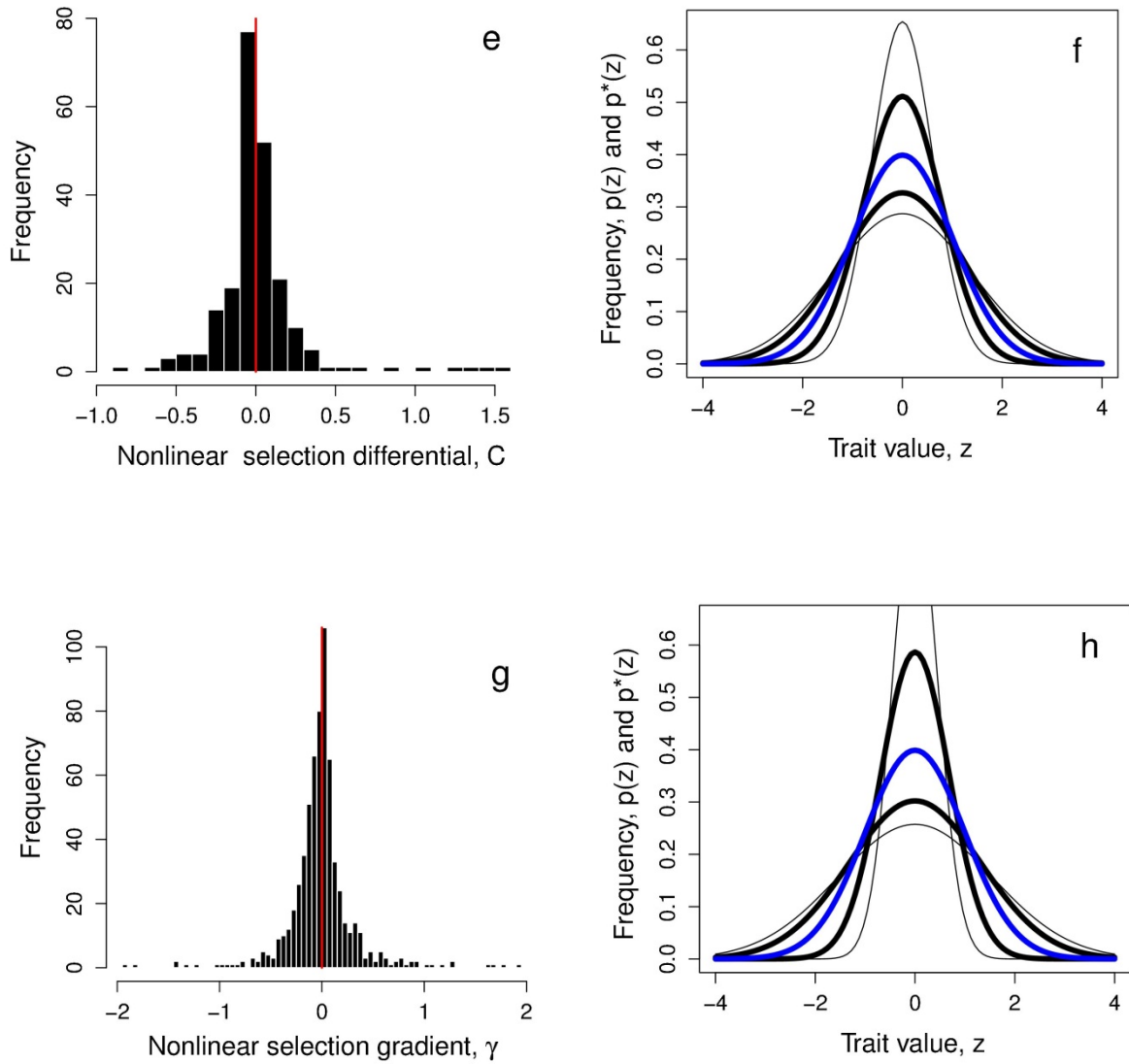


Figure 2.5 Histograms of selection gradients and differentials paired with frequency distributions that portray the magnitude of effects on means and variances. (a) Histogram of the absolute values of directional selection differential estimates,  $s$ ; 746 values from Kingsolver et al 2001 database. Three values greater than  $\text{abs}(2.0)$  are not

included. (b) Shifts in mean corresponding to the directional selection differentials in Fig. 2.5a. Shifts corresponding to the five bins on the right-most side of the distribution (0.05-0.45) are shown in black and account for 92% of the observations. (c) Histogram of the absolute values of directional selection gradient estimates,  $\beta$ ; 992 values from Kingsolver et al 2001. Three values for  $s$  greater than  $\text{abs}(2.0)$  were not included. (d) Shifts in mean corresponding to the directional selection gradients in Fig. 2.5c. Shifts corresponding to the five bins on the right-most side of the distribution (0.05-0.45) are shown in black and account for 90% of the observations. (e) Histogram of nonlinear selection differential estimates,  $C = (P^*-P+s^2)/P$ ; 220 values from Kingsolver et al 2001 database. Five values greater than  $\text{abs}(2.0)$  are not included. The vertical red line separates the distribution into negative and positive estimates. (f) Shifts in variance corresponding to the nonlinear selection differentials shown in Fig. 2.5e. Shifts corresponding to the four most populated bins in the center the distribution (-0.15 to 0.15) are shown in black and account for 78% of the observations. (g) Histogram of nonlinear selection gradient estimates,  $\gamma$ ; 653 values from the Stinchcombe et al 2008 database, after deleting 7 values of  $\gamma > 2$  and 4 values  $< -2$ . (h) Shifts in variance corresponding to the nonlinear selection gradients shown in Fig. 2.5g. Shifts corresponding to the 16 most populated bins in the center the  $\gamma$  distribution (-0.4 to 0.4) are shown in black and account for 86% of the observations.

permeate the literature prior to 2008. They resampled the studies compiled by Kingsolver et al (2001) and corrected those errors in  $\gamma$  and added many additional studies. That new database was used to make the histogram shown in Fig. 2.5g.

From a statistical point of view, distributions of selection differentials and gradients are extremely similar. We get the same overall picture of directional selection, for example, whether we look at the differential,  $s$ , or the gradient,  $\beta$ . In both cases we see a distribution that is negative exponential in appearance with a modal value close to zero and with the vast majority of estimates in the range 0 to 0.5 (Fig. 2.5 a, Fig. 2.5c). In qualitative terms, directional selection tends to be weak, rarely shifting mean by more than half a within-population phenotypic standard deviation. The similarity between the distributions of  $s$  and  $\beta$  suggest that the indirect effects of selection, arising from phenotypic correlations between traits, make at most a minor contribution to the overall picture.

Turning to the distributions of nonlinear selection differentials and gradients, we again see much the same distributional picture. Both selection coefficients show leptotic (peaked) distributions that are almost symmetrically centered about zero (Fig 2.5e, Fig 2.5g). The selection differential  $C$  is slightly biased towards negative values (stabilizing selection), while the gradient  $\gamma$  has a slight bias in the other direction, towards

disruptive selection. The overall effect of indirect effects appears to inflate the absolute values of  $C$ , so that its distribution is less leptotic than that of  $\gamma$ . Judging from the distribution of  $\gamma$ , it is unusual for direct nonlinear selection to increase or decrease trait variance by more than 40%. A comparison of the distribution of  $\gamma$  compiled by Kingsolver et al. (2001) with the one compiled by Stinchcombe (2008) yields a surprising result. The two distributions are virtually identical! Although individual estimates of  $\gamma$  may be inaccurate by a considerable amount prior to 2008, in the aggregate the errors appear to cancel out.

## Chapter 3: The Selection Surface and Adaptive Landscape for a Single Trait

© Stevan J. Arnold 2016

**Overview.-** Selection on a single trait can be visualized as a curve that relates trait values to fitness, the ISS. The fundamental properties of this curve (slope and curvature) are intimately related to the changes in trait mean and variance that are induced by selection within a generation. For example, a steep selection curve dramatically shifts the mean. A  $\cap$ -shaped curve reduces trait variance within a generation. Although we generally will not know the shape of the ISS, we can deduce its properties and approximate its shape with various functions. To make predictions about how the trait will change from one generation to the next, we need a related curve, one that is averaged over the trait distribution. This curve is called the adaptive landscape (AL).

### 3.1 The individual selection surface, ISS.

The idea that selection is some kind function is implicit in the names used to describe selection; e.g., directional, stabilizing, truncation, etc. In this chapter we will make this idea explicit in a way that helps us visualize selection in its many guises. Imagine selection described by some continuous function. In particular, imagine relative fitness of individuals of phenotype  $z$  as a function of trait values,  $z$ . An overall positive slope implies directional selection favoring higher values (Fig. 3.0a), while an overall negative slope implies directional selection for smaller values. Downward curvature that straddles the phenotypic mean implies stabilizing selection in the sense that selection encourages the mean to reside in a specified range (Fig. 3.0b, c). Upward curvature has the opposite effect, the sign of disruptive selection

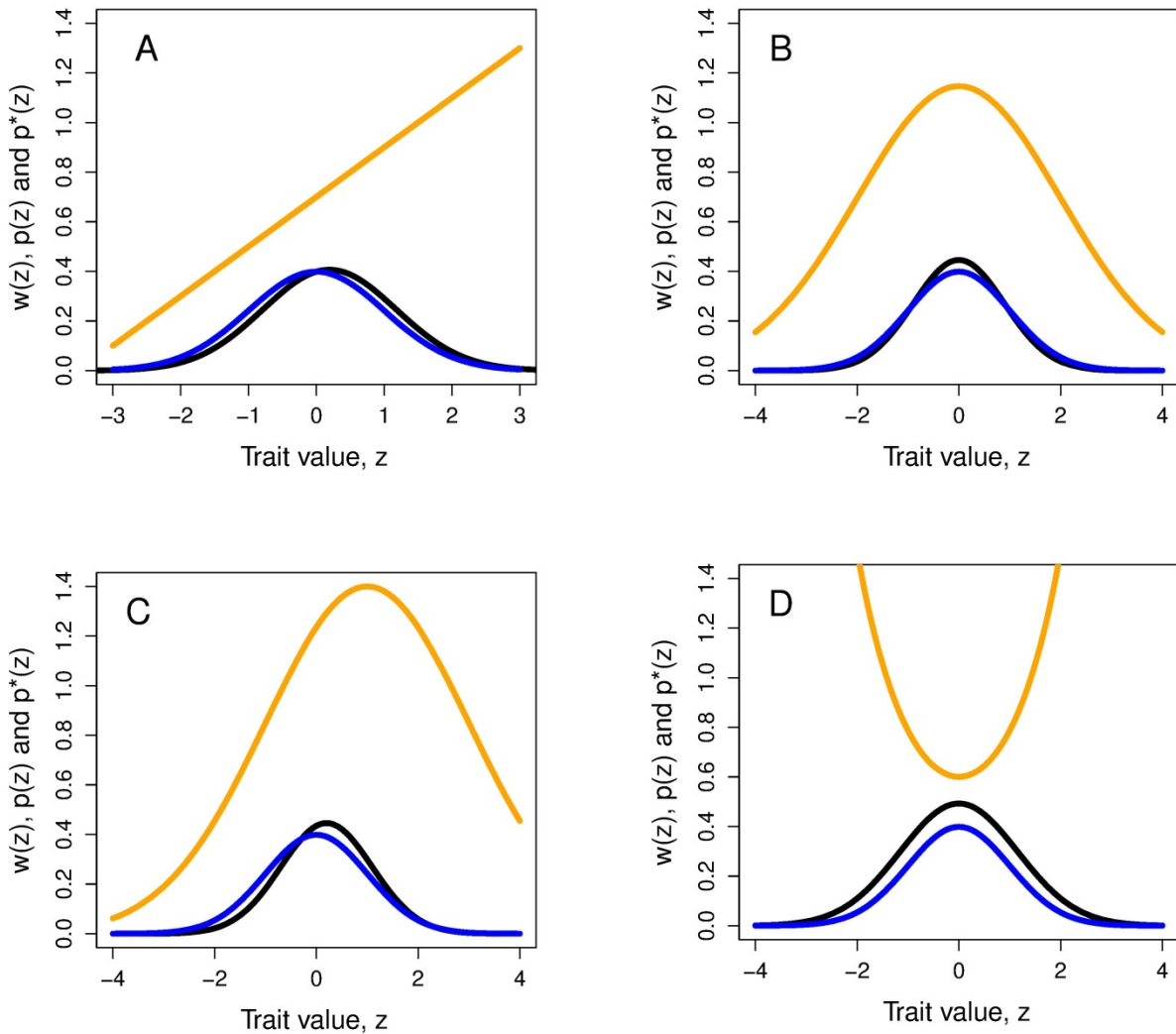
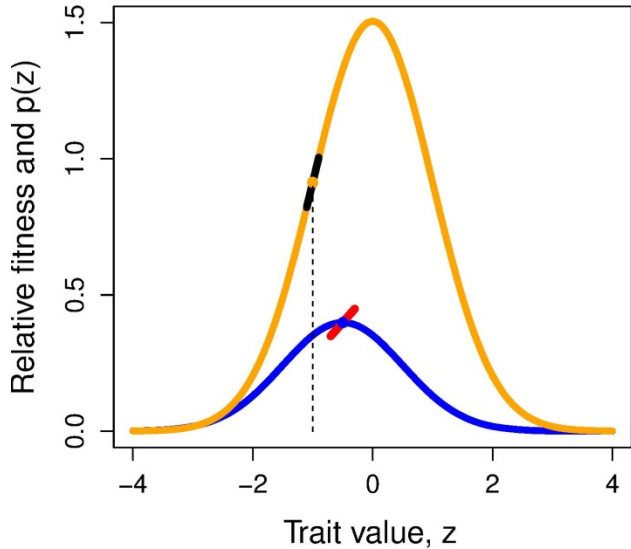


(Fig. 3.0d) . We will refer to the function in question as  $w(z)$  and call it the *individual selection surface*, the ISS.

**Figure 3.0** Examples of individual selection surfaces, ISSs, showing their effects on trait distributions. The statistics of the trait distributions before selection (blue),  $p(z)$ , and after (black) selection,  $p(z)^*$ , are given in Fig. 1.1. The ISS,  $w(z)$ , is shown as an orange curve. (a) Directional selection. The ISS is a linear function,  $w(z) = \alpha + \beta z$ ,  $\alpha = 1$ ,  $\beta = 0.2$ . The orange line has been shifted down 0.3 units for graphic effect. (b) Stabilizing selection. The ISS is a Gaussian function with  $\theta = 0$ ,  $\omega = 4$ . (c) Directional and stabilizing selection. The ISS is a Gaussian function with  $\theta = 1$ ,  $\omega = 4$ . (d) Disruptive selection. The ISS is a Gaussian function with  $\theta = 0$ ,  $\omega = -4$ . The orange curve has been shifted down 0.8 units for graphic effect.

Our concern with the ISS is local in the sense that we will focus on its shape in the region of trait values in which individuals are likely to be observed within our focal population. For example, consider the issue of the average slope of the ISS. To calculate that average slope, we would need to take the slope or first derivative of the function at a particular value of  $z$ ,  $\partial w(z)/\partial z$  (Fig. 3.1), weight that slope by

**Figure 3.1.** The directional selection gradient,  $\beta$ , as the weighted average of first derivatives of the ISS. The ISS is the orange curve; the trait distribution before selection,  $p(z)$ , is shown in blue. The first derivatives of the ISS for  $z=-1$  is shown as the slope of the black, straight line segment superimposed on the ISS. The average of all such slopes, weighted by  $p(z)$ , is the directional selection gradient,  $\beta$ , shown as the slope of the red line segment. In this illustration, the ISS is a Gaussian function ( $\theta = 0$ ,  $\omega = 1$ ) and  $p(z)$  is a normal distribution ( $\bar{z} = -0.5$ ,  $P = 1$ ).



the frequency of individuals at that point,  $p(z)$ , repeat these operations over the entire range of occupied values of  $z$ , and then add up all those weighted slopes,  $p(z)\partial w(z)/\partial z$ . This average slope turns out to be a familiar commodity, the directional selection gradient,

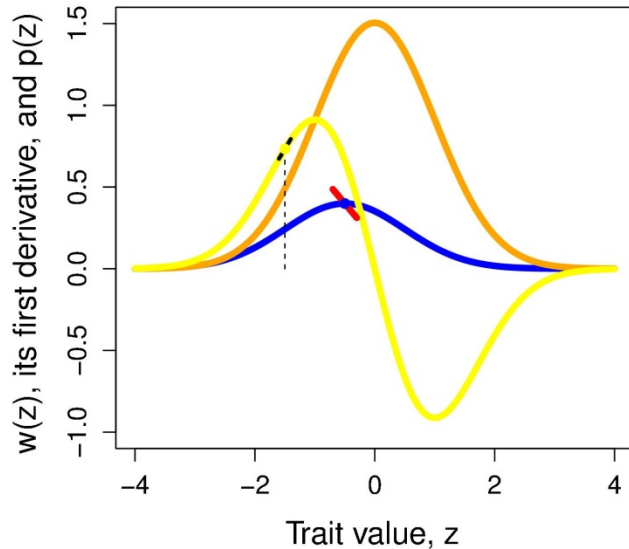
$$\beta = \int p(z) \frac{\partial w(z)}{\partial z} dz \quad (3.00)$$

(Lande & Arnold 1983). By a similar set of operations, we can evaluate the average curvature of the ISS,  $\partial^2 w(z) / \partial z^2$  at each point, and calculate the average of those curvatures (Fig. 3.2). This average is equivalent to the nonlinear selection gradient,

$$\gamma = \int p(z) \frac{\partial^2 w(z)}{\partial z^2} dz \quad (3.01)$$

Surprisingly, these equivalencies hold whatever the form of the ISS so long as it is continuous and differentiable, and the trait is normally distributed before selection (Lande & Arnold 1983).

**Figure 3.2.** The nonlinear selection gradient,  $\gamma$ , as the weighted average of second derivatives of the ISS. The ISS is the orange curve,  $w(z)$ ; the trait distribution before selection,  $p(z)$ , is shown in blue. The first derivative of the ISS is the yellow curve. A first derivative of this yellow curve (which is the second derivative of the ISS) at  $z=-1.5$  is shown as a black line segment superimposed on the yellow curve. The average of all such slopes, weighted by the trait distribution, is the nonlinear selection gradient,  $\gamma = -0.4375$ , shown as the slope of the red line segment. In this illustration, the ISS is a Gaussian function ( $\theta = 0, \omega = 1$ ) and  $p(z)$  is a normal distribution ( $\bar{z} = -0.5, P = 1$ ).



### 3.2 Linear and quadratic approximations to the ISS.

Unless we are prophets, as we pretended to be in Figd. 3.1 and 3.2, the ISS is not revealed to us directly, so we must deduce the properties of the ISS from data on relative fitness,  $w(z)$ , as a function of trait values,  $z$ . Suppose, for example, instead of an ISS revelation, we have instead the data plot shown in Fig. 3.3. We can bypass the problem of the actual shape of the ISS and try to estimate the selection gradients,  $\beta$  and  $\gamma$ . It turns out that these gradients can be estimated by the familiar statistical procedures of linear and quadratic regression (Lande & Arnold 1983). Before fitting the regressions, it is useful to standardize the trait before selection so that it has a zero mean and a standard deviation of one. Fitness should be standardized in a different way so that it has a mean of one. These standardizations yield selection gradients in readily interpretable units. Having accomplished these standardizations , we first estimate  $\beta$  by fitting a linear approximation to the ISS,

$$w(z) = \alpha + \beta z + \varepsilon, \quad (3.02)$$

$\varepsilon$  is the deviation of a particular observation from the regression line (Fig. 3.3a). The usual assumption in statistical inference is that  $\varepsilon$  is normally distributed with a mean of 0. To estimate  $\gamma$  , we need to use a second-order polynomial function, a quadratic function, to approximate the ISS,

$$w(z) = \alpha + \beta z + \frac{1}{2} \gamma z^2 + \varepsilon \quad (3.03)$$

(Fig. 3.3b). The factor of  $\frac{1}{2}$  is included so that  $\gamma$  will be the second derivative of the function, a measure of curvature.

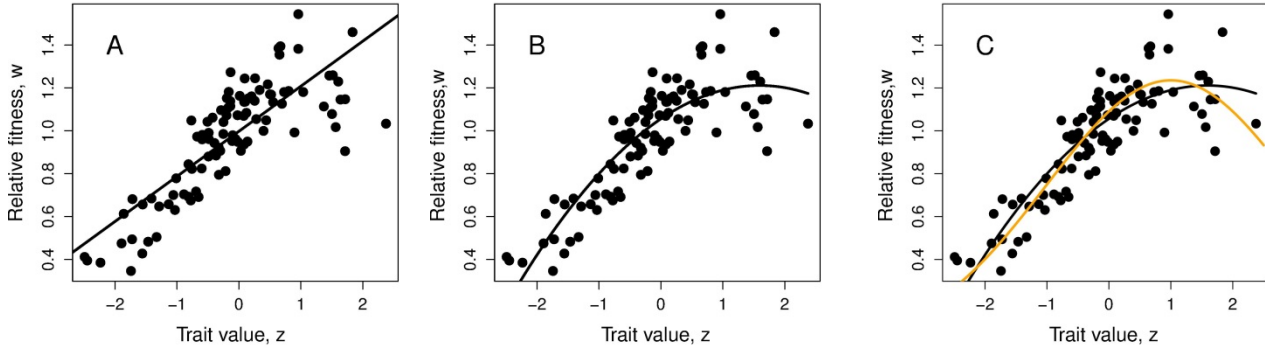


**Figure 3.3.** Linear and quadratic approximations to the ISS in a hypothetical example. (a) A linear fit to the data (Fig. 1.x) using (3.02),  $\alpha = 1$ ,  $\beta = 0.21 \pm 0.02$  s.e. (b) A quadratic fit using (3.03),  $\alpha = 1$ ,  $\beta = 0.20 \pm 0.01$  s.e.,  $\gamma = -0.12 \pm 0.02$  s.e. (c) The actual ISS is a Gaussian function (3.07), shown in orange,  $\theta = 1$ ,  $\omega = 4$ . The data points were generated by taking a random sample of trait values,  $z$ , from a normal distribution ( $\bar{z} = 0$ ,  $P=1$ ). Those trait values were used in conjunction with the specified Gaussian function to produce corresponding, expected values of  $w$ . Values of  $\varepsilon$  were drawn from a normal distribution (mean = 0, variance = 0.01) and added to expected value of  $w$  to produce the points in the figure ( $n=100$ ).

A few words about the actual steps in performing these two regressions may be useful. For the standardization of trait values before selection, one simply subtracts the raw trait mean from each value and divides each of those new values by the raw trait standard deviation, producing a desired new trait with zero mean and standard deviation of one. The raw values of fitness are divided by the raw fitness mean to produce a new fitness variable (relative fitness) with a mean of one. If one wished to draw or express the two regressions, (3.02) or (3.03), one ignores the estimated value of  $\alpha$  and sets its value to one. Why is this? The value of  $\varepsilon$  on the regression curve is zero, so it is dropped from the equation. Finally, to draw or express (3.03), one takes the value of  $\beta$  estimated from (3.02) and the value of  $\gamma$  estimated from (3.03). This last point may seem mysterious, but it is a practical solution to a bias problem. In general, if the trait distribution is not perfectly normal before selection, the standardized trait values,  $z$ , will be correlated with their squared values,  $z^2$ . This correlation will bias the estimate of  $\beta$  obtained from (3.03). A simple solution to this problem is to use the value of  $\beta$  estimated from the linear regression (3.02), which will produce an unbiased estimate (Lande & Arnold 1983).

Neither of these approximations, (3.02) and (3.03), is meant to actually imitate asymmetry or the bumps and grinds that might be present in the ISS. Linear and quadratic functions are used because they enable us to estimate parameters of selection. For example, in the hypothetical example shown in Fig. 3.1, the ISS was actually a Gaussian function (Fig. 3.3c), which is only roughly approximated by a quadratic function. Despite the relatively poor fits of the linear and quadratic functions to this ISS, those fits do provide correct estimates of  $\beta$  and  $\gamma$ . Nevertheless, the actual shape of the ISS is also of interest. A variety of procedures and functions might be used to more accurately describe the shape of the ISS. We will consider one of these in the next section.

In passing, we note that in the univariate case, selection gradients and selection differentials are equivalent when fitness and trait values are standardized. Under that standardization scheme, relative fitness has a mean of one, and the trait values have a mean of one, with  $P=1$  (section 1.4). With this standardization, we see from (2.2 and 2.9) that  $\beta=s$  and  $\gamma=C$ , but these relationships will not hold in the multivariate case.

### 3.3 Cubic spline approximation to the ISS.

The power of the quadratic approximations just described is that we can use them to estimate the selection coefficients  $\beta$  and  $\gamma$ . It is a remarkable fact that this estimation is legitimate and accurate even if the ISS is not quadratic. In some situations, however, quadratic approximation may lead us astray even though it does its job of estimating  $\beta$  and  $\gamma$ . One such case is shown in Fig. 3.4. In this hypothetical example, truncation selection acts on the population. The actual shape of the ISS is step function with a step at a phenotypic value of +1. Quadratic regression will do a poor job of approximating the ISS for it will yield a disruptive curve with an inflection point near -1. In general, when the shape of the ISS is of interest, regression techniques more sophisticated than quadratic regression can be used to approximate its shape. Schlüter (1988) introduced the use of regression with cubic splines to describe fitness functions, and many subsequent studies have successfully used this approach to approximate the ISS.

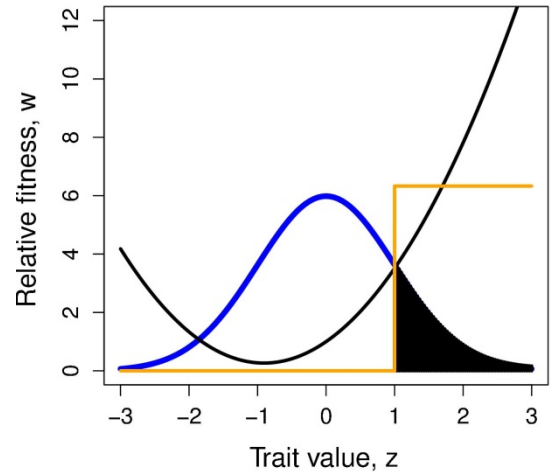
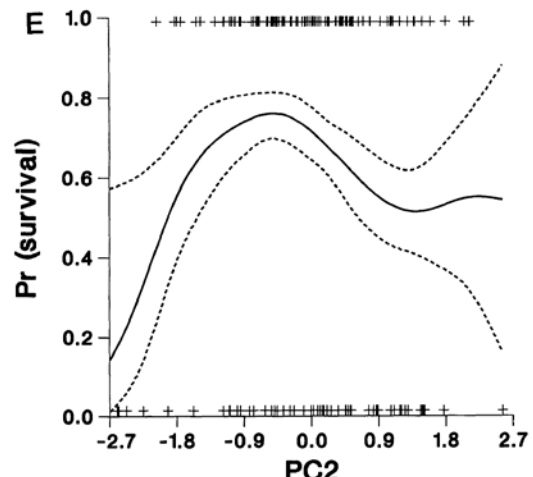


**Figure 3.4.** A hypothetical example in which a quadratic approximation to the ISS is misleading in shape. The sample before selection is shown as a blue curve, a normal distribution with a mean of zero and a standard deviation of 1. The actual ISS, which exerts truncation selection, is shown in orange (estimated using 3.03). The sample after selection is shown in black. The quadratic approximation to the ISS is shown as a black curve. This curve was estimated by fitting a quadratic regression to a sample of 1000 individuals drawn from the normal distribution before selection and assigned relative fitnesses according to the truncation-function ISS. Although the black curve gives a poor idea of the ISS, it does give a good estimate of the selection gradients ( $\beta = 1.62 \pm 0.04$  s.e.,  $\gamma = 1.79 \pm 0.07$  s.e.) (after Schlüter 1988).

An example of a cubic spline approximation to an unknown ISS is shown in Figure 3.5. Here survivorship of song sparrows (*Melospiza melodia*) is shown as a function of a linear combination of morphological measurements (PC2). As in the preceding example, fitness is binary. Measurements in the sample after selection are clustered near the middle of the range in trait values. The cubic spline approximation appropriately shows a convex function with an inflection near the trait mean (stabilizing selection). The minor curves in the fitted function were not anticipated by the authors and are probably of no interest to readers. In this sense, a simple quadratic approximation, which would be a smooth convex function, would do just as well, while estimating  $\beta$  and  $\gamma$ . In some situations, however, minor curves or non-quadratic shapes will have biological significance.

**Figure 3.5.** An example of a cubic spline approximation to an unknown ISS. The solid black curve is a cubic spline of overwinter survival of male song sparrows ( $n=152$ ) as a function of morphological measurements (PC2). The dashed curves show  $\pm 1$  standard error of the



function, estimated by bootstrapping. The crosses at the top and bottom show the absolute fitness and trait values of males that did and did not survive winters. From Schluter 1988.

### 3.3 The adaptive landscape, AL.

Another fitness function, distinct from the ISS, will be important to us. This important function is known as the *adaptive landscape*, the AL. In the AL, average fitness of the population,  $\bar{W}$ , is a function of its average trait value,  $\bar{z}$ . For our focal population, we can evaluate the AL at a single point, the trait mean,  $\bar{z}$ . That narrow perspective on the AL, however, is sufficient to tell us the slope and curvature of the AL at that point. In particular,

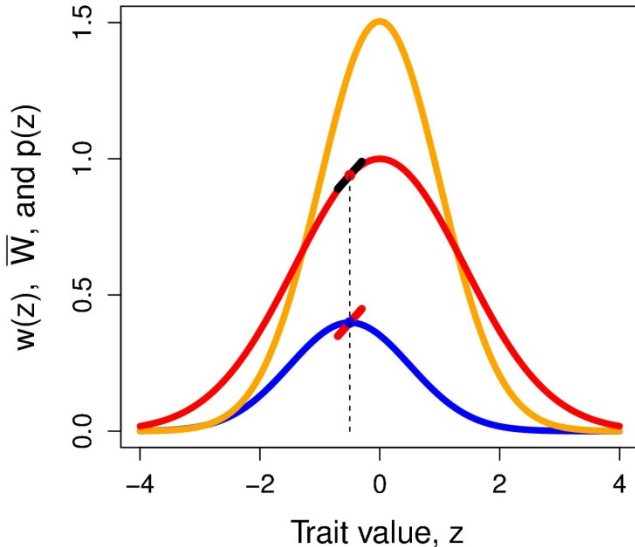
$$\beta = \frac{\partial \bar{W}}{\bar{W} \partial \bar{z}} = \frac{\partial \ln \bar{W}}{\partial \bar{z}} \quad (3.04)$$

and

$$\gamma - \beta^2 = \frac{\partial^2 \bar{W}}{\bar{W} \partial \bar{z}^2} = \frac{\partial^2 \ln \bar{W}}{\partial \bar{z}^2}, \quad (3.05)$$

where  $\ln \bar{W}$  means the natural logarithm of average absolute fitness in the population (Lande 1979, Arnold & Lande 1983). The directional selection gradient,  $\beta$ , as the slope of the AL evaluated at the trait mean is portrayed in Fig. 3.6.

**Figure 3.6.** The directional selection gradient,  $\beta$ , as the first derivative of the AL, evaluated at the trait mean before selection,  $\bar{z} = -0.5$ . The AL is shown as a red Gaussian curve with an optimum  $\theta = 0$  and width parameter  $(\omega + P) = 2$ . The directional selection gradient is shown at two sites connected by a dashed vertical line: at the mean of  $p(z)$ , where it is shown as a red line segment, and at the point of evaluation on the AL, where it is shown as a black line segment. Other conventions as in Fig. 3.1.



Just as we can imagine that the ISS is a function that extends beyond the occupied region of phenotypes for our population, the same might be so for the the AL. We also need to imagine that hypothetical probability distributions for  $z$ , so that we can average the ISS over those hypothetical distributions to visualize the correponding AL. An easy way to generate these hypothetical distributions of  $z$  is to keep the variance,  $P$ , constant and simply shift the mean before selection,  $\bar{z}$ . The extension is especially simple if we assume that  $p(z)$  is a normal distribution, and the ISS is a Gaussian function (Haldane 1954, Lande 1976) so that

$$p(z) = (\sqrt{2\pi P})^{-1} \exp\left\{-\frac{(z - \bar{z})^2}{2P}\right\} \quad (3.06)$$

and

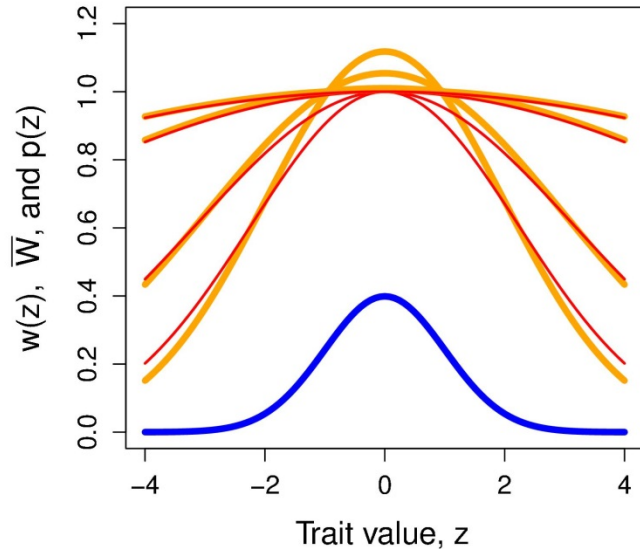
$$w(z) = \exp\left\{-\frac{(z-\theta)^2}{2\omega}\right\}, \quad (3.07)$$

where  $\theta$  is the optimum and  $\sqrt{\omega}$  is the width of the function, analogous to a standard deviation ( $\omega$  is analogous to a variance) (Fig. 3.0e). If  $p(z)$  keeps its shape (constant variance) while translating it mean, averaging the ISS over this translated function yields a Gaussian-shaped AL,

$$\bar{W} \propto \exp\left\{-\frac{(\bar{z}-\theta)^2}{2(\omega+P)}\right\}, \quad (3.08)$$

with the same optimum as the ISS,  $\theta$ , but a larger ‘variance’,  $\omega + P$  (Fig. 3.65). The first derivative or

**Figure 3.65** Gaussian ISSs and their corresponding Gaussian ALs for a range of values of  $\omega$ . The blue curve shows a normal trait distribution before selection,  $p(z)$ , with a mean of 0 and a variance,  $P=1$ . The wide orange curves show the individual selection surfaces for  $\omega = 99$  (at the top), 49, 9, and 4 (at the bottom). The narrow red curves show the corresponding adaptive landscapes with width parameters  $\omega+P = 100, 50, 10$ , and 5.



slope of the AL, evaluated at the population mean, is

$$\frac{\partial \ln \bar{W}}{\partial \bar{z}} = (\omega + P)^{-1}(\theta - \bar{z}) \quad (3.09a)$$

and its curvature is

$$\frac{\partial^2 \ln \bar{W}}{\partial \bar{z}^2} = -(\omega + P)^{-2} = \gamma - \beta^2 \quad (3.09b)$$

(Lande 1979, Phillips & Arnold 1989, Jones et al. 2004). When the trait mean is at the optimum and  $\omega \gg P$ ,

Lande (pers. comm.) showed that

$$\gamma = -\frac{1}{\omega} \left( \frac{\omega}{\omega + P} \right)^{\frac{3}{2}}.$$

A useful approximation for converting between  $\gamma$  and  $\omega$  under Gaussian assumptions is

$$\gamma \approx -\frac{1}{\omega}, \quad (3.10)$$

An expression that works best when  $\gamma$  is close to zero or with a trait value close to the optimum when  $\gamma > -1$  (Fig 3.7a).

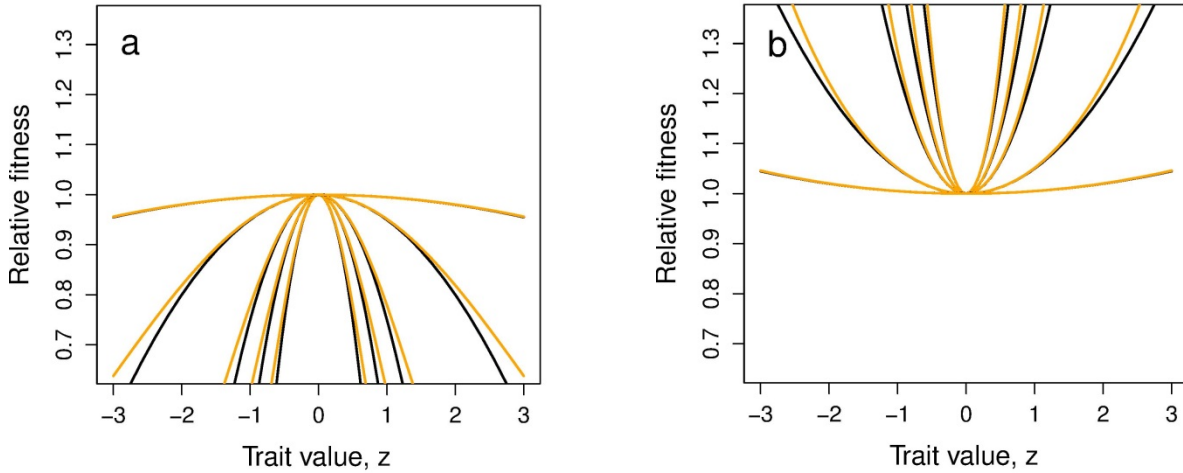


**Figure 3.7.** Gaussian approximations to quadratic individual selection surfaces (ISSs). Quadratic ISSs are shown as black curves and their Gaussian approximations are shown as orange curves. Expression 3.10 was used to approximate  $\omega$  from  $\gamma$ . Optimum or pessimum of quadratic surface set at zero. When  $\omega$  is 0.5 or -0.5 the approximation is so close that the quadratic curves are barely visible. (a) Gaussian approximations of stabilizing quadratic selection curves. From the top curve to the lowest,  $\gamma(\omega)$  values are -0.01(100), -0.1(10), -0.5(2), -1(1), and -2 (0.5). (b) Gaussian approximations of disruptive quadratic selection curves. From the lowest curve to top,  $\gamma(\omega)$  values are 0.01(-100), 0.1(-10), 0.5(-2), 1(-1), and 2 (-0.5).

In general, by taking the second derivative of (3.03) and setting it equal to zero, we find that the distance to the optimum (or pessimum) from the trait mean is

$$(\bar{z} - \theta) = \beta / -\gamma \quad (3.11)$$

(Mitchell-Olds & Shaw 1987, Phillips & Arnold 1989).

The Gaussian form of the ISS (3.07) is also useful in theoretical work because it allows us to immediately solve for the mean and variance after selection. If a trait is normally-distributed before

selection and subjected to Gaussian selection (3.07), it will be normally-distributed after selection with mean and variance,

$$\bar{z}^* = (\bar{z}\omega + \theta P) / (\omega + P) \quad (3.12a)$$

and

$$P^* = \omega P / (\omega + P) \quad (3.12b)$$

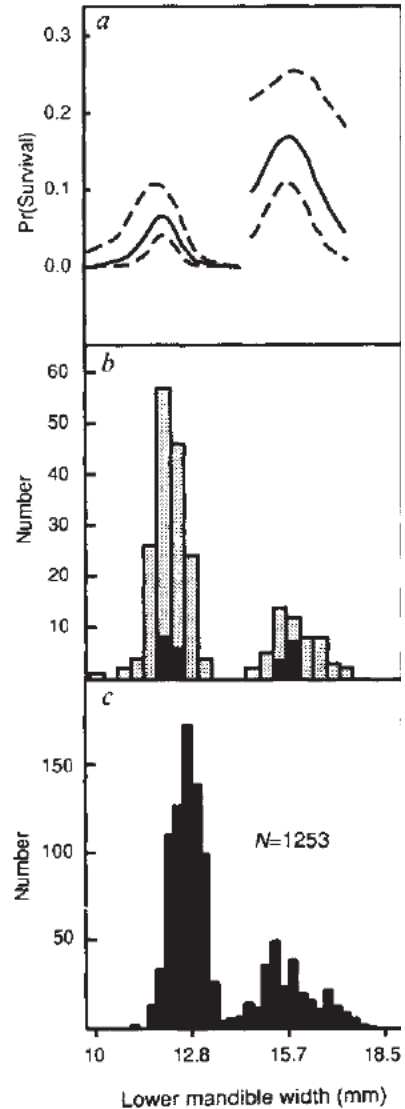
Lande (1981).

### 3.4 Empirical approximations to the ISS

Fig. 3.5 = Univariate examples of linear, quadratic and cubic spline approximations to ISS, do this with the Galapagos finch data?

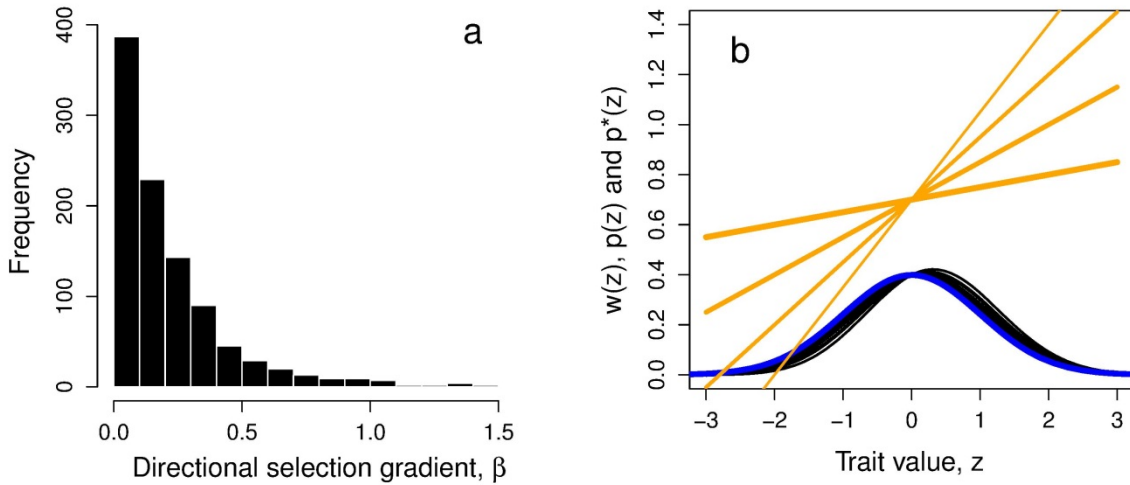
.... empirical focus on  $\beta$ , neglect of  $\gamma$  ... related to the sample size problem, exacerbated by including many traits ...

**Figure 3.75.** Disruptive selection on bill size in the African finch *Pyrenestes ostrinus*. (a) Cubic spline approximation to the ISS fitted separately for small and large billed morphs. Confidence limits (dashed lines) estimated by bootstrapping. (b) Trait distribution of juveniles that did not survive (shaded) and that did survive (black). (c) Trait distribution in adults. From Smith (1993).



### 3.5 Surveys of univariate selection surfaces and adaptive landscapes

Here we focus on the shapes of ISSs that emerge from the two surveys summarized in Chapter 2, Kingsolver et al. 2001 and Stinchcombe et al. 2008. The most basic result is that the most frequent result from empirical studies is an almost flat curve with almost no slope and no curvature. We reach this conclusion by noting that the most frequent estimate of  $\beta$  is very close to zero (Fig. 3.8a). This fact is poorly reflected in Fig 3.8b, in which the widest ISS is for a bin category centered at  $\beta=0.05$ . Also note that the histogram in Fig. 3.8a is for the absolute value of  $\beta$ . If we had plotted the estimated values, in which the signs are arbitrary functions of measurement scale, the plot would be approximately symmetrical about zero. Turning to  $\gamma$ , we see such an approximately symmetrical histogram in Figure 3.8c, which implies that the most frequent  $\gamma$  estimate is very close to zero, which implies a nearly flat curve that is bowed slightly upward or downward. Curves corresponding to four bin categories ( $\gamma = 0.3, 0.1, -0.1$ , and  $-0.3$ ) are shown in Fig. 3.8d. In other words, the most frequent result in empirical studies is to find that the individual selection surface is nearly flat. It is unusual to estimate a slope steeper than the thinnest orange line in Figure 3.8b or more curved than the thinnest curves in Figure 3.8d.



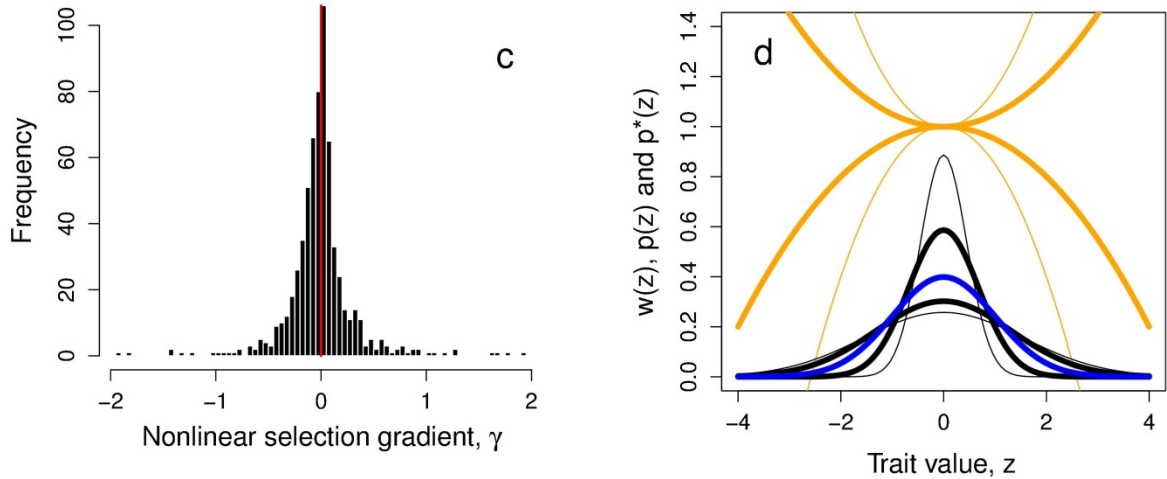


**Figure. 3.8** Histograms of selection gradients paired with frequency distributions that portray corresponding selection surfaces and the magnitude of effects on means and variances. Trait distributions before and after selection are shown in blue and black, respectively. (a) Histogram of the absolute values of directional selection gradient estimates,  $\beta$ ; 992 values from Kingsolver et al 2001. (b) Shifts in mean corresponding to the directional selection gradients in Fig. 3.8a. Shifts corresponding to the four bins on the right-most side of the distribution (0.05-0.45) are shown as black curves whose widths correspond to bin frequency. Orange curves show the fitness functions (ISSs) corresponding to those 4 bin categories, with widths corresponding to bin frequency. (c) Histogram of nonlinear selection gradient estimates,  $\gamma$ ; 653 values from the Stinchcombe et al 2008 database, after deleting 7 values of  $\gamma > 2$  and 4 values  $< -2$ . (d) Shifts in variance corresponding to the nonlinear selection gradients shown in Fig. 3.8c . Shifts corresponding to the 16 most populated bins in the center the  $\gamma$  distribution (-0.4 to 0.4) are shown as four black curves (accounting for 86% of the observations) with width representing four bin category frequency. Orange curves show the fitness functions (ISSs) corresponding to those 4 bin categories, with widths corresponding to bin category frequency.

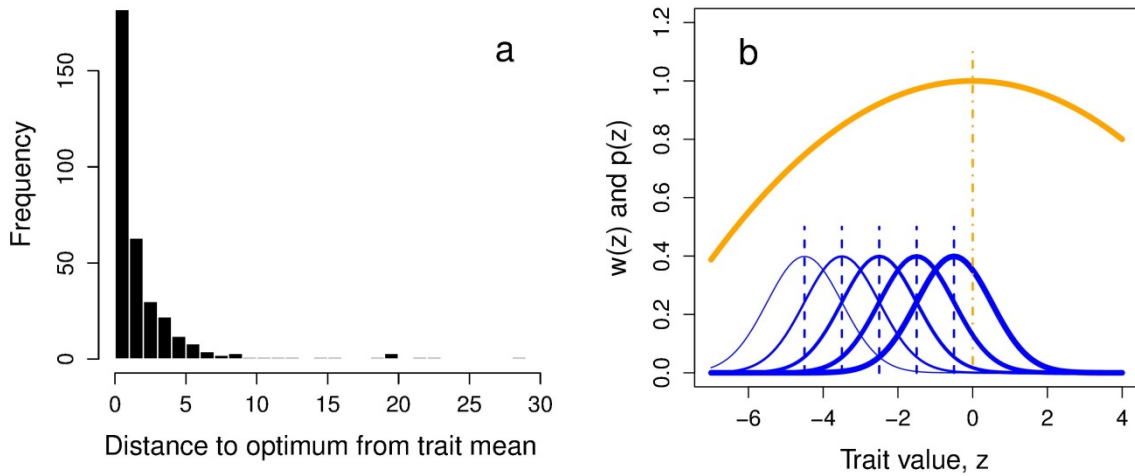


**Fig. 3.9** Histogram of distances of the phenotypic mean from the intermediate optimum,  $\theta$ , in natural populations, with blue curves portraying the most frequent values of those distances. (a) Values were calculated using (3.11) with paired values of negative  $\gamma$  and absolute values of  $\beta$  from the Stinchcombe et al. (2008) database ( $n = 339$ , dropping two values greater than 50). Distance to the optimum is measured in units of within-population phenotypic standard deviation before selection. The median value is 0.906. (b) The orange curve shows the most frequency value of  $\gamma$  with a negative value in the histogram shown in Fig. 3.8c (bin centered at  $\gamma = -0.025$  with a count of 80). The optimum,  $\theta$ , is shown with a vertical dash-dot line. The blue curves show means of  $p(z)$  at distances of  $-0.5, -1.5, -2.5, -3.5$  and  $-4.5$  from  $\theta$ , corresponding to the first 5 bins in the histogram with relative frequencies portrayed with line widths. The positions of trait means are shown with vertical dashed lines.

We can also calculate the distances to the optimum of the ISS (which are equivalent to distances from the optimum of the AL), assuming a convex ISS, using (3.11). Taking the median values of those distances, we find that most trait means are within one trait phenotypic standard deviation of the optimum and that it is unusual for the trait mean to be more than 5 standard deviations from the optimum (Fig. 3.9a).

### 3.6 The ecology of selection

The simplicity of the function describing stabilizing selection (probably the commonest mode of selection) gives conceptual power but it should not hide the fact that many ecological factors and features of biological design are responsible for the particular location of the optimum and

downward curvature at the two ends of the function (Travis 1989). If we consider the length of the tail in a hypothetical bird, for example, it seems likely that a tail that is too short fails to provide aerodynamic lift at take off, while a tail that is too long interferes with maneuverability and landing. In other words, different kinds of performance and selective agents are likely to cause downward curvature at the two ends of the ISS. The ISS is complex in the sense that it summarizes the interaction of a set of traits with an environment of selective agents and contexts.

### **3.7 Technical issues in estimating and interpreting selection surfaces**

No one mode of selection analysis is likely to satisfy all the expectations of the investigator or reader. Selection gradients, for example, provide useful measures of the intensity of selection in the same form that appears in response to selection equations, but they may fail to describe the actual shape of the ISS. Consequently, a quadratic approximation (section 3.2) to the ISS might be used to estimate  $\beta$  and  $\gamma$ , but a cubic spline (section 3.3) or some other averaging function may be needed to accurately describe the shape of the ISS.

The ISS is a multivariate beast whose overall appearance cannot generally be appreciated by viewing it one trait at a time. Even in the simple case in which only two traits are under selection, each of the two univariate views of selection may be misleading. Plotting fitness as a function of a shape trait may show a flat trend line because strong selection for increasing values of shape prevails in small individuals, while strong selection for decreasing values of shape prevails in large individuals. In this case, averaging selection across one trait (shape) masks the true mode of selection acting on another trait (size). In general, we must be wary that a univariate view or coefficient accurately describes selection. Usually it will not. In the next chapter we will consider truly multivariate visions of the selection beast.

## Chapter 4: The Selection Surface and Adaptive Landscape for Multiple Traits

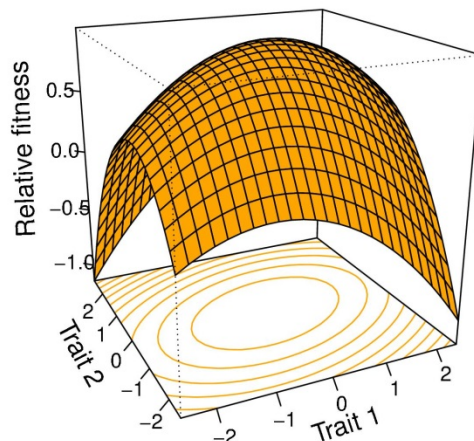
© Stevan J. Arnold 2016

**Overview.-** Selection on multiple traits can be visualized as a surface that relates fitness to the values of two or more traits in individuals. Such a surface can help us visualize the direct effects of selection on trait distributions. Indeed, under some conditions, this surface can take account of the indirect effects of selection induced by trait correlations. In the case of two traits, analysis of selection in natural populations often reveals a hill- or ridge-shaped surface that depicts bivariate stabilizing and correlational selection. The corresponding adaptive landscape has a similar shape but with less curvature.

Natural selection acts simultaneously on many traits. An important consequence of this fact of nature is that we need a multivariate conceptualization of selection to deal with selection and evolution in the natural world. Textbooks in evolutionary biology have been slow to embrace these multivariate inevitabilities. Instead, depictions of selection remain locked on a vision of selection in which selection acts on single traits and is purely directional, a vision developed in the 1940-1960 world of plant and animal breeding. That world included the origin of selection indicies, a multivariate tool for handling directional selection on multiple traits (Hazel 1944), but the conceptualization of multivariate stabilizing selection is a relatively recent development (Lande & Arnold 1983, Phillips & Arnold 1989).

Many important features of the effects of multivariate selection on trait distributions can be appreciated by considering bivariate selection that is stabilizing. The selection surface corresponding to this form of selection is convex (Fig. 4.0) with the optimum situated near the bivariate mean of the trait distribution before selection. Fitness falls off in all directions away from the optimum.

**Figure 4.0** Bivariate stabilizing selection represented as a convex selection surface. Relative fitness,  $w(z)$ , corresponds to points on the surface as a function of the values of two traits,  $z_1$  and  $z_2$ . A contour representation of the surface is projected onto the  $z_1 \times z_2$  plane with contours at increments of 0.2 in relative fitness. This surface is quadratic with  $\alpha = 1$ ,  $\beta_1 = 0.22$ ,  $\beta_2 = -0.08$ ,  $\gamma_{11} = -0.31$ ,  $\gamma_{22} = -0.18$ , and  $\gamma_{12} = 0.07$ .

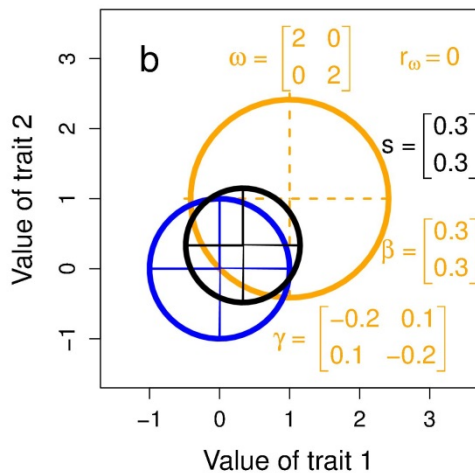
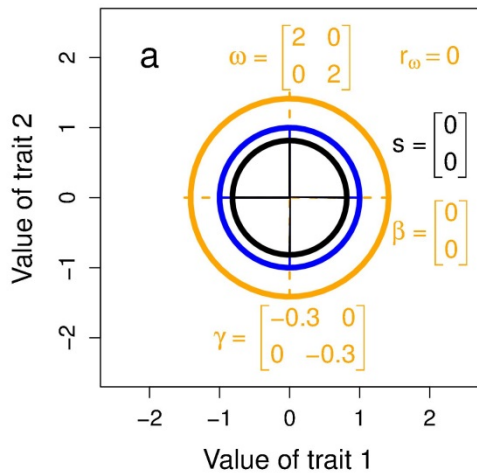
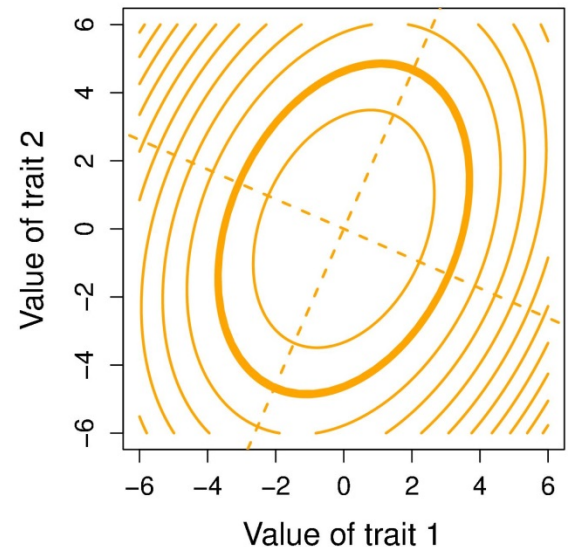


Another convention that will prove useful later is the representation of bivariate stabilizing selection with a single contour line and its eigenvectors. In Fig. 4.1 we show this representation for an inclined surface that exerts strong correlational selection. Consider first a familiar bivariate normal distribution of phenotypes,  $p(z)$ . The 95% confidence ellipse for the bivariate mean is 1.96 phenotypic standard deviations from the mean along each of its principal axes or eigenvectors. The eigenvalues corresponding to each eigenvector are analogous to variances. Likewise, a selection surface has principal axes (section 2.55), shown in Fig. 4.1 as dashed orange lines. The eigenvalues ( $\lambda$ ) for this surface are also analogous to variances. Consequently an ellipse analogous to the 95% confidence ellipse for  $p(z)$ , is situated  $1.96\sqrt{\lambda_i}$  along each

of the two eigenvectors,  $i = 1$  and  $2$ , from the stationary point (where the eigenvectors intersect). This confidence ellipse is shown in Fig. 4.1 as a bold orange ellipse. The smaller this ellipse, the stronger the stabilizing selection. The further the optimum of the surface from the bivariate mean, the stronger the directional aspect of selection.

**Figure 4.1** Contour and confidence ellipse portrayal of a selection surface. The optimum of the surface is at  $z_1=0$  and  $z_2=0$ . The thin orange ellipses represent equal values of relative fitness at increments of 0.2. The bold orange ellipse represents the analog to a 95% confidence ellipse. See text for more details.

Other examples of stabilizing selection surfaces are shown in Fig. 4.2 using the confidence ellipse portrayal. Such convex surfaces can be circular (Fig. 4.1a,b), elliptical with a positive (Fig. 4.1 c, d) or a negative inclination (Fig. 4.1e, f). Many other configurations are possible as well. When the optima of these concave surfaces are located away from the bivariate mean before selection, directional selection is imposed and the bivariate mean is pulled in that direction (Fig. 4.0b, c, f). In the rest of this chapter we will elaborate on these concepts of multivariate selection and make them more precise. In the process we will see that the selection depicted in Fig. 4.0 is substantially stronger than we expect to see in nature.



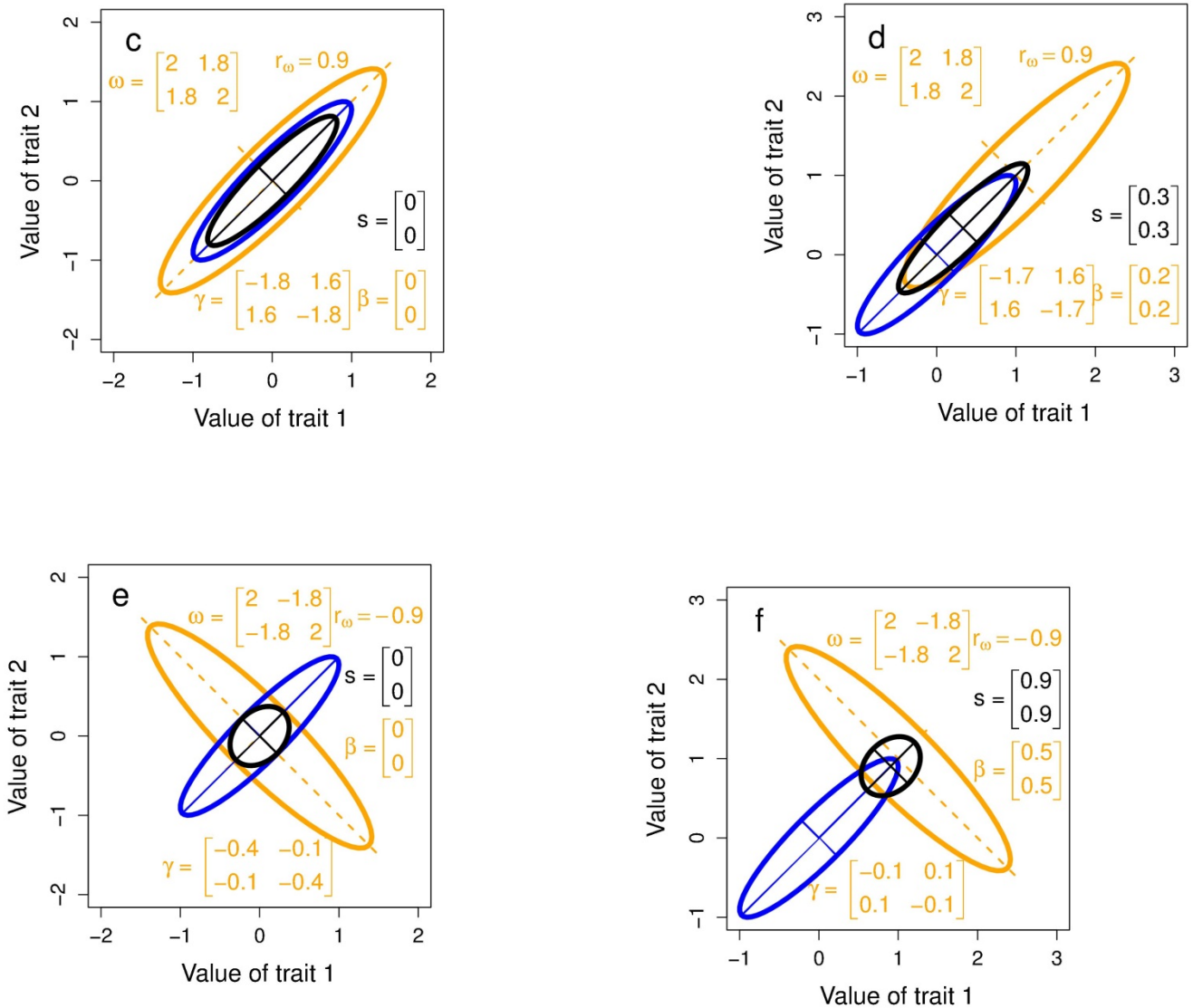


**Figure 4.2.** Various forms of Gaussian selection and their effects on bivariate trait distribution. Ellipses comparable to 95% confidence ellipses are shown for Gaussian ISSs (orange). Phenotypic trait distributions are bivariate normal before (blue 95% confidence ellipses) and after selection (black 95% confidence ellipses). Bivariate means, variances and covariances, before and after selection, are given in the caption for Fig. 2.2. The relationship of the  $\gamma$ -matrix to the  $\omega$ -matrix will be discussed in section 4.4. In the left-hand panel, the trait distribution experiences nonlinear selection, but no directional selection. In the right-hand panel, directional selection has been added by shifting the position of the optimum,  $\theta$ . (a) Symmetrical stabilizing selection contracts the trait variance without shifting the mean. (b) When the optimum is displaced from trait mean in both directions, the trait distribution after selection shifts towards the optimum. (c) Positive correlational selection is reflected in the positive inclination of the  $\gamma$ -ellipse. When this ellipse is aligned with the  $P$ -

ellipse (blue), the inclination of the  $P^*$ -ellipse (black) is not changed by selection. (d) Displacement of the optimum from the trait mean, combined with aligned  $\gamma$ - and  $P$ -matrices, shifts the trait distribution towards the optimum. (e) Nonalignment of the  $\gamma$ - and  $P$ -matrices causes a dramatic change in trait covariance (compare  $P$ - and  $P^*$ -ellipses). (f) Nonalignment of the  $\gamma$ - and  $P$ -matrices, combined with a displaced optimum, shifts the trait distribution towards the optimum.

In Figures 4.0 and 4.1, we specified selection, imposed it on trait distributions and observed the consequences within a generation. We now want to consider the problem of deducing the shape of the selection surface from actual data. Those data might take one of two forms: (1) a sample of individuals together with their trait measurements before selection and a estimate of each individual's fitness, or (2) one sample of individuals and their trait measurements before selection and a second sample, with measurements, taken after selection. In either case, we want to deduce the properties of the ISS from the data. The properties we have in mind are the average slopes and curvatures of the ISS, properties that we wish to mathematically connect to actual observations. We will need to begin by defining the properties of multivariate slope and curvature

#### 4.1 Key properties of the individual selection surface, ISS, for multiple traits.

In general, we want to think of the relative fitness of individuals,  $w(z)$ , as a continuous function or surface of the values of two or more traits,  $z$ . This surface might have a complicated shape, but we will be concerned only with simple quadratic shapes ... (possible new figure = use as an example a complex surface with just one peak but with a few bumps, perhaps a sum of two or three Gaussian surfaces. Such an example will make clear the distinction between the actual ISS and its quadratic approximation). If we consider a particular point on a 2-trait version of this surface (Fig 4.0), the slope at that point is a vector,

$$\begin{bmatrix} \partial w(z)/\partial z_1 \\ \partial w(z)/\partial z_2 \end{bmatrix}, \quad (4.0a)$$

and the curvature at that point is described by a matrix,

$$\begin{bmatrix} \partial^2 w(z)/\partial z_1^2 & \partial^2 w(z)/\partial z_1 \partial z_2 \\ \partial^2 w(z)/\partial z_1 \partial z_2 & \partial^2 w(z)/\partial z_2^2 \end{bmatrix}. \quad (4.0b)$$

The two elements in the vector (4.0a) give the slope in each of the two trait directions,  $z_1$  and  $z_2$ , with a positive sign indicating that fitness increases with trait values, a negative sign indicating the opposite. The diagonal elements in the matrix (4.0b) give the curvature in those same two directions, with negative sign denoting downward (stabilizing) curvature and positive sign denoting upward (disruptive) curvature. In our illustrated example, Fig 4.0, the signs of two diagonal curvature measures is negative (downward curvature). The off-diagonal element in the matrix describes a curvature phenomenon, correlational selection, that has no analog in the univariate case. A positive sign for this element,  $\partial^2 w(z)/\partial z_1 z_2$ , means that the surface is titled so that it promotes a positive correlation between the two traits, while a negative sign means that the surface is tilted so that it promotes a negative correlation. In the illustrated case  $\partial^2 w(z)/\partial z_1 z_2$  is positive.

As in the univariate case, the average slope and curvature of the multivariate ISS are equivalent to our familiar selection gradients,  $\beta$  and  $\gamma$ , which are now, respectively, a column vector and a matrix.

$$\beta = \int p(z) \frac{\partial w(z)}{\partial z} dz = \begin{bmatrix} \int p(z) \frac{\partial w(z)}{\partial z_1} dz \\ \int p(z) \frac{\partial w(z)}{\partial z_2} dz \end{bmatrix} \quad (4.1a)$$

and

$$\gamma = \int p(z) \frac{\partial^2 w(z)}{\partial z^2} dz = \begin{bmatrix} \int p(z) \frac{\partial^2 w(z)}{\partial z_1^2} dz & \int p(z) \frac{\partial^2 w(z)}{\partial z_1 \partial z_2} dz \\ \int p(z) \frac{\partial^2 w(z)}{\partial z_1 \partial z_2} dz & \int p(z) \frac{\partial^2 w(z)}{\partial z_2^2} dz \end{bmatrix} \quad (4.1b)$$

(Lande & Arnold 1983). These are the same averaging functions as in (3.00, 3.01), except that now the averaging is for each of two elements in  $\beta$  and for each of three distinct elements in  $\gamma$ . {address qualifiers discussed in Taylor expansion sect of Phillips & Arnold 1989, p. 1214, or in the next section}

#### 4.2 Linear and quadratic approximations to the ISS.

The elements in the multivariate selection gradients  $\beta$  and  $\gamma$  can be estimated by approximating the ISS with linear and quadratic surfaces. (Note that in the discussions that follow, we assume that each of the traits has been standardized so that each mean is zero, and  $w(z)$  has been standardized so that its mean is 1). For example, in the 2-trait case, we can estimate  $\beta$  by fitting a linear regression model to the data on relative fitness and trait values,

$$w(z) = \alpha + \beta^T z + \varepsilon = \alpha + \beta_1 z_1 + \beta_2 z_2 + \varepsilon. \quad (4.2)$$

The fitted surface is a plane, with  $\alpha=1$  describing its elevation,  $\beta_1$  and  $\beta_2$  its inclination, and  $\varepsilon$  representing the departure of individual data points from the regression surface in the vertical dimension (Fig. 4.1). We can estimate the elements in  $\gamma$  fitting a curvilinear regression model that corresponds to a quadratic surface,

$$w(z) = \alpha + \beta^T + \frac{1}{2} z^T \gamma z + \varepsilon = \alpha + \beta_1 z_1 + \beta_2 z_2 + \frac{1}{2} \gamma_{11} z_1^2 + \frac{1}{2} \gamma_{22} z_2^2 + \gamma_{12} z_1 z_2 + \varepsilon, \quad (4.3)$$

where  $z_1^2$ ,  $z_2^2$ , and  $z_1 z_2$  are the squares and products of trait values, so-called quadratic variables. (Note that these are the same as  $\tilde{z}_1^2$ ,  $\tilde{z}_2^2$ , and  $\tilde{z}_1 \tilde{z}_2$  in sec. 2.5, but here we have deleted the tildas for simplicity.) As in the univariate case,  $\gamma_{11}$  and  $\gamma_{22}$  are *stabilizing selection gradients*, describing downward curvature (stabilizing selection) when their signs are negative and upward curvature (disruptive selection) when their signs are positive. And, as in the univariate case, the factors of  $\frac{1}{2}$  are present so that the stabilizing selection gradients are second derivatives (Stinchcombe et al. 2008). A new kind of coefficient is represented by  $\gamma_{12}$ . This *correlational selection gradient* describes orientation of the ISS in the  $z_1$  by  $z_2$  dimensions, with a positive sign corresponding to an upward tilt and a negative sign corresponding to a downward tilt.

Note that (4.2) provides a statistical model that can be used to estimate the elements of  $\beta$  and  $\gamma$ . The requisite data are measures of trait values and relative fitness for each individual in a sample. Such data are *longitudinal* in the sense that ordinarily individuals must be literally or figuratively followed through time to estimate relative fitness. Fitting the quadratic regression model (4.2) with least-squares is a standard problem in multivariate statistics than can be accomplished in many statistics packages. Extracting actual estimates of  $\beta$  and  $\gamma$ , however, requires some attention to details, which are discussed below.

The rationale for treating the estimation of  $\beta$  as a regression problem (4.2) is very strong.

Because  $s$  is a vector of covariances between relative fitness and traits (2.2), comparison of  $P^{-1}s$  with the definition of partial regression coefficients (Kendall & Stuart 1979) reveals that  $\beta$  is a vector of partial regression coefficients (Lande & Arnold 1983). For example, the directional selection gradient for the first of  $n$  traits,  $\beta_1$ , is the partial regression of relative fitness on  $z_1$ , holding all the other traits constant. By analogy and assuming multivariate normality of the trait distribution,  $\gamma$  is a matrix of partial regression coefficients, where each element represents a partial regression of relative fitness on quadratic variables, holding all the other quadratic variables constant (see eq. 2.8 and 2.9).

Since all the elements of  $\beta$  and  $\gamma$  are contained in one quadratic regression model, one is tempted to use just (4.3) to estimate all the elements in these gradients. One should resist this temptation! If the distributions of the traits are not perfectly symmetrical, as they are in the multivariate normal case, skewness in the distributions will cause the regular trait values,  $z_1$  and  $z_2$ , to be correlated with the quadratic variables,  $z_1^2$ ,  $z_2^2$ , and  $z_1 z_2$ . These correlations will distort the estimates of  $\beta$ . A simple way to avoid this problem (the heartbreak of multivariate skewness) is to use (4.2) to estimate  $\beta$  and (4.3) to estimate  $\gamma$ . Another, more complicated solution involving orthogonal polynomials is discussed by Lande & Arnold (1983).

Despite the simplicity of the quadratic approximation to the ISS (4.3), it can be used to represent large variety of selection possibilities. In the 2-trait case, for example, quadratic surfaces may be hill (Fig. 4.2a), a saddle (Fig. 4.2b), a nearly level ridge (Fig. 4.2c), a rising ridge (Fig. 4.2d), as well as other possibilities. Fig. 4.2 also illustrates the point that it is generally difficult to visualize the quadratic surface that is specified by even a  $2 \times 2$  matrix of  $\gamma$  values. All four surfaces illustrated in Fig. 4.2 have the same value and sign (negative) for their stabilizing selection coefficients,  $\gamma_{11}$  and  $\gamma_{22}$ . All of the correlational selection coefficients,  $\gamma_{12}$ , have the same sign (positive), but differ in magnitude from surface to surface. The position of the bivariate mean (denoted with an  $x$ ) varies from surface to surface. The directional selection gradient,  $\beta$ , is the direction of steepest uphill slope from that position, and consequently it varies from surface to surface in Fig. 4.w. If the bivariate mean were located at a stationary point on the surface (the intersection of the two eigenvectors), both of the elements in  $\beta$  would be zero, i.e., there would be no directional selection.

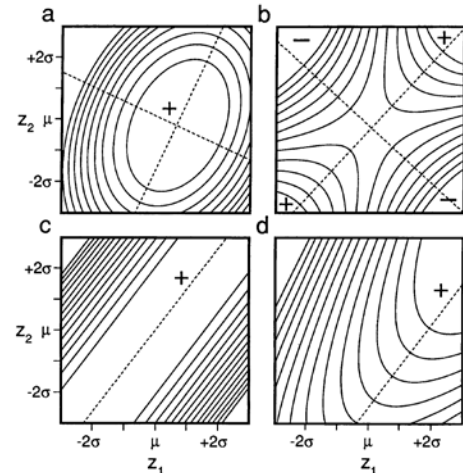


**Figure 4.2.** Hypothetical quadratic ISSs for two traits. Peaks are denoted with a + sign and depressions with a - sign. Dotted lines represent the canonical (principal) axes of the surface. Traits means are denoted with  $\mu$  and phenotypic standard deviation with  $\sigma$ . Despite the differences in the appearance of these surfaces, the values of the elements in their  $\gamma$ -matrices are only slightly different. See Phillips & Arnold 1989 for details. From Phillips & Arnold 1989.

### 4.3 Canonical analysis of the quadratic approximation to the ISS

Figure 4.2 illustrates the important point that we can not deduce the shape of the fitted quadratic surface from a simple inspection of the  $\gamma$ -matrix. The four surfaces illustrated in Fig. 4.2 differ radically in shape yet their  $\gamma$ -matrices are extremely similar. One can determine the shape of the surface by plotting expression (4.2) or, more elegantly, by conducting a canonical analysis of the  $\gamma$ -matrix (section 2.65) that yields its eigenvalues,  $\lambda$ , and eigenvectors. Recalling our earlier discussion (2.65), the eigenvectors are a rotation of the original trait axes which have the property that the first eigenvector is in the direction that has the greatest curvature, the second eigenvector is in an orthogonal direction with the next greatest

curvature, and so on. The eigenvectors of the surfaces illustrated in Fig. 4.2 are shown as dotted lines. These eigenvectors and their associated eigenvalues are calculated directly from  $\gamma$ -matrix (Phillips & Arnold 1989). Using the  $\gamma$ -matrix one can also determine the *stationary point*,  $z_0$ , on the fitted quadratic surface, which may be a fitness maximum, minimum or saddle point. The distance from the mean to this stationary point is

$$z_0 = -\gamma^{-1}\beta, \quad (4.03)$$

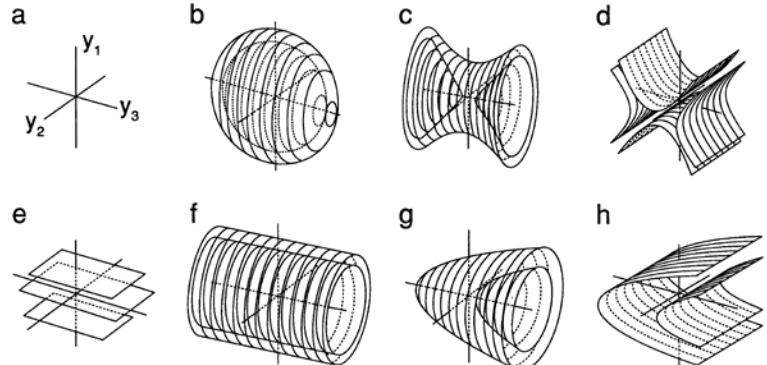
and the value of relative fitness at the stationary point is

$$w_0 = \alpha + \frac{1}{2}\beta^T z_0 \quad (4.04)$$

(Phillips & Arnold 1989). By calculating the eigenvalues of a surface, one can deduce its properties. If all the eigenvalues of  $\gamma$  are negative the surface is a dome (convex); if they are all positive the surface is a bowl (concave). Mixed signs indicate a saddle-shaped surface, with a stationary point at the saddle. See Phillips & Arnold (1989) for further discussion.

When the eigenvalues of  $\gamma$  are of mixed sign, it will often be useful to order them using their absolute values,  $|\lambda_i|$ , that is to say, by greatest curvature, whether concave or convex (Brooks & Blows 2003). The contrasting convention used by most computational algorithms is to rank eigenvalues by their raw values, so that all eigenvalues with positive sign receive higher rank than all eigenvalues with negative sign, irrespective of the magnitude of curvature. The distinction becomes important when we wish to determine the direction on the surface that has the least effect on relative fitness. We can call this direction  $\gamma_{min}$ . It is the direction given by the eigenvector with the minimum value of  $|\lambda_i|$ , which can be thought of as a *selective line of least resistance*. In all the plots shown in Fig. 4.2, the selective lines of least resistance are inclined at about a 45 degree angle in trait space.

In the 3-trait case, the variety of ISSs that can be approximated with quadratic surfaces is also very large (Phillips & Arnold 1989). Seven varieties are shown in Fig. 4.4, where the canonical axes are denoted  $y_1$ ,  $y_2$ , and  $y_3$ , but are not ordered by the size of their eigenvalues. Each of the nested surfaces in each figure represents equal values for relative fitness. Perhaps the easiest 3-trait case to visualize is stabilizing selection on all three axes, shown in Fig. 4.4a. Here the the fitness optimum,  $\theta$ , a stationary point, is situated at the intersection of the axes. Fitness falls off as concentric spheres about this point. In Fig. 4.4f, the optimum is a line corresponding to  $y_3$ , with stabilizing selection on  $y_1$  and  $y_2$ , but no selection along the  $y_3$ -axis.



#### 4.4 The adaptive landscape.

The adaptive landscape relates population mean fitness to average trait values in the multivariate case, just as it does in the univariate case. The slope and curvature of the AL, evaluated at the trait mean,  $\bar{z}$ , are related to the selection gradients. In general and in the 2-trait case,

$$\boldsymbol{\beta} = \frac{\partial \bar{W}}{\bar{W} \partial \bar{z}} = \frac{\partial \ln \bar{W}}{\partial \bar{z}} = \begin{bmatrix} \partial \ln \bar{W} / \partial \bar{z}_1 \\ \partial \ln \bar{W} / \partial \bar{z}_2 \end{bmatrix} = \begin{bmatrix} \beta_1 \\ \beta_2 \end{bmatrix} \quad (4.05)$$

and

$$\gamma - \boldsymbol{\beta}\boldsymbol{\beta}^T = \frac{\partial^2 \bar{W}}{\bar{W} \partial \bar{z}^2} = \frac{\partial^2 \ln \bar{W}}{\partial \bar{z}^2} = \begin{bmatrix} \partial^2 \ln \bar{W} / \partial \bar{z}_1^2 & \partial^2 \ln \bar{W} / \partial \bar{z}_1 \partial \bar{z}_2 \\ \partial^2 \ln \bar{W} / \partial \bar{z}_1 \partial \bar{z}_2 & \partial^2 \ln \bar{W} / \partial \bar{z}_2^2 \end{bmatrix} = \begin{bmatrix} \gamma_{11} - \beta_1^2 & \gamma_{12} - \beta_1 \beta_2 \\ \gamma_{12} - \beta_1 \beta_2 & \gamma_{22} - \beta_2^2 \end{bmatrix}. \quad (4.06)$$

The directional selection gradient,  $\boldsymbol{\beta}$ , gives the direction of steepest uphill slope (first derivatives) from the multivariate mean,  $\bar{z}$  (Lande 1979). The matrix  $\gamma - \boldsymbol{\beta}\boldsymbol{\beta}^T$  describes the curvature (second derivatives) of the AL at the multivariate mean (Lande 1979, Lande & Arnold 1983). Notice that the sign elements in the second term in (4.06) are always negative, so we can conclude that the curvature of the AL ( $\gamma - \boldsymbol{\beta}\boldsymbol{\beta}^T$ ) is always less than the curvature of the ISS ( $\gamma$ ).

To visualize the AL as a surface, we need to average the ISS over translations (lateral shiftings) of the trait distribution,  $p(z)$ . Building on our discussion of the univariate case (sec. 3.3), this averaging is easy if  $p(z)$  is multivariate normal (2.0) and if the ISS is approximated by a multivariate Gaussian surface,

$$W(z) = \exp\{-\frac{1}{2}(z - \theta)^T \boldsymbol{\omega}^{-1}(z - \theta)\} \quad (4.07)$$

(Lande 1979, 1980, or 1981?). The  $\boldsymbol{\omega}^{-1}$  term is the inverse of the  $\boldsymbol{\omega}$ -matrix, which in the 2-trait case takes the form

$$\boldsymbol{\omega} = \begin{bmatrix} \omega_{11} & \omega_{12} \\ \omega_{12} & \omega_{22} \end{bmatrix}, \quad (4.08)$$

with  $\omega_{11}$  and  $\omega_{22}$  analogous to variances. When these two coefficients are positive, the ISS may be a bell-shaped hill (or any one of the other surfaces shown in Fig. 4.w!). The off-diagonal term,  $\omega_{12}$ , is analogous to a covariance. When it is positive, the hill is tilted upward in the  $z_1 \times z_2$  dimension. When  $\omega_{12}$  is negative the hill is tilted downward. We can produce a multivariate AL by averaging this Gaussian ISS over a multivariate normal trait distribution. The resulting adaptive landscape is also multivariate Gaussian,

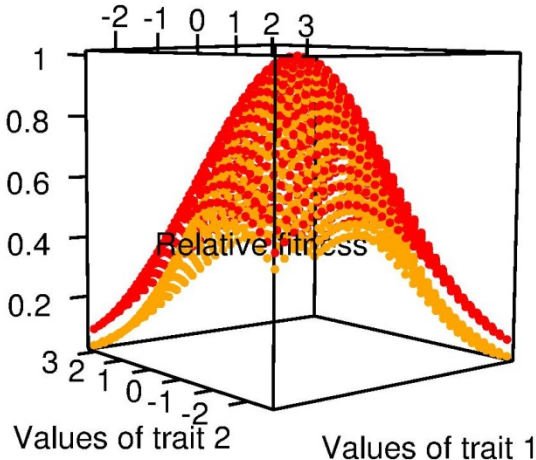
$$\bar{W} \propto \exp\{-(\bar{z} - \theta)^T (\boldsymbol{\omega} + P)^{-1}(\bar{z} - \theta)\}, \quad (4.09)$$

where  $\boldsymbol{\omega} + P$  is a shape and orientation matrix

(Lande 1979). In the 2-trait case,

$$\boldsymbol{\omega} + P = \begin{bmatrix} \omega_{11} + P_{11} & \omega_{12} + P_{12} \\ \omega_{12} + P_{12} & \omega_{22} + P_{22} \end{bmatrix}, \quad (4.10)$$

where, as in  $\boldsymbol{\omega}$ , the diagonal terms are analogous to variances and the off-diagonal terms are analogous to a covariance, and both kinds of terms carry the



same kinds of geometric interpretations. Because  $P_{11}$  and  $P_{22}$  are always positive, the AL will be somewhat flatter than the ISS, but its tilt may differ if  $\omega_{12}$  and  $P_{12}$  differ in sign. If stabilizing selection is weak, however, so that  $\omega \gg P$ , the ISS and AL will be very similar in configuration (Fig. 4.5).

**Figure 4.5.** A Gaussian ISS and corresponding Gaussian AL are similar in configuration if stabilizing selection is weak, as in this example: Gaussian ISS (orange) with  $\theta = (0,0)$  and  $\omega = (5,2.5,2.5,5)$  and the corresponding Gaussian AL with  $\omega + P = (6,2.5,2.5,6)$ , where  $P = (1,0,0,1)$ .

A Gaussian form for the ISS is also useful in theoretical work because it enables us to solve for the multivariate trait distribution after selection. If the trait distribution,  $p(z)$ , is multivariate normal before selection and the ISS is Gaussian (4.07), the phenotypic trait distribution is normal after selection with means and variance-covariance matrix given by

$$\bar{z}^* = (\omega + P)^{-1}(\omega\bar{z} + P\theta)$$

and

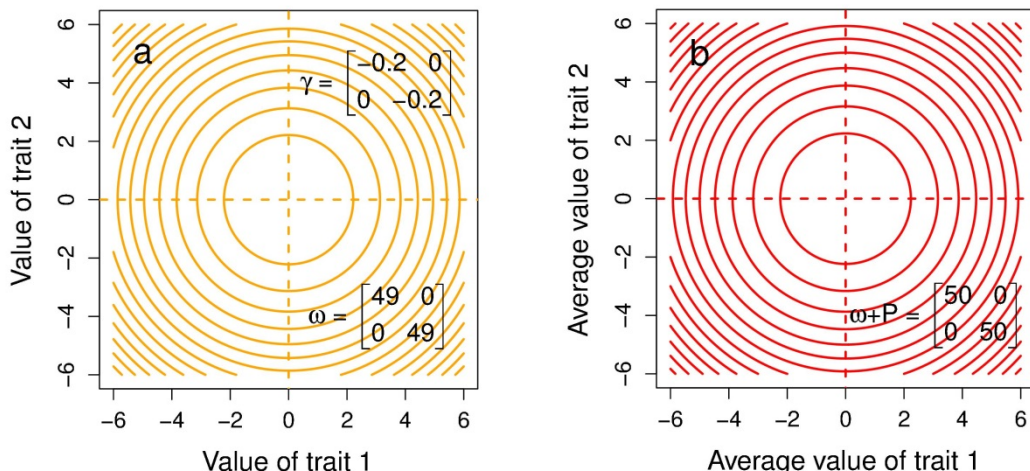
$$P^* = (\omega + P)^{-1}\omega P,$$

which are generalizations of Lande's (1981) results for the univariate case (3.12). In these forms, we see that the AL exerts its effects on  $p(z)^*$  via its shape matrix,  $\omega + P$ . **What is the formula for beta when the ISS is Gaussian?\*\***

When multivariate stabilizing selection is weak, we can estimate  $\omega$  from the negative inverse of the  $\gamma$ -matrix,

$$\omega = -\gamma^{-1}, \quad (4.11)$$

which is the multivariate generalization of (3.10). From this approximation of  $\omega$ , we can easily approximate  $\omega + P$ . Ordering eigenvalues by their absolute values (section 4.3), the  $\omega$ - and  $\gamma$ -matrices have the same eigenvectors but in reverse order, so  $\omega_{max}$  corresponds to  $\gamma_{min}$ , the direction in trait-space in which the ISS has the weakest curvature. In other words,  $\omega_{max}$  is the eigenvector of  $\omega$  with the largest eigenvalue, giving the direction in trait space that is most forgiving with respect to selection, a selective line of least resistance. Similarly,  $\omega + P_{max}$  is the eigenvector of  $\omega + P$  with the largest eigenvalue, which is likely to be similar to  $\omega_{max}$  if multivariate stabilizing selection is weak (Fig. 4.6).



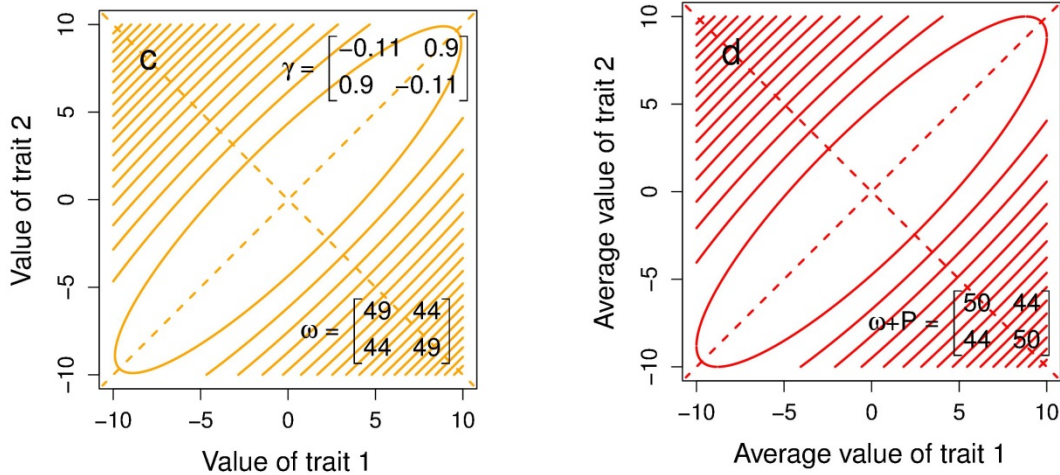


**Figure 4.6** Contour plot portrayals of weak bivariate Gaussian ISSs and their corresponding adaptive landscapes. In each figure the optimum is at  $z_1=0$  and  $z_2=0$ ,  $P=(1,0,0,1)$ . Eigenvectors are shown as dashed lines. Matrix representations are superimposed on each surface. (a) An ISS with equally strong stabilizing selection on each trait with no correlational selection. Contours show equal values of relative fitness,  $w(z)$ . (b) The AL corresponding to Fig. 4.6a. Contours show equal values of average absolute fitness,  $\bar{W}$ . (c) An ISS with equally strong stabilizing selection on each trait and strong correlational selection,  $r_\omega=0.9$ . (d) The AL corresponding to Fig. 4.6c.

In conclusion, we note while the ISS is useful as a local description of selection, the AL is useful because it is the surface on which  $\bar{z}$  evolves. Because of this distinction, we will need a vision of the AL in our later discussion of evolution. We adopt a Gaussian framework because it gives us that needed vision.

#### 4.5 Examples of quadratic approximations of the ISS

We can appreciate the relationship of selection gradients to the ISS by returning to the example of how crawling speed in newborn garter snakes is affected by body and tail vertebral counts (Arnold 1988, Arnold & Bennett 1988). In Chapter 2 we showed how the gradients in this example could be estimated by comparing samples before and after selection (2.02, 2.09), but here we show estimation by linear and quadratic regression. The directional selection gradients were estimated by linear regression (4.2) and the nonlinear selection gradients were estimated by quadratic regression (4.3) (Table 4.1). Bootstrap estimates of 95% confidence limits suggest that the point estimates of  $\beta_1$ ,  $\beta_2$ ,  $\gamma_{11}$  and  $\gamma_{22}$  are not different from zero. Point estimates of standard errors provided by regression analysis without bootstrapping provide a similar picture (Table 4.1). In contrast, the correlational selection gradient,  $\gamma_{12}$ , is positive and substantially different from zero. To visualize the ISS that corresponds to these selection gradients, we plot the corresponding surface,

$$w(z) = 1.0 + 0.031z_1 - 0.011z_2 + \frac{1}{2}(-0.011)z_1^2 + \frac{1}{2}(-0.006)z_2^2 + 0.079z_1z_2,$$

and compare that surface with the one described by the selection gradients estimated in Chapter 2,

$$w(z) = 1.0 + 0.031z_1 + 0.002z_2 + \frac{1}{2}0.097z_1^2 + \frac{1}{2}0.116z_2^2 + 0.176z_1z_2.$$

The gradient estimates are subtly different as a consequence of different estimation procedures, but how different are the two surfaces? Contour plots reveal that the surfaces are remarkably similar and saddle-shaped in both cases (Fig. 4.2). Both surfaces curve slightly upward from the bottom lefthand corner to

the upper, right-hand corner, and slightly downward from the upper left-hand corner to the bottom right-hand corner.

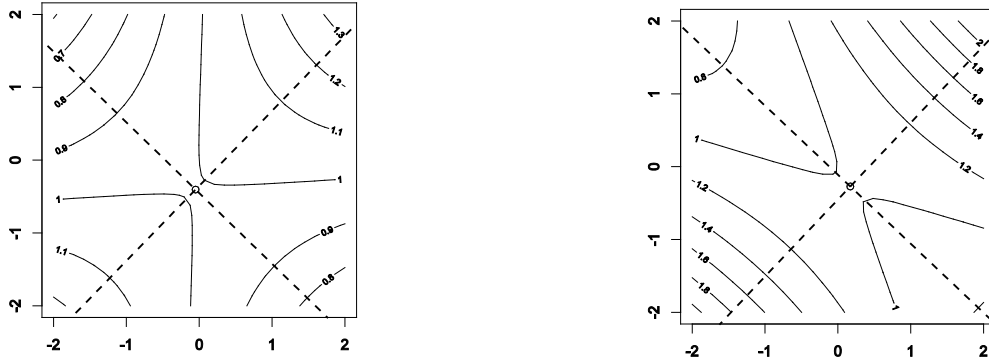


Figure 4.z Crawling speed performance surfaces as a function of body and tail vertebral numbers, estimated by two different procedures. Eigenvectors are shown in dotted lines. Stationary points, calculated using (4.03), are shown as open circles, near the center of each plot. A. (left) Contour surface drawn using selection gradients estimated by linear and quadratic regression. The slope of the leading eigenvector is 0.971 ( $\lambda_1=0.071$ ,  $\lambda_2=-0.087$ ). B. (right) Contour surface drawn using selection gradients estimated by comparing samples before and after selection (2.02, 2.09). The slope of the leading eigenvector is 1.055 ( $\lambda_1=0.282$ ,  $\lambda_2=-0.069$ ).

The new axes described by the eigenvectors are biologically informative. Eigenvectors are linear combinations of the original axes. In the case of selection surfaces, each eigenvector consists of a series of weights (loadings) each of which describes how a particular trait contributes to the new axis. When all the weights are positive the weighting produces a combination that is the weighted average (sum) of the traits. When the weights have a mixture of signs, the weighting produces a combination that is difference or contrast in traits. Thus, the leading eigenvectors of the surfaces in Fig. 4.z, with slopes close to one, represent the sum of the two vertebral counts, whereas the second eigenvectors, with slopes close to minus one, represent the difference in the two vertebral counts. In Fig. 4.za, curvature is about the same in both the sum and difference directions ( $|0.071| \approx |-0.087|$ ), but in Fig. 4.zb, curvature is substantially stronger in the sum direction ( $|0.282| > |-0.069|$ ) telling us that variation in the sum of counts is tolerated less than variation in direction of the count difference.

This example also illustrates the utility of eigenvectors and eigenvalues in comparing surfaces. Although the similarity of the two surfaces is not apparent from their  $\gamma$ -matrices, it is readily deduced from their eigenvectors and eigenvalues (Fig. 4.z). In both cases the slope of the leading eigenvector is nearly one, selection in that direction is disruptive, as indicated by the positive sign of the corresponding eigenvalue, whereas selection in the opposite direction is stabilizing, as indicated by the negative sign and magnitude of the eigenvalue corresponding to that eigenvector. In contrast, the values of  $\beta_1$  and  $\beta_2$  tell us little about the surface. Instead, they describe slope of surface at the location of the bivariate mean, which in the present case is very close to the stationary point.

The illuminating properties of the eigenvectors and eigenvalues suggest that they are best platform to explore the sampling properties of the ISS, however it is estimated. In particular, a bivariate plot of the two eigenvalues estimated for each bootstrapped sample can tell us how often the ISS takes the

form of a saddle (versus other shapes). When the ISS is estimated by multiple regression, the ISS most often takes a saddle shape ( $\lambda_1$  positive,  $\lambda_2$  negative), but a bowl-shaped surface is relatively common ( $\lambda_1$  positive,  $\lambda_2$  positive) (Fig. 4.zzb). The distribution of slopes for the leading eigenvector is bimodal, and straddles zero with a slight preponderance of negative values (Fig. 4.zza). When the ISS is estimated from samples before and after selection, the shapes of the ISS show the same split between saddle and bowl shapes. In this case, however, the distribution of slopes for the leading eigenvector is unimodal with a mode close to one, and nearly all values are positive.

Bootstrap sampling of the two estimation procedures is revealing because it tells us that our visualization of the ISS is fragile. Our vision of the ISS changes shape from boot to boot. The slope of the leading eigenvector is, however, a more stable feature of the ISS when it is estimated by samples before and after selection. In that case, a confidence interval could easily be specified about the strong mode (near one). In the case of estimation by regression, however, a confidence interval would be misleading in and of itself, because the distribution of slopes shows two modes (one near 2 and one near -2). The results in the two case do not recommend one estimation procedure over the other. Instead, this case study emphasizes the point that when curvature of the ISS is slight, our confidence in shape of the ISS and in its major axis is compromised.

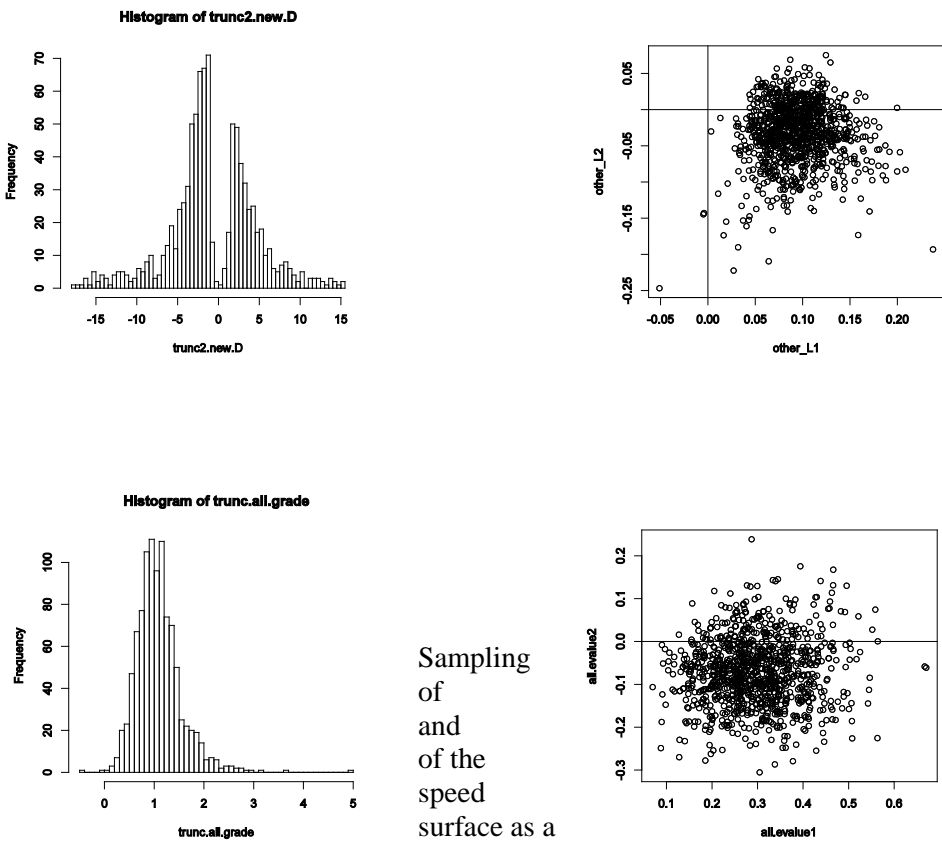


Fig. 4.zz  
distributions  
eigenvalues  
eigenvectors  
crawling  
performance  
function of

vertebral numbers, estimated by bootstrapping two different estimation procedures ( $n=1000$  samples with replacement). A. (upper left) The bootstrap distribution of slopes of the leading eigenvector of the  $\gamma$ -matrix, estimated by multiple regression. B. (upper right) Bootstrap values of  $\gamma_2$  plotted against  $\gamma_1$ , when the  $\gamma$ -matrix is estimated by multiple regression. C. (lower left) The bootstrap distribution of slopes of the leading eigenvector of the  $\gamma$ -matrix, estimated from samples before and after selection. D. (lower right)

Sampling  
of  
and  
of the  
speed  
surface as a  
body and  
tail

Bootstrap values of  $\gamma_2$  plotted against  $\gamma_1$ , when the  $\gamma$ -matrix is estimated from samples before and after selection.

Finally, we can use our regression estimate of the  $\gamma$ -matrix to illustrate approximations of  $\omega$  and  $\omega+P$ . Using 4.xx, we find that \*\*Note that the values of gamma here and in Table 4.1 need to be reconciled with the values used in plotting the selection surface\*\*

$$\omega = -\gamma^{-1} = -\begin{bmatrix} -0.011 & 0.079 \\ 0.079 & -0.006 \end{bmatrix}^{-1} = \begin{bmatrix} -0.957 & -12.784 \\ -12.784 & -1.711 \end{bmatrix}.$$

The negative inverse operation converts a matrix of second derivatives for a quadratic surface,  $\gamma$ , into a matrix of variance- and covariance-like elements that describes a Gaussian surface,  $\omega$ . When the variance-like diagonal elements of  $\omega$  are positive the Gaussian surface is convex, like a familiar bell curve, but when the diagonal elements are negative, the Gaussian surface is concave, like an upside down bell curve. The canonical form of  $\gamma$ , with eigenvalues on the main diagonal, is

$\begin{bmatrix} -0.088 & 0 \\ 0 & 0.071 \end{bmatrix}$ , with the eigenvectors of  $\gamma$  given by the columns of  $\begin{bmatrix} -0.718 & -0.696 \\ 0.696 & -0.718 \end{bmatrix}$ . The canonical form of  $\omega$  is  $\begin{bmatrix} -14.123 & 0 \\ 0 & 11.455 \end{bmatrix}$ , with eigenvectors given by the columns  $\begin{bmatrix} 0.697 & -0.717 \\ 0.717 & 0.697 \end{bmatrix}$ .

As expected, the eigenvectors of  $\gamma$  and  $\omega$  are the same but in reverse order. The selective line of least resistance is given by  $\gamma_{min} = [-0.696 \quad -0.718]^T$ , or equivalently  $\omega_{max} = [0.697 \quad 0.717]^T$

Because our vertebral count distributions are approximately normal before selection, and because the trait variances have been standardized to one before selection, we can readily visualize the curvature of the Gaussian  $\omega$ -surface in relation to our trait variances. A first eigenvalue of -14.123 tells us that the Gaussian surface is concave in the direction of the first eigenvector with a ‘variance’ about 14 times larger than our trait variance. Similarly, a second eigenvalue of 11.455 tells us that the surface is convex in an orthogonal direction with a ‘variance’ about 11 times larger than our trait variances.

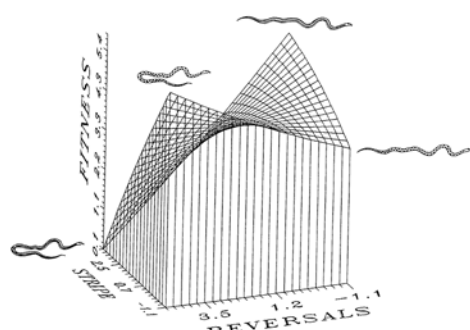
Our corresponding estimate of  $\omega+P$ , using values of  $P$  from Table 4.1, is

$$\omega + P = \begin{bmatrix} -0.957 & -12.784 \\ -12.784 & -1.711 \end{bmatrix} + \begin{bmatrix} 1.000 & 0.073 \\ 0.073 & 1.000 \end{bmatrix} = \begin{bmatrix} 0.043 & -12.711 \\ -12.711 & -0.711 \end{bmatrix}$$

with canonical form  $\begin{bmatrix} -13.051 & 0 \\ 0 & 12.383 \end{bmatrix}$  and eigenvectors given by the columns  $\begin{bmatrix} 0.697 & -0.718 \\ 0.718 & 0.697 \end{bmatrix}$ .

As expected, the canonical forms of  $\omega$  and  $\omega+P$  are very similar. The selective line of least resistance determined from  $\omega + P$  is  $[0.697 \quad 0.718]^T$ .

Brodie’s (1992) study of how viability in garter snakes is affected by coloration and behavior provides another illuminating example of selection surface analysis. This study was motivated by the observation that coloration pattern and antipredator behavior coevolve in snakes, so that higher taxa fall out along a bivariate continuum (Jackson et al. 1976). At one end of



the continuum are slow-moving snakes with blotched color patterns that rely on crypsis to evade predators. At the other end are fast-moving snakes with stripes or no pattern that rely on speed and optical illusion to escape predators. Remarkably, this same coloration-behavior continuum occurs within individual populations of the garter snake *Thamnophis ordinoides*. On the continuum, the population includes blotched snakes that tend to reverse directions and striped snakes that crawl in a straight line, but off-continuum snakes are also well represented (striped, reversing snakes and blotched, straight-crawling snakes). Despite this bivariate smear before selection, the connection to the interspecific continuum becomes clear when we visualize the viability selection surface. That visualization reveals that snakes that fall out along the continuum are favored by selection, but selection acts against snakes with the maladaptive combinations of striped-reversal and blotched-straight crawl (Fig. 4. zw). Turning to the selection coefficient that exerts the most influence on the portrayal of the surface, this example bears many similarities to the *T. radix* crawling speed-vertebral count example that we just discussed. As in the *T. radix* example, it is a correlational selection differential and corresponding gradient that are sufficiently large to attain statistical significance. Bivariate selection on coloration pattern and behavior affects the correlation between those traits. In a later section we will discuss the significance of the fact that this bivariate selection has also resulted in a genetic correlation between these two traits (Brodie 1993).

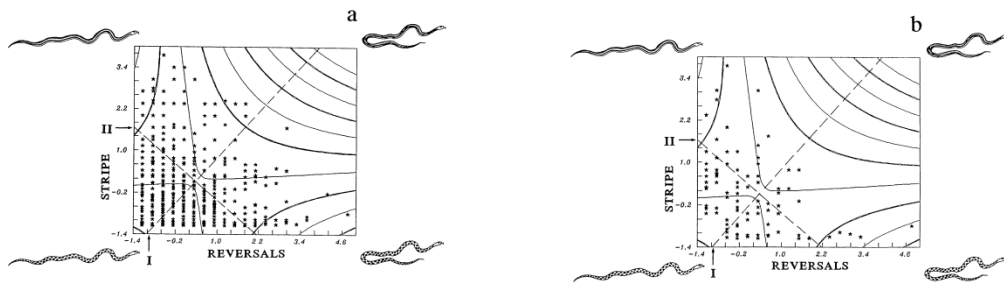


**Figure 4.zx** Viability selection as a function of coloration pattern and antipredator behavior in *T. ordinoides*. Survival in the field is shown as a function of reversals (the tendency to reverse directions during simulated predation exposure in the laboratory) and stripe (overall stripedness of the color pattern). Contours show relative fitness (survival) as a quadratic function of reversals and stripe. Eigenvectors are shown as dashed lines. Selection is stabilizing (concave) along the leading eigenvector (I) and disruptive (convex) along the second eigenvector (II). (a) The bivariate sample before selection ( $n=646$ ). (b) The bivariate sample after selection ( $n=101$ ). (c) Surface plot of the quadratic selection function.

#### 4.9 Surveys of quadratic approximations to the ISS

We would like to know what multivariate form of selection is most prevalent in nature. From a theoretical standpoint we can expect quadratic approximations to take a variety of shapes (bowl, dome, saddle, rising ridge, etc.), but which of these shapes is most commonly encountered? Blows & Brooks (2003) have taken a major step towards answering this question by surveying studies that tackled the issue of shape in three or more dimensions (Table 4.az). The surprising answer was that in 17 of 19 cases the surface was saddle-shaped (one bowl and one dome accounted for the other two cases). This answer is surprising because a saddle is inherently unstable. For this very reason theoreticians often employ a multivariate dome to describe selection on continuous traits. Dome-shaped selection tends to move the trait mean towards a stable local optimum. Why is this multi-stabilizing form of selection so rare? One possible reason – among many – for the disconnect between theoretical expectation and empirical realization is that we nearly always measure components of fitness, not lifetime fitness in studies of selection surfaces. Arnold & Bennet (1988) and Brodie (1992), for example, assessed selection over the first few weeks or years of life, not over the entire life span.

... another possibility is that when curvilinear selection is weak, a point estimate may often have the opposite curvature to the parametric surface ... \*illustrate with boot-strapping of radix performance surface\*

Table A1: Comparative data set

$n$	Largest $\gamma_{ii}$	$\lambda$	Type of surface	Type of selection	Reference
5	.044	.062	Saddle	O	Mitchell-Olds and Bergelsson 1990
4	-.457	-1.262	Saddle	F	Moore 1990
4	-.550	-.714	Saddle	M	Moore 1990
4	-.707	-1.093	Saddle	F	Moore 1990
4	-.498	-.729	Saddle	M	Moore 1990
4	.102	.155	Saddle	M	Moore 1990
4	-.538	-.650	Saddle	F	Moore 1990
4	-.122	-.273	Saddle	S	Brodie 1992
3	-.874	-.875	Saddle	F	Nunez-Farfan and Dirzo 1994
3	.370	.552	Saddle	F	O'Connell and Johnston 1998
3	1.180	1.709	Bowl	F	O'Connell and Johnston 1998
3	.770	1.124	Saddle	F	O'Connell and Johnston 1998
3	.260	.283	Saddle	F	O'Connell and Johnston 1998
3	.200	.305	Saddle	F	O'Connell and Johnston 1998
3	.23	.26	Saddle	F	O'Connell and Johnston 1998
5	.994	.999	Saddle	F	Simms 1990
3	-.019	-.021	Peak	S	Kelly 1992
4	.016	.027	Saddle	S	Kelly 1992
5	.112	.214	Saddle	F	Kelly 1992

Note: Analysis of nonlinear selection in 19 data sets identified by Kingsolver et al. (2001) involving three or more traits. We have presented the largest  $\gamma_{ii}$  and  $\lambda_i$  from each  $\gamma$ . The type of surface is based on the signs of all eigenvalues, following the descriptions used by Phillips and Arnold (1989); if eigenvalues were all negative, the surface has a peak; if all were positive, the surface is a bowl; and if some were negative and positive, the surface is a saddle. The type of selection follows the categories used by Kingsolver et al. (2001): S = survival, M = mating success, F = fecundity/fertility, O = other.  $n$  = number of traits measured in each study.

#### 4.10 Cubic spline approximation to the ISS

The cubic spline solution to the problem of estimating the shape of the ISS (section 3.3) can be generalized to multiple traits (Schluter & Nychka 1994). A 2-trait example is shown in Fig. 4.5

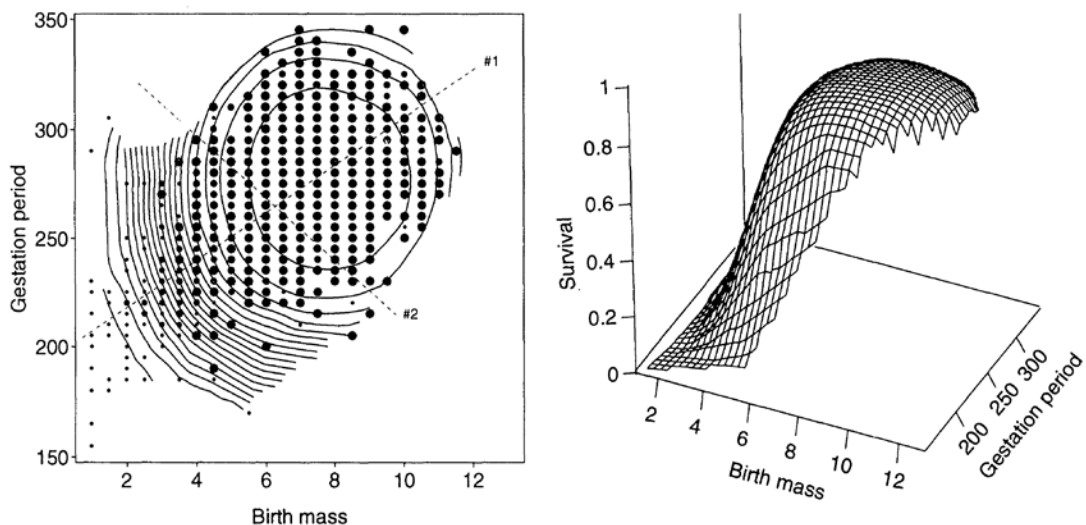
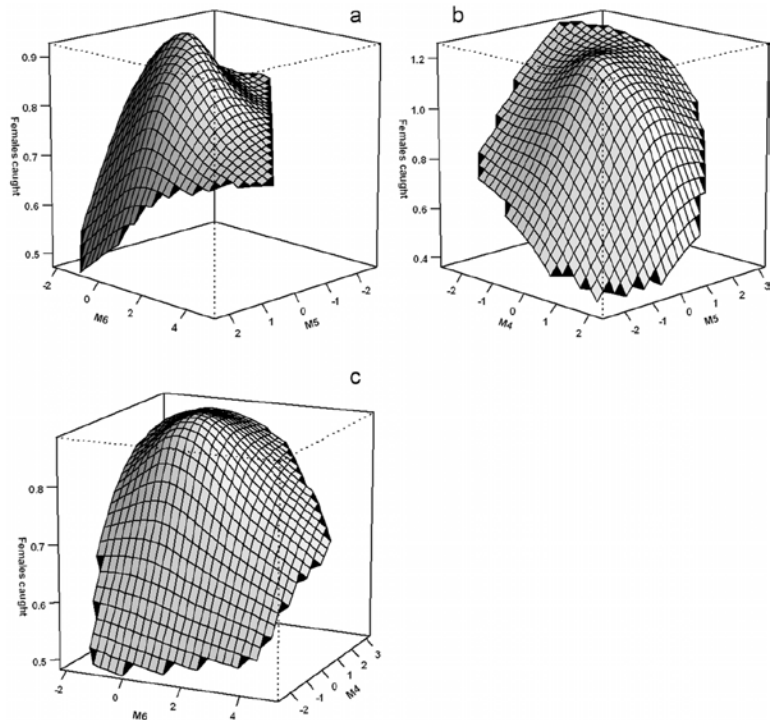


FIG. 5.—Survival probability of male human infants as a function of birth mass (pounds) and gestation period (days). The surface was approximated using two directions (table 3) indicated by the *dashed lines*. Fitness contours in the *left panel* are in increments of 0.5. They describe a dome rising steeply from lower left to a broad plateau above and right of center, declining slightly along its outer edges. *Right panel* gives three-dimensional perspective. Symbol size increases with increasing average survival of individuals in each mass (rounded to nearest 0.5 lb.) and gestation class (rounded to nearest 5 d); differences in symbol size are exaggerated in the range 0.90–1.00 to highlight slight survival differences. The most extreme observation at large mass was excluded from the analysis.  $\ln(\lambda) = -10$ ;  $n = 7,036$ .

Bentson et al. (2006) ... cricket vocalizations ...

**\*\*Responses of crickets to artificial calls\*\***



**Bentson et al. 2006** Figure 2: Thin-plate spline visualizations of the fitness surfaces, which demonstrate significant convex stabilizing selection between  $m_5$  and  $m_6$  (a),  $m_4$  and  $m_5$  (b), and  $m_4$  and  $m_6$  (c).

**4.11 Technical issues in estimating and interpreting the ISS** {Consider moving this section to before the survey section}

Over the last few decades, the trend in selection studies has been to include portrayals of the ISS, as well as tables of  $\beta$  and  $\gamma$  estimates and their standard errors. In part this trend reflects increasing appreciation of the fact the ISS cannot be visualized from a table of  $\beta$  and  $\gamma$  estimates (Phillips & Arnold 1989). The other growing realization is that the ISS is an object of interest in its own right (Blows 2007). Accurate portrayals of the ISS can summarize complex modes of selection, provide a vision of the AL, and may point to important avenues of evolution during adaptive radiations (Chapter 17). Nevertheless, a disturbing fraction of selection studies fail to report coefficients of nonlinear selection (often estimates of  $\gamma_{ij}$  are missing, but sometimes estimates of  $\gamma_{ii}$  as well).

Using multivariate regression to capture a vision of the ISS immediately places us in a quandry of how many traits to include. The quandry arises because the vagaries of sampling force us to consider the over-all shape of the ISS rather than just the values and significance of individual elements in  $\beta$  and  $\gamma$  and because the actual targets of selection (the real subset of traits under the strongest directional or nonlinear selection) are usually unknown to us. To capture the real targets, we could include more traits in the selection analysis, but – because  $\gamma$  is a matrix – the number of coefficients to be estimated goes up as the square of the number of traits. Increasing the number of traits may increase our chances of including real targets, but as we attempt to estimate more coefficients our power to detect selection goes down (i.e., more of our estimates are nonsignificant). Unfortunately, this multivariate quandry has no universal solution, although it can often be mitigated by two considerations. The first is that ecological or biomechanical arguments may enable us to narrow the field of possible traits. For example, in the case of Galapagos finches, a host of ecological observations and biomechanical analogies, bolster a priori the choice of beak depth and length as probable targets of selection (Grant xxxx, Grant & Grant yyyy). On this basis the investigators restricted their selection analysis to just two traits. The second consideration is that selection can sometimes be profitably viewed as acting on combinations of traits. Taking this approach, one can analyze selection on principal components or other linear combinations of traits and thereby reduce the trait number to one, two or three. This tact works best if the linear combinations are readily interpretable. For example, if the traits are linear measurements, the first principal component can often be interpreted as a measure of overall size, while components with small eigenvalues represent measures of shape (Jolicoeur & Mosimann 1960).

A variety of other issues are in general endemic to multivariate statistical analyses, not just to selection analysis. Although these issues are not peculiar to selection analysis by multiple regression, they should be considered in using this approach or in interpreting results (Lande & Arnold 1983, Mitchell-Olds & Shaw 1987, Brodie et al. 1995). (1) The problem of *multicollinearity* arises if a subset of traits is highly correlated. In this circumstance, the analysis can fail to fully account for correlations among traits, with resulting distortions of estimated coefficients. As in the quandry discussed above, two useful approaches are to reduce the number of traits (using outside criteria) or to use principal components. (2) Multiple regression results are always conditional on the proviso that all correlated traits under selection have been included in the analysis. To the extent that correlated, unmeasured traits are exposed to selection, their exclusion may have distorted estimates of selection coefficients. While this proviso may at first sound fatal, most investigators feel that it is better to account for some correlations than to fall back on univariate analyses. (3) Stepwise regression and related strategies are useful statistical solutions to the problem of sorting through a large field of possible explanatory variables. These approaches are problematic in selection analyses, however, because of the biases they cause in the estimates of  $\beta$  and  $\gamma$ . (4) Variance in relative fitness (the *opportunity for selection*) can limit the power to detect selection and should be taken into account in designing selection studies (Hersch & Phillips 2004). (5) A dichotomous fitness measure (e.g., survivors and nonsurvivors) complicates the estimation of standard errors for  $\beta$  and  $\gamma$ . Janzen & Stern 1998 describe a solution that employs logistic regression.

A technical problem plagues published estimates of nonlinear selection coefficients,  $\gamma$ . Recall that in the quadratic regression equation (4.3) the nonlinear coefficient for  $z_i^2$  is  $\frac{1}{2}\gamma_{ii}$  so that  $\gamma_{ii}$  is a second derivative of the ISS. Stinchcombe et al (2008) queried the authors of 32 papers published in the period 2002-2007 and found that in a sizeable fraction of those papers (78%), the authors failed to take the factor of  $\frac{1}{2}$  into account. The consequence is that the published estimates labeled  $\gamma_{ii}$  are actually  $\frac{1}{2}\gamma_{ii}$ . Because the diagonal elements of  $\gamma$ -matrix are under-estimated by a factor of 2, while the off-diagonal elements are not, portrayals of the ISS can be affected. Unless authors specifically state that the factor of  $\frac{1}{2}$  was taken into account or reproduce (4.3), a cautious reader should assume that published values of  $\gamma_{ii}$  are likely to be in error.

Under certain circumstances one must assume that nonlinear selection is weak ( $\omega \gg P$  or  $P \gg |\gamma|$ ).

One such circumstance arises when one wishes to claim that a quadratic or Gaussian approximation provides a good representation of the ISS. If the actual ISS is asymmetric or stabilizing or disruptive selection is strong, neither of these approximations is likely to be satisfactory. Likewise, when ... {need to write a simple R program to devise some rules} the simple formula for converting between  $\gamma$  and  $\omega$  (3.10) is inaccurate.

... computational strategies {see papers by Blows, Brooks and colleagues with focus on ISS rather than on the elements of  $\gamma$ } ... parts of fitness, not all ... only parts of the ISS and the AL

#### 4.12 Why the multivariate view of selection is important.

... hazards in taking a univariate view of selection ... ridges not apparent in univariate views refer back to the discussion of the Phillips & Arnold 1989 quad plots ... slight change in  $\gamma$ -coefficients, big impact of appearance of surface ... and amplify on those conclusions